FILM BOILING OF POTASSIUM ON A HORIZONTAL PLATE

Andrew Padilla, Jr.

A dissertation submitted in partial fulfillment
of the requirements for the degree of
Doctor of Philosophy in the
University of Michigan
1966

Doctoral Committee:

Associate Professor Richard E. Balzhiser
Associate Professor Robert H. Kadlec
Professor Donald L. Katz
Associate Professor Herman Merte, Jr.
Professor Edwin H. Young

Film Boiling of Potassium on A Horizontal Plate

by Andrew Padilla, Jr.

ABSTRACT

The purpose of this investigation was to experimentally determine the heat transfer to potassium in the stable film-boiling regime. The experiments were conducted on a stainless steel pool-boiling apparatus utilizing a 3-inch diameter horizontal surface facing upwards and the heat flux-temperature difference at various pressures were obtained.

The liquid potassium was slowly charged to a hot surface at low pressure, thus establishing film boiling directly without passing over the maximum heat flux. The film-boiling curve was then obtained by raising or lowering the power to the heaters. Operation at higher pressures was accomplished by slowly bleeding helium into the system.

Film boiling data were obtained for pressures between 2 mm Hg and 300 mm Hg, corresponding to liquid temperatures between 714°F and 1243°F. Two runs were made at constant pressures of 2 mm Hg and 50 mm Hg. A third run consisted of increasing the pressure in small increments at essentially constant power input. Nucleate boiling data were also obtained for pressures of 1-2 mm Hg and 602-751 mm Hg. Heat fluxes up to 63,600 BTU/hr-sq ft were obtained for temperature differences between 15°F and 49°F with essentially no difference between the low- and high-pressure data.

The heat fluxes encountered for the film boiling of potassium were substantially above the theoretical predictions of Zuber and Berenson. For a pressure of 2 mm Hg, the minimum heat flux was 2,000 BTU/hr-sq ft at a $T_{wall}-T_{sat}$ of 400°F and the heat flux increased to 16,000 BTU/hr-sq ft at a $T_{wall}-T_{sat}$ of 873°F. For 50 mm Hg, the heat flux varied from 8,800 BTU/hr-sq ft at a $T_{wall}-T_{sat}$ of 432°F to 12,000 BTU/hr-sq ft at a $T_{wall}-T_{sat}$ of 665°F. After correction for the effects of radiation and the vapor-phase dimerization reaction were made, the experimental results for potassium at moderate temperature differences of approximately 200°F beyond the minimum heat flux, as well as for the previous experimental results of Berenson for n-pentane and carbon tetrachloride and Hosler and Westwater for Freon-11 and water, were found to be correlated to within 22% by the equation

$$h = 0.97 \left[\frac{k_v^3 \rho_v (\rho_l - \rho_v) g L'}{\mu_v \Delta T D_b} \right]^{1/4}$$

where the bubble diameter D_b is given by

$$D_b = 4.7 \sqrt{\frac{3 g_c \sigma}{g(\rho_l - \rho_v)}}$$

This represents heat transfer coefficients approximately 35% above those predicted by Berenson's correlation. The film-boiling heat transfer to potassium, as well as to some non-metallic fluids, was found to increase much more rapidly at high temperature differences than could be accounted for by this or any other correlation.

ACKNOWLEDGEMENTS

This study was made possible by support from the United States Air Force, Aeronautical Systems Division, Contracts AF33(616)-8277 and AF33(657)-11548, under the direction of Professor R. E. Balzhiser.

The author wishes to acknowledge the assistance of the members of his doctoral committee. Special thanks are due to Professor R. E. Balzhiser, Chairman of the Committee.

CONTENTS

LIST OF TABLES

LIST OF FIGURES

LIST OF FIGURES (Continued)

LIST OF APPENDICES

NOMENCLATURE

a	Constant defined by Equation (21)
a'	Constant defined by Equation (25)
A	Area, sq ft
b	Power in Equation (19)
c	Constant defined by Equation (6)
C_p	Heat capacity, BTU/lb-^oF
D	Diameter, ft
g	Acceleration of gravity, ft/hr^2
g_c	Conversion factor, 4.17×10^8 (lb_m/lb_f) ft/hr^2
Gr'	Modified Grashof number
h	Heat transfer coefficient, BTU/hr-sq ft-^oF
k	Thermal conductivity, BTU/ft-hr-^oF
L	Latent heat of vaporization, BTU/lb
L'	Effective latent heat of vaporization, BTU/lb
Nu	Nusselt number
Pr	Prandtl number
q	Heat transferred, BTU/hr
Ra'	Modified Rayleigh number
r_e	Electrical resistivity, ohm-cm
T	Temperature, ^oR
ΔT	Temperature difference between surface and liquid, ^oF

Greek Symbols

ϵ_o	Normal emissivity
μ	Viscosity, lb/ft-hr
ρ	Density, lb/ft^3
σ	Surface tension, lb/ft

Subscripts

b	Bubble
l	Liquid property
v	Vapor property
min	At the minimum heat flux

I. INTRODUCTION

The design of high-temperature heat transfer systems utilizing high surface heat fluxes has led to the relatively recent interest in liquid metals. The low vapor pressure of liquid metals compared to that of water and organic fluids makes lighter designs possible. Their high thermal conductivity affords potentially higher heat transfer rates which would result in a substantial reduction in the required heat transfer area. Much of the current research being carried out on liquid metals has resulted from the feasibility of their being used as the working fluid in energy conversion cycles with nuclear reactors, especially in space applications. Even with terrestial nuclear power stations, the use of liquid metals over other fluids would greatly increase the thermodynamic efficiency of the power cycle.

Useful design information for liquid metal systems can be provided by relatively simple pool boiling experiments. They are considerably easier to set up than forced convection loops and would determine the lower heat transfer limit of the flowing system. Furthermore, the qualitative effects of additives and other similar changes in loop operation can be more easily obtained.

Unlike nucleate boiling, the film-boiling regime has been the subject of relatively few analytical and experimental

investigations. Energy transfer in film boiling occurs by conduction, convection, and radiation across a layer of vapor which separates the liquid from the heating surface. Since the fluxes attainable in film boiling are usually much lower than in nucleate boiling, equipment is invariably operated to avoid passing into this regime. However, it is advantageous to operate as close as possible to the critical heat flux thus increasing the possibility of encountering film boiling. A knowledge of the entire boiling curve and the thermal capacity of a system would help the designer to determine whether transition from nucleate to film boiling would result in catastrophic failure of the heat transfer surface.

Except for mercury, which film boils at a relatively low temperature difference between the heating surface and the liquid because of its non-wetting characteristics, there has been little pool boiling data in the film regime for liquid metals. The object of this investigation was to experimentally determine the heat transfer to potassium in the stable film-boiling regime. The experiments were conducted on a pool-boiling apparatus utilizing a 3-inch diameter horizontal surface facing upwards and the heat flux-temperature difference relationship at various pressures were obtained. The experimental results were used to test existing correlations for film boiling.

II. LITERATURE REVIEW

1. Film Boiling Correlations

Although the first definite observation of film boiling occurred in 1934 by Nukiyama (34), the first analytical treatment did not appear until 1950 when Bromley (7) presented his theory of stable laminar film boiling from a horizontal cylinder based on Nusselt's derivation for laminar film condensation. His results can be expressed as

$$h = 0.62 \left[\frac{k_v^3 \rho_v (\rho_l - \rho_v) g L'}{D \, \Delta T \, \mu_v} \right]^{1/4} \tag{1}$$

Equation (1) can be rearranged into the following form:

$$\frac{hD}{k_v} = 0.62 \left[\frac{D^3 \rho_v (\rho_l - \rho_v) g}{\mu_v^2} \; \frac{L'}{C_{pv} \, \Delta T} \left(\frac{C_p \, \mu}{k} \right)_v \right]^{1/4} \tag{2}$$

or,

$$Nu = 0.62 \, (Ra')^{1/4} \tag{3}$$

where Ra' denotes a modified Rayleigh number

Bromley corrected his heat-transfer coefficient for radiation by assuming infinite parallel-plate radiation.

In 1959, Chang (8) introduced his wave theory for film boiling from a horizontal surface based on hydrodynamic con-

siderations alone. He assumed that the phenomenon would exhibit waves whose lengths would be equal or less than the critical value for the existence of a standing wave over a horizontal surface. He then utilized the concept of an equivalent thermal diffusivity of the vapor-liquid interface due to phase change and derived an expression for the heat transfer coefficient for a saturated liquid:

$$h = \left[\frac{k_v^2 \rho_v (\rho_l - \rho_v) g L}{4 \pi^2 \Delta T \mu_v}\right]^{1/3} \tag{4}$$

Zuber (44, 45) later followed the approach suggested by Chang and assumed that a more significant wavelength might be the most dangerous wavelength; that is, the one for which the amplitude of the vapor-liquid interface grows most rapidly. By assuming that the process is governed by a two-phase Taylor instability, he derived an equation for predicting the minimum heat flux:

$$(q/A)_{min} = cL'\rho_v \left[\frac{\sigma g_c g(\rho_l - \rho_v)}{(\rho_l + \rho_v)^2}\right]^{1/4} \tag{5}$$

where the constant c can have the range

$$\frac{\pi}{24} \frac{1}{(3)^{1/4}} \leqslant c \leqslant \frac{\pi}{24} \frac{0.4\,\pi\sqrt{2}}{(3)^{1/4}} \tag{6}$$

The uncertainty in the constant c arises because of the uncertainty of various assumptions in the derivation. Zuber's analysis predicts the minimum heat flux from the bubble spacing, bubble size, and bubble frequency from hydrodynamic considerations alone and does not take into account any thermal transport process.

Berenson (3 , 4) modified and extended Zuber's approach and obtained relations for the heat-transfer coefficient, the minimum heat flux, and the temperature difference at the minimum:

$$h = 0.425 \left[\frac{k_v^3 \rho_v (\rho_l - \rho_v) g L'}{\mu_v \Delta T \sqrt{\frac{g_c \sigma}{g(\rho_l - \rho_v)}}} \right]^{1/4} \tag{7}$$

$$(q/A)_{min} = 0.09 \, \rho_v L' \left[\frac{g(\rho_l - \rho_v)}{\rho_l + \rho_v} \right]^{1/2} \left[\frac{g_c \sigma}{g(\rho_l - \rho_v)} \right]^{1/4} \tag{8}$$

$$\Delta T_{min} = 0.127 \frac{\rho_v L'}{k_v} \left[\frac{g(\rho_l - \rho_v)}{\rho_l + \rho_v} \right]^{2/3} \left[\frac{g_c \sigma}{g(\rho_l - \rho_v)} \right]^{1/2} \left[\frac{\mu_v}{g_c (\rho_l - \rho_v)} \right]^{1/3} \tag{9}$$

Equation (7) can be rearranged into the following form:

$$\frac{h}{k_v} 4.7 \sqrt{\frac{g_c \sigma}{g(\rho_l - \rho_v)}} = 0.63 \left[\left(4.7 \sqrt{\frac{g_c \sigma}{g(\rho_l - \rho_v)}} \right)^3 \frac{\rho_v (\rho_l - \rho_v) g}{\mu_v^2} \frac{L'}{C_{pv} \Delta T} \left(\frac{C_p \mu}{k} \right)_v \right]^{1/4} \tag{10}$$

Since Berenson predicts that the diameter of bubbles produced during film boiling from a horizontal surface is given by

$$D_b = 4.7\sqrt{\frac{g_c\sigma}{g(\rho_l-\rho_v)}} \tag{11}$$

equation (10) can be written as

$$\frac{hD_b}{k_v} = 0.63\left[\frac{D_b^3\rho_v(\rho_l-\rho_v)g}{\mu_v^2}\ \frac{L'}{C_{pv}\Delta T}\ \left(\frac{C_p\,\mu}{k}\right)_v\right]^{1/4} \tag{12}$$

or,

$$Nu = 0.63\ (Ra')^{1/4} \tag{13}$$

Hence, Berenson's correlation for film boiling from a horizontal surface is practically identical with Bromley's correlation for a horizontal tube if the proper characteristic length is used.

Frederking, et al (15) analyzed film boiling about a sphere assuming a turbulent, free convection process and obtained:

$$h = 0.14\left[\frac{k_v'^2\rho_v(\rho_l-\rho_v)gL'}{\mu_v\,\Delta T}\right]^{1/3} \tag{14}$$

Note that no effect of size is predicted. This is because the correlation was derived in the form:

$$Nu = 0.14\ (Ra')^{1/3} \tag{15}$$

or,

$$\frac{hD}{K_v} = 0.14\left[\frac{D^3\rho_v(\rho_l-\rho_v)g}{\mu_v^2}\ \frac{L'}{C_{pv}\,\Delta T}\ \left(\frac{C_p\,\mu}{k}\right)_v\right]^{1/3} \tag{16}$$

Equation (15) is similar in form to Bromley's correlation for a horizontal tube (Equation (3)). Bromley's coefficient is 0.62 instead of 0.14 and his exponent is 1/4 instead of 1/3.

The correlations above have been presented because they involve film boiling from a horizontal surface or can be compared to correlations for horizontal surfaces. Other film-boiling correlations are discussed in several literature surveys: Drew and Mueller (11), Westwater (43), McFadden and Grosh (31, 32), Balzhiser, et al (1), and Kepple and Tung (22).

2. Liquid Metal Film Boiling Experiments

Lyon (28) was the first investigator to make an extensive study of boiling heat transfer to liquid metals. The metals considered were mercury, mercury containing 0.10% sodium, mercury containing 0.02% magnesium and 0.0001% titanium, sodium, sodium-potassium alloy (56-59 wt % K), and cadmium. The test section consisted of a 3/4-inch OD horizontal cylinder 5 inches long made from type 316 stainless steel. Lyon experienced only film boiling for pure mercury and cadmium and attributed this effect to their non-wetting characteristics. Figure 1 shows Lyon's film-boiling data along with Bromley's correlation for comparison.

Bonilla (6) also studied the pool boiling of mercury with and without wetting agents. The apparatus consisted of a horizontal surface made of low carbon steel fitted with a 3-inch OD stainless steel tube which served as a container and condenser. Figure 2 shows the results for mercury boiled in a 2-cm-deep pool at various pressures. Bonilla concluded that all of the 50 to 200 mm curves represented film boiling. In the initial runs, film

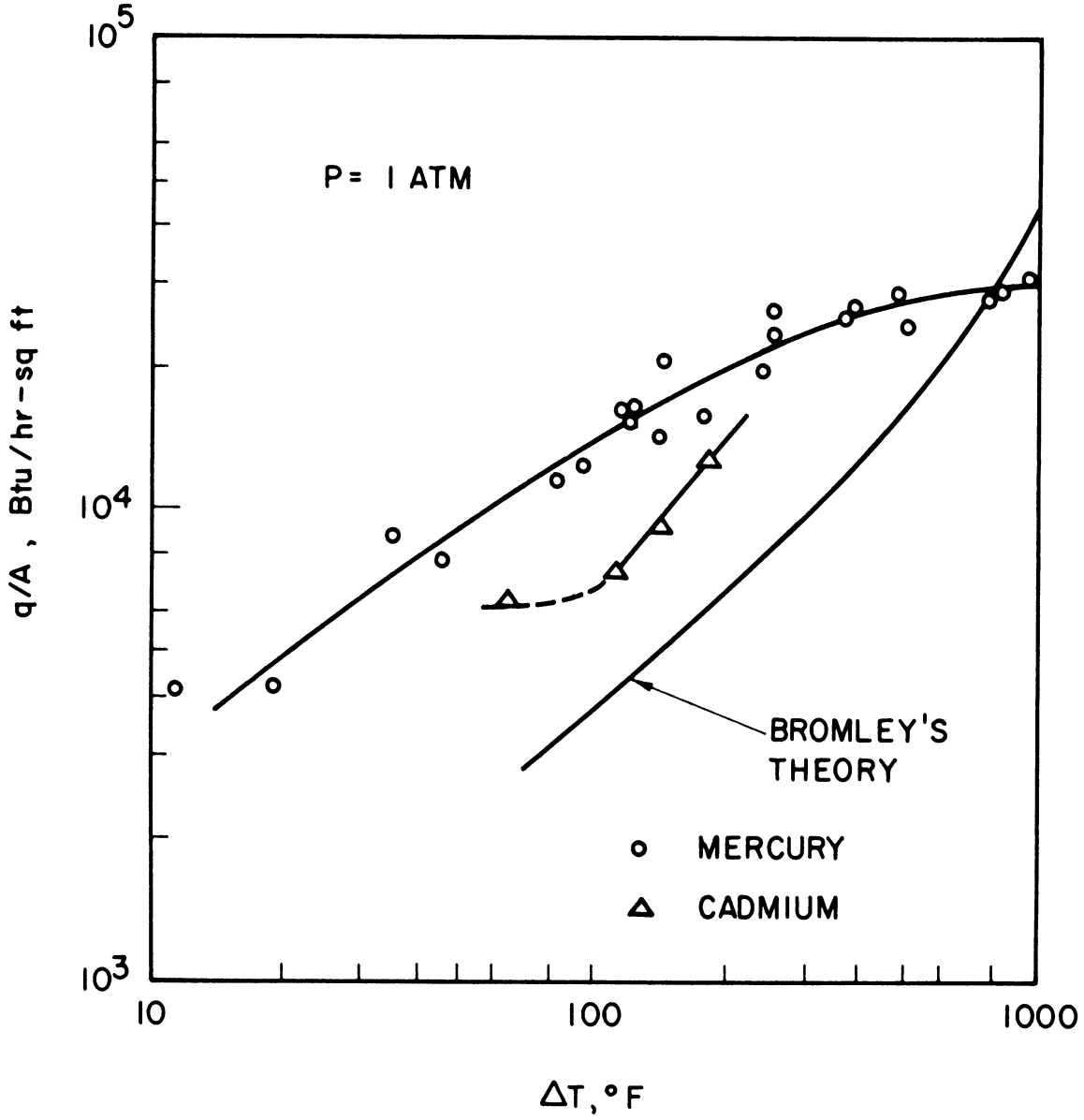

Figure 1. Data of Lyon (28) for Film Boiling of Mercury and Cadmium

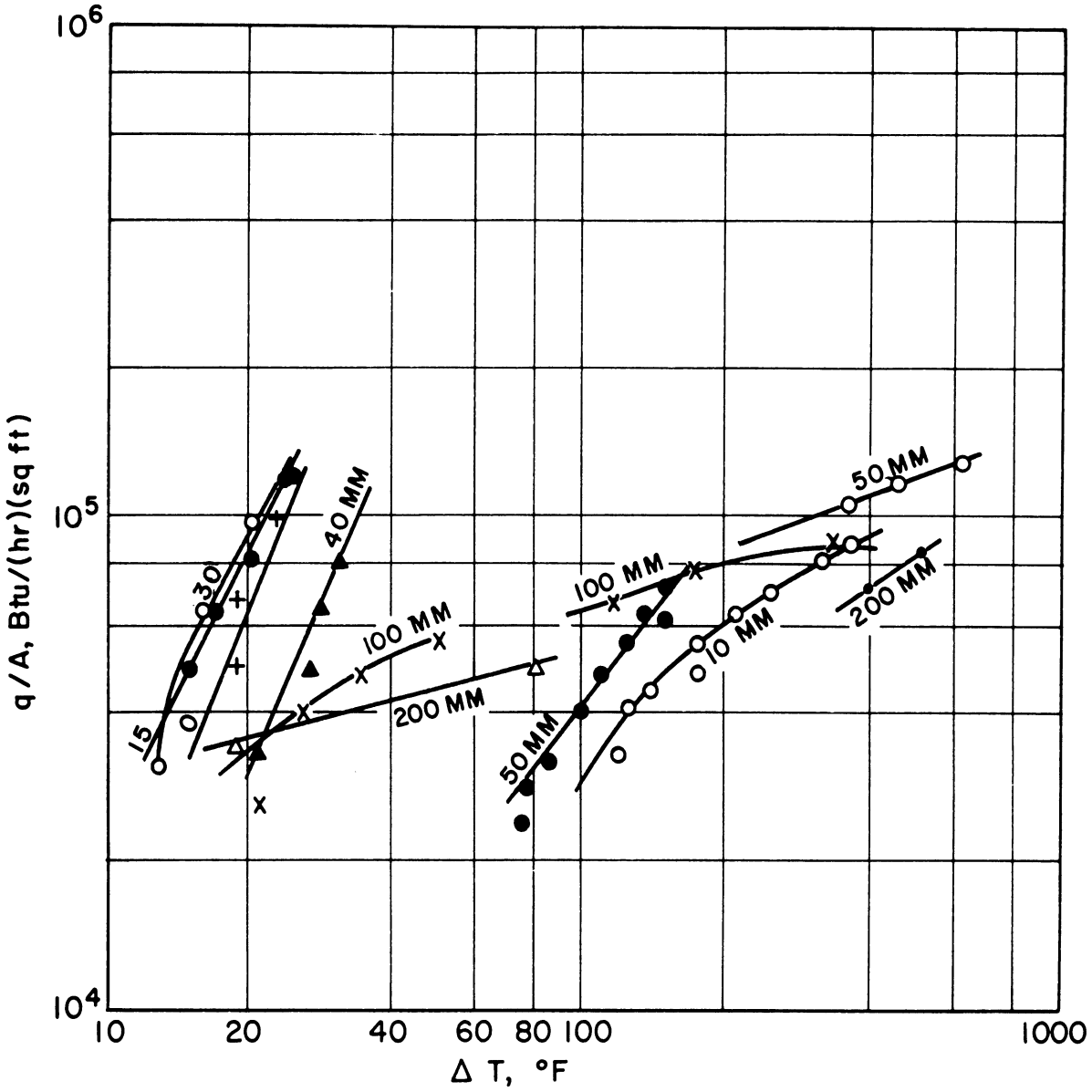

Figure 2. Data of Bonilla (6) for Pool Boiling of Mercury; parameter: pressure over the liquid in mm Hg absolute or lb/sq in. gauge

boiling was invariably obtained regardless of how low the heat flux was. After the boiling surface had been in frequent operation for a few weeks, film boiling was never obtained. This was attributed to the mechanical removal of oxygen or oxide which yielded better wetting of the surface by the mercury.

Lin, et al (26) performed experiments with pure mercury at atmospheric pressure. No mention was made in the article about the experimental apparatus and procedure. The system was observed to enter the film-boiling regime at very low temperature differences.

It was found that the heat-transfer coefficient could be expressed by

$$h = 4850\ (q/A)^{-0.26}\ \text{Kcal/hr-in}^2\text{-°C} \tag{17}$$

The experimental values correlated by equation (17) fell about 50% above the theoretical line corresponding to Bromley's prediction.

Merte (33) traversed the entire boiling curve in studies with mercury using a 2-inch diameter horizontal surface made of type 347 stainless steel. The data is shown in Figure 3 along with Berenson's correlation for comparison. To determine the approximate region of the minimum heat flux, the power was reduced in small increments until the system reverted to nucleate boiling. The minimum heat flux occurred within the range 23,000-27,000 BTU/hr-sq ft at a ΔT of approximately 140°F.

Although there have not been any pool boiling studies of potassium for film boiling, data is available for droplet vaporization and forced convection. Poppendiek, et al (35, 36, 37) have

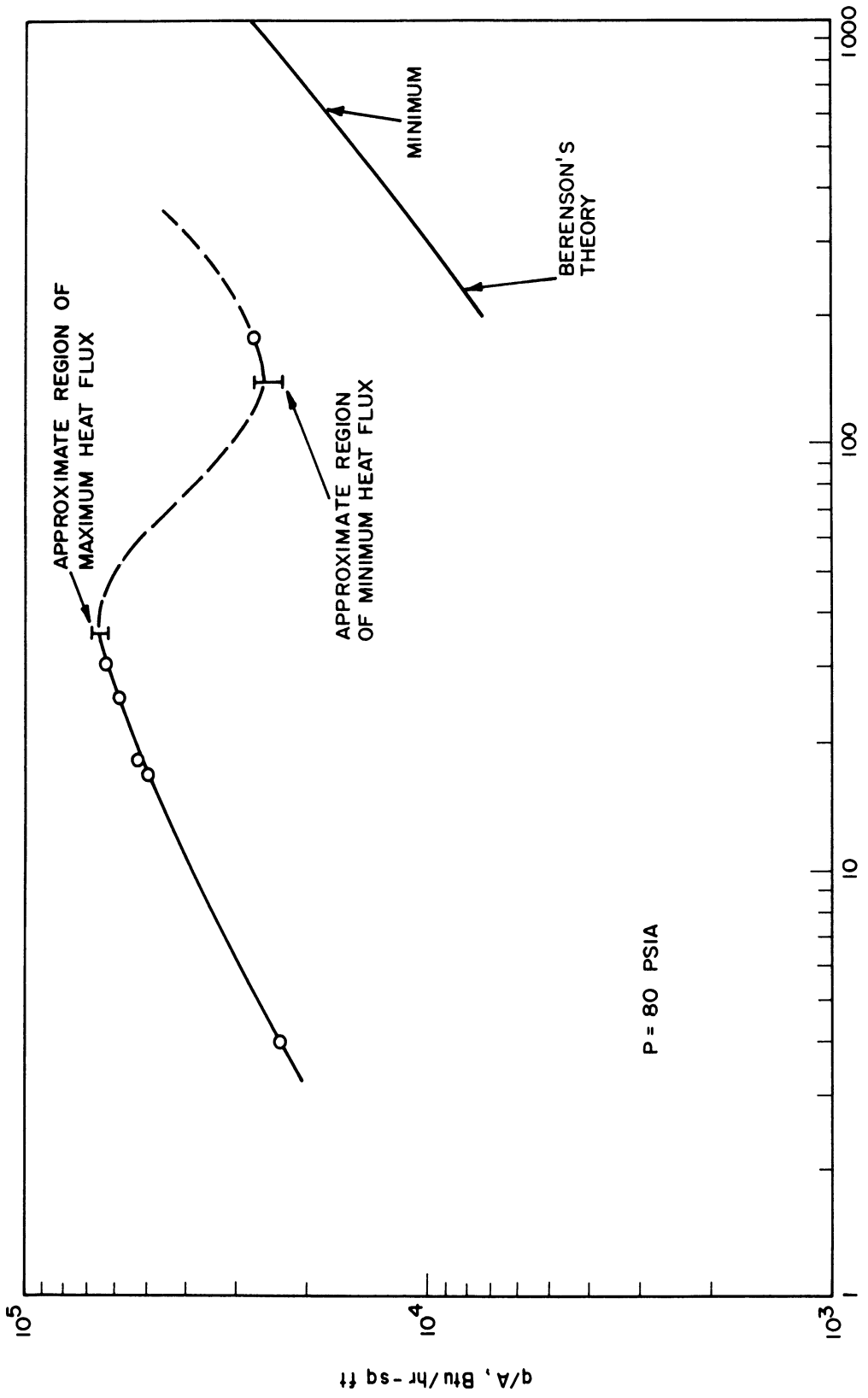

Figure 3. Data of Merte (33) for Saturated Pool Boiling of Mercury

carried out analytical and experimental studies on the vaporization of droplets suspended above a hot surface by a vapor film. They experimentally measured the lifetimes of droplets of water, mercury, potassium, benzene, Freon-11 and Freon-114 and compared them with their predictions. For the vaporization of mercury droplets on a nickel-plated copper plate, 87% of the data fell within 20% of the predicted lifetimes. The potassium droplet experiments were carried out in an argon atmosphere on nickel, stainless steel, Haynes 25, iron, and tantalum surfaces. In most of the runs, a definite surface conditioning process was observed such that the observed lifetimes increased with the number of droplets vaporized on the surface. However, the stainless steel surfaces did not appear to be subject to conditioning. With the exception of the tantalum surface, the lifetimes observed for quiet, stable film boiling droplets of potassium fell about the same amount (30-50%) above the predicted curve as did the other liquids. A marked increase in droplet lifetime occurred at a surface-to-drop temperature difference of approximately 350^{o}F, indicating the onset of complete film boiling. The lifetimes of two steady potassium droplets on a heated tantalum surface were almost a factor of two higher than the predictions.

Boiling coefficients for potassium in forced convection have been obtained by the General Electric Co. (16) using a 0.938 inch ID Mo-0.5% Ti boiler tube. The transition and film-boiling coefficients for qualities between 30% and 90% are shown in Figure 4. Extrapolation of the curve to 100% quality gives an estimated film-boiling coefficient range of 30-70 BTU/hr-sq ft-^{o}F.

3. Discussion

Film-boiling data for non-metallic fluids have been used to test the correlations discussed in Section 1. Berenson (4) found that his results for n-pentane and CCL_4 on a 2-inch diameter horizontal surface agreed within ± 10% with his predictions. Hosler and Westwater (19) obtained data for water and Freon-11 on an 8-inch-square horizontal surface and concluded that Berenson's method for predicting the film-boiling curve is good, but his predictions for the ΔT at the minimum flux are not reliable. They also found that a good estimate of the minimum flux was given by the higher estimate of Zuber and that the method of Chang for predicting the film-boiling curve was not reliable. The data of Lewis, et al (25) for the film boiling of nitrogen on the surface of 1-inch, $\frac{1}{2}$-inch, and $\frac{1}{4}$-inch spheres agreed well with the correlation of Frederking.

The available pool-boiling data for mercury of Lyon (28), Bonilla (6), Lin (26), and Merte (33) are characterized by relatively high fluxes at moderate temperature differences and are considerably above the predicted curves. However, there is no reason to suspect a priori that potassium will also not agree with the available correlations. The droplet vaporization studies of Poppendiek (37) suggest that the film-boiling process for potassium is not much different from that of water, benzene, and Freon. The forced convection studies of the General Electric Co. show that the upper limit of the film-boiling coefficient for potassium is of the same order of magnitude as the coefficients of Hosler and Westwater for water and Freon-11.

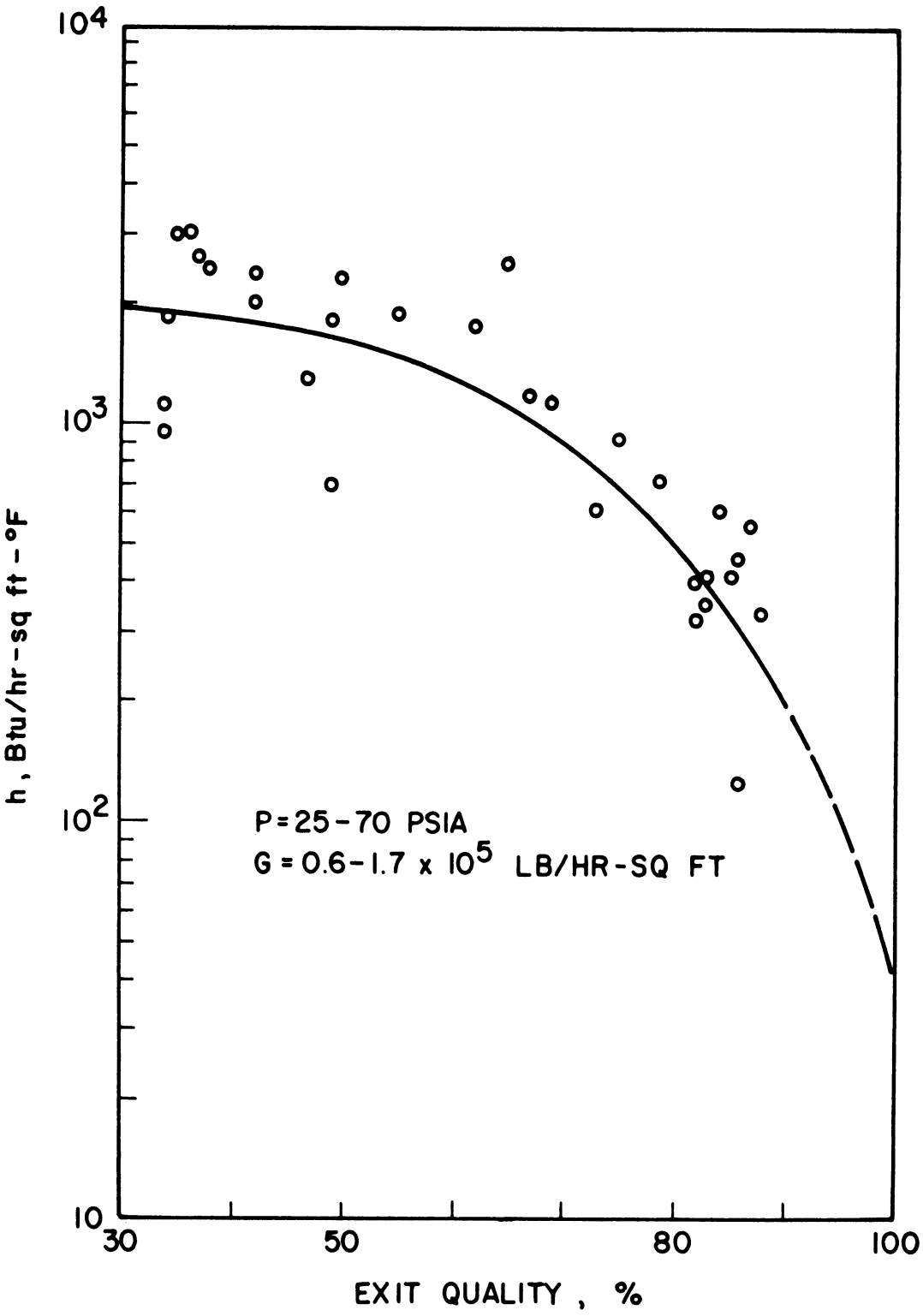

Figure 4. Data of the General Electric Company (16) for Average Transition and Film Boiling Coefficients of Potassium in Forced Convection.

III. DESCRIPTION OF EQUIPMENT

1. Introduction

The most obvious method of obtaining film boiling, i.e., traversing the nucleate boiling curve and passing over the maximum heat flux, would require high capacity equipment. Since the flux levels in film boiling would probably be only a small fraction of the maximum heat flux, it was decided to adopt a technique used by Hosler and Westwater (19). This consisted of heating the dry boiler to a temperature above that required to obtain film boiling and then slowly charging liquid into the boiler, thus establishing film boiling directly without having to pass over the maximum heat flux. Hosler and Westwater found that a short free fall for the liquid return to the boiler of approximately 1 inch was necessary to avoid reverting to nucleate boiling. The apparatus used in this investigation was designed using the above criteria.

A schematic diagram of the film boiling apparatus is shown in Figure 5. Figure 6 is a general view of the environmental vessel, potassium reservoir, instrument panel, vacuum system, and power supply.

2. Environmental Vessel

The environmental vessel consists of a 21-inch diameter by 27-inch long main section and a 13-inch diameter by 6-inch long top section. The main section is directly flanged to a

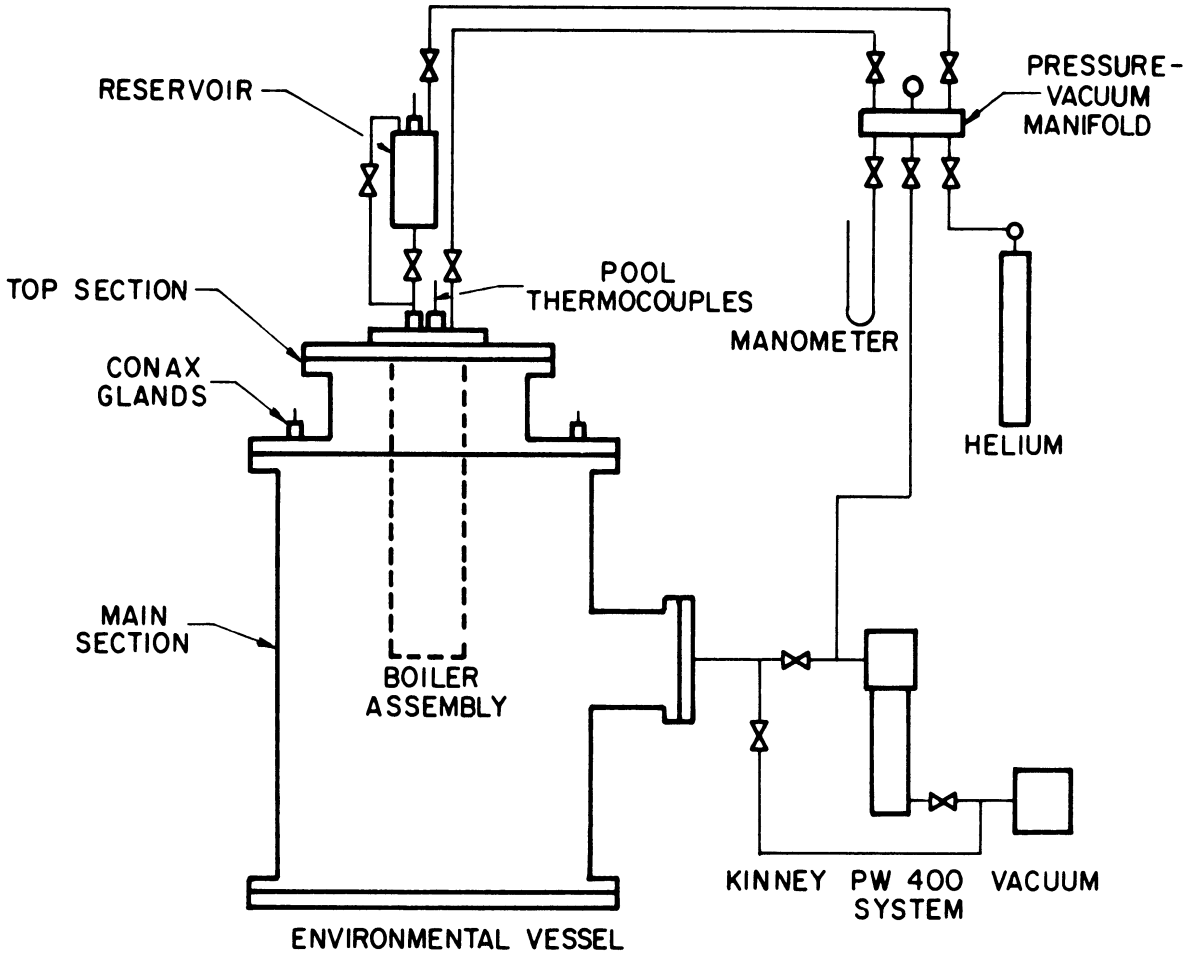

Figure 5. Schematic Diagram of Film Boiling Apparatus

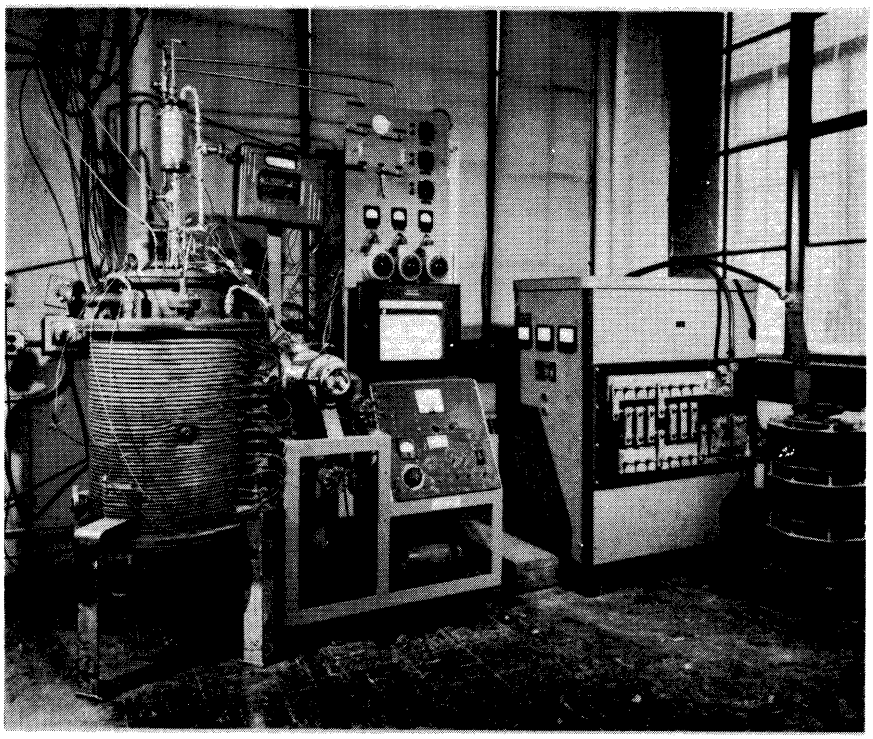

Figure 6. General View of Experimental Apparatus

Kinney PW 400 vacuum system which includes a 4-inch diffusion pump and a Welsch Duo-Seal vacuum pump. The top section contains a viewing port and six Conax glands for power leads and thermocouples. The flange for the top section has a $5\frac{1}{2}$-inch diameter opening through which the boiler assembly is lowered into the environmental vessel. The cooling coils around the main section are designed to keep the vessel cool but it was not found necessary to use them.

3. Boiler Assembly

The boiler assembly is shown in Figure 7 after it has been lowered into the $5\frac{1}{2}$-inch diameter opening in the flange to the top section of the environmental vessel. It consists of the top flange through which the fill line and pool thermocouples are inserted, the condenser, the drip plate, the boiling chamber, the boiling plate, the main heater along with its busbars and electrical insulators, and the compression plate with its springs for obtaining good electrical contact between the busbars and the heater.

The top flange is an 8-inch diameter by 3/4-inch thick plate of type 304 stainless steel. Eight equally-spaced Conax 3/16-inch OD MPG glands are silver-soldered to the flange around a 2 inch diameter. One of the glands is used for pressurizing and evacuating the condenser and the remaining seven are used for thermocouple wells to be lowered into the boiling chamber. At the center of the flange is a 3/8-inch OD Veeco gland welded to a 4-inch-long 3/4-inch OD extension. The gland, which allows the fill line to be raised and lowered, uses a

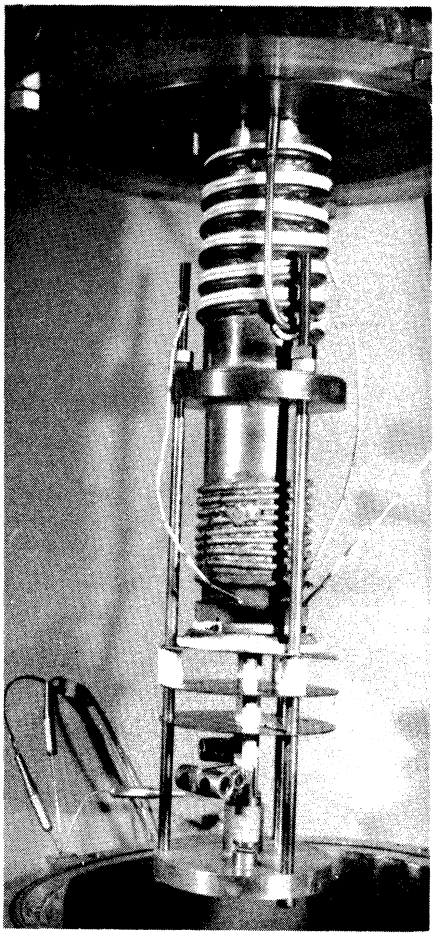

Figure 7. Boiler Assembly

Viton O-ring to insure that the fill line can be heated above the melting point of potassium during charging.

The condenser is a 9-inch-long section of schedule 40 Haynes 25 pipe. This portion of the boiler assembly would have normally been made of stainless steel, but the Haynes pipe was used because it was already available and could be readily welded to the other stainless steel components. The cooling coil welded to the outside of the condenser was made from 10 feet of 1/4-inch OD stainless steel tubing and is silver-soldered to the top flange. A 400-watt beaded Nichrome wire heater is wrapped around the condenser to insure that it can be always kept above the melting point of potassium.

Figure 8 is a section of the stainless steel drip plate. The purpose of the drip plate is to insure that all of the vapor generated in the boiling chamber reaches the condenser. An earlier design had indicated that liquid flowing down the walls of the boiling chamber may have disrupted the film boiling process. Liquid flowing down the walls of the condenser is prevented from dripping through the slots by $\frac{1}{2}$-inch-high weirs to avoid a high free fall. The condensate flows down the downcomer which ends one inch above the boiling surface.

The boiling chamber is a $3\frac{1}{4}$-inch OD by 3-inch ID by 8-inch long section of type 316 stainless steel tubing. A 3/16-inch OD by 93-inch long guard heater is Nicrobrazed to the boiler wall. The heater consists of two Nichrome wires insulated by magnesium oxide inside of a swaged Inconel sheath and is rated at 1 kilowatt at 115 volts AC.

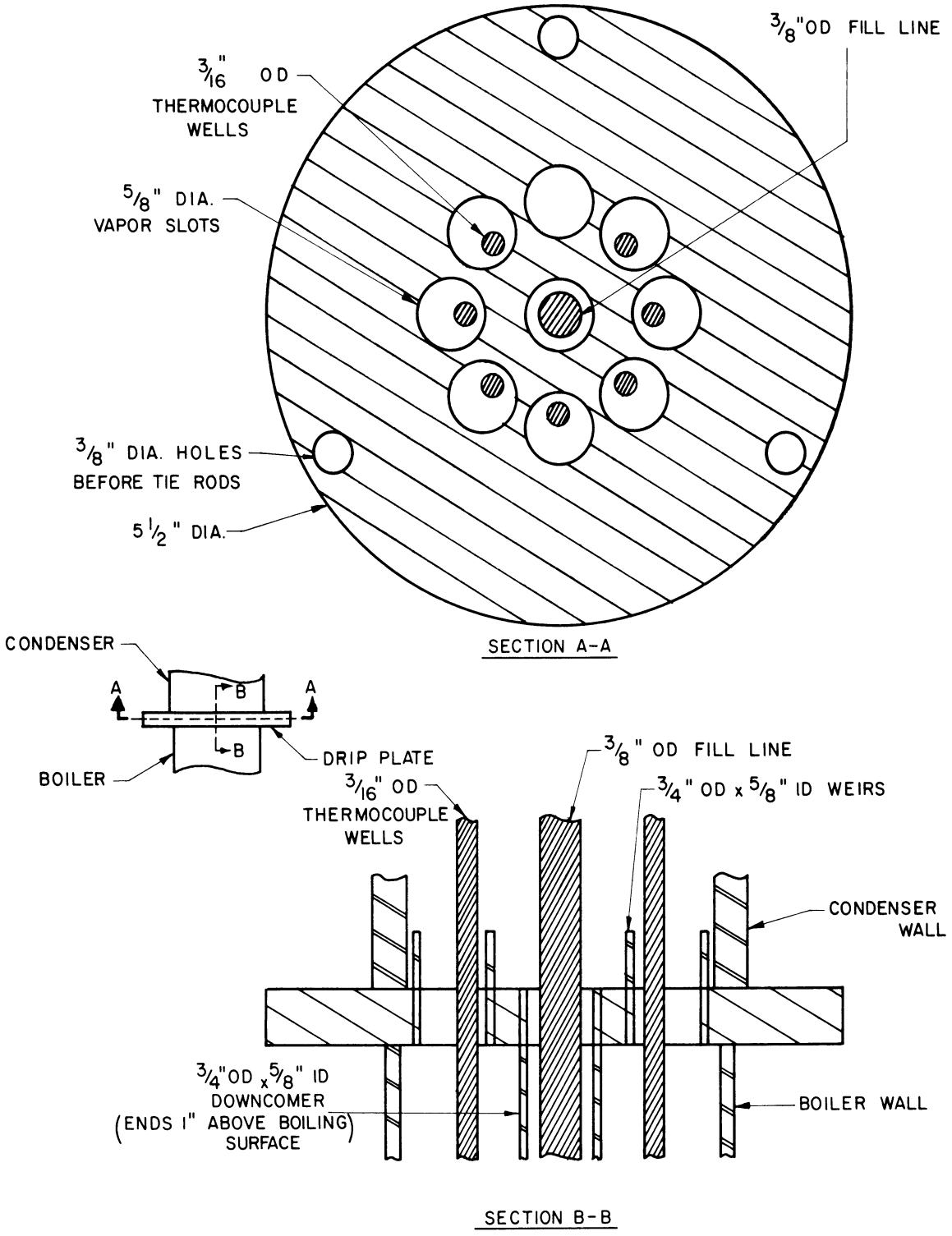

Figure 8. Diagram of Drip Plate

The boiling plate is shown in Figure 9. To avoid a weld or undue thermal stress at the outer edge of the boiling surface, the plate was machined from solid bar stock $3\frac{1}{2}$-inch in diameter by $1\frac{1}{2}$-inch long of type 316 stainless steel. The plate section is 0.504-inch thick and contains six 1/16-inch diameter holes for thermocouples. Figure 10 shows the location of the holes and their distances from the boiling surface. The 0.050-inch thick by $\frac{1}{2}$-inch long thin-walled section above the boiling plate is designed to minimize heat conduction from the plate to the walls of the boiling chamber. The final preparation of the 3-inch diameter boiling surface consisted of polishing with 500 grit aluminum oxide cloth and then with 600 grit boron carbide powder.

Figure 11 shows the main heater which is made from a $3\frac{1}{2}$-inch diameter by $\frac{1}{4}$-inch thick plate of National Carbon grade ATJ graphite. It has a measured resistance of approximately 0.14 ohm at room temperature. The heater is insulated from the boiling plate by a 1/32-inch-thick layer of alumina and was assembled according to the following procedure. High-purity alumina powder was mixed with water to trowelling consistency and allowed to stand for 24 hours in an airtight container. Spacers which consisted of 1/32-inch diameter alumina rods were placed on the bottom surface of the boiling plate and the thick alumina slurry was poured over the spacers. The graphite heater was then placed on the slurry and pressed down until contact was made with the spacers. The excess alumina slurry flowed out at the edges and through the slits in the graphite heater and were wiped off. Weights were then

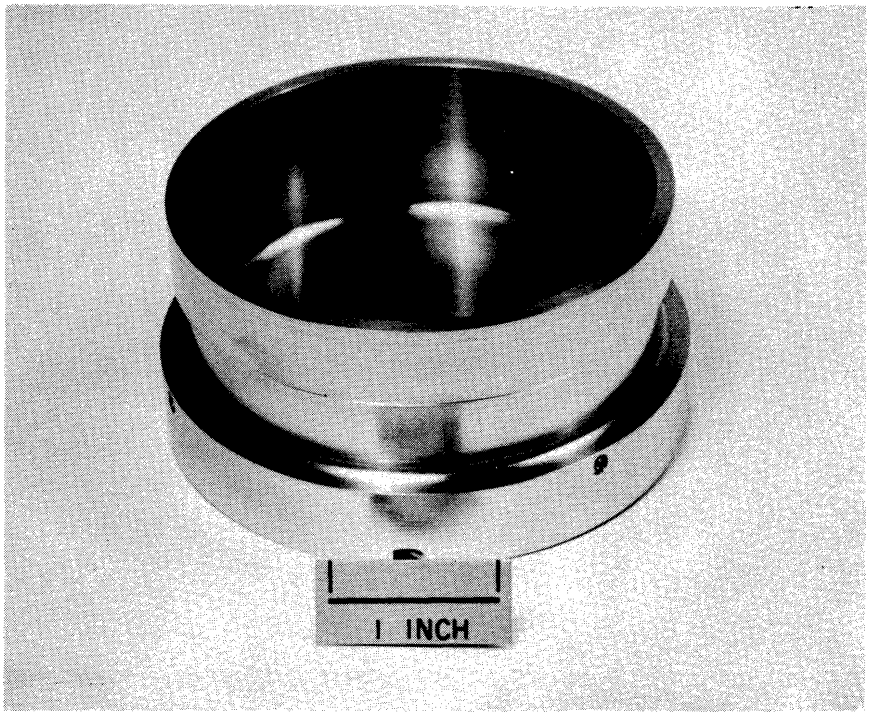

Figure 9. Boiling Plate

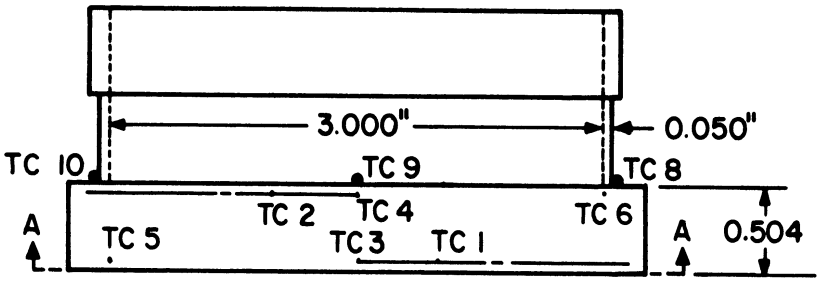

DISTANCE BETWEEN CENTERLINE OF THERMOCOUPLE HOLES AND BOILING SURFACE:

TC 1	.436"
TC 3	.438"
TC 5	.439"
TC 2	.072"
TC 4	.076"
TC 6	.072"

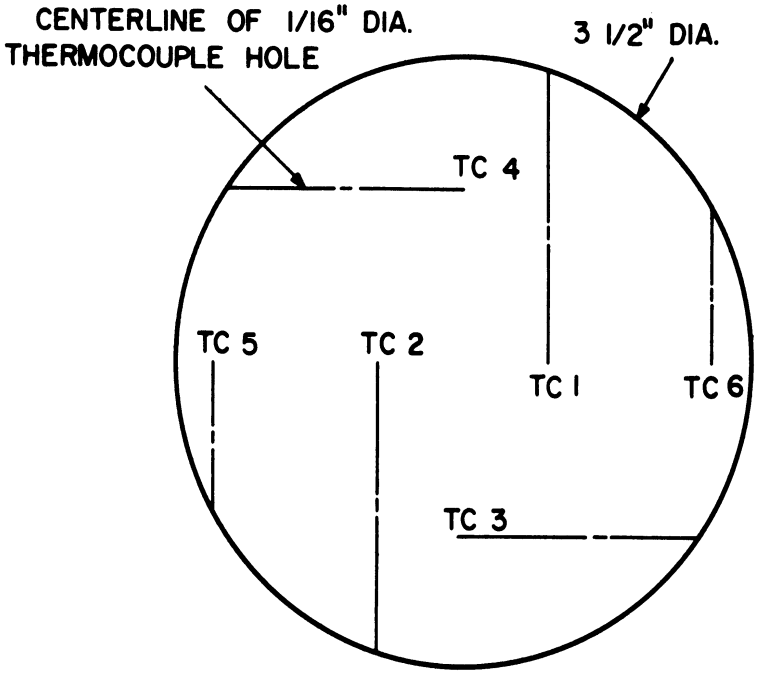

SECTION A-A

Figure 10. Location of Boiling Plate Thermocouples

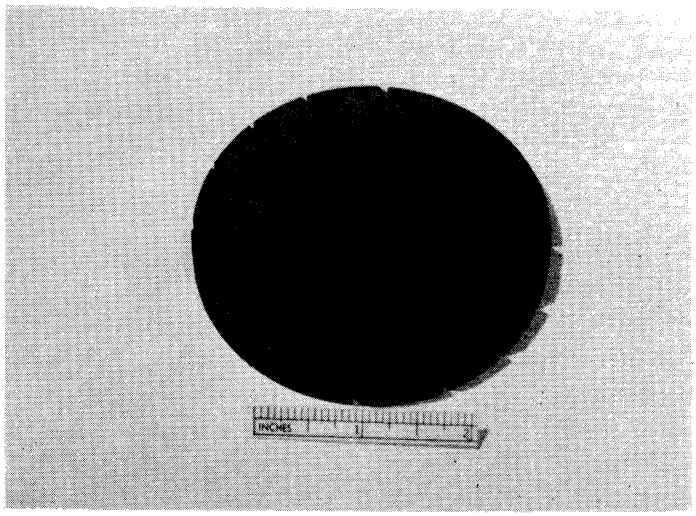

Figure 11. Graphite Main Heater

placed on the graphite heater until the alumina dried and hardened.

A $4\frac{1}{2}$-inch diameter zirconia crucible cover acts as the bottom insulator for the graphite heater and also as a guide for the two molybdenum busbars. Copper strips are heli-arc welded to the bottom of the busbars with Everdur filler and mechanical clamps are bolted to the copper strips for connection to the copper braid. The molybdenum busbars are forced against the graphite heater by means of stainless steel springs to insure good electrical contact. Another spring allows for thermal expansion to avoid cracking the graphite heater. Compression of the springs is accomplished by tightening three 3/8-inch diameter stainless steel tie rods connecting the compression plate and the drip plate. The three radiation shields below the zirconia insulator are intended to keep the springs cool. Another radiation shield is placed around the graphite heater to cut down radial losses.

Figure 12 shows the boiler assembly with all the thermocouples and power leads hooked up prior to insulating the boiling chamber, boiling plate, and graphite heater assembly with several layers of Fiberfrax insulation. In Figure 13, the Fiberfrax insulation has been applied and the top section of the environmental vessel is ready to be lowered to the main section.

4. Charging System

Figure 14 is a schematic diagram of the charging system. The potassium reservoir consists of a $3\frac{1}{4}$-inch OD by 7-inch long

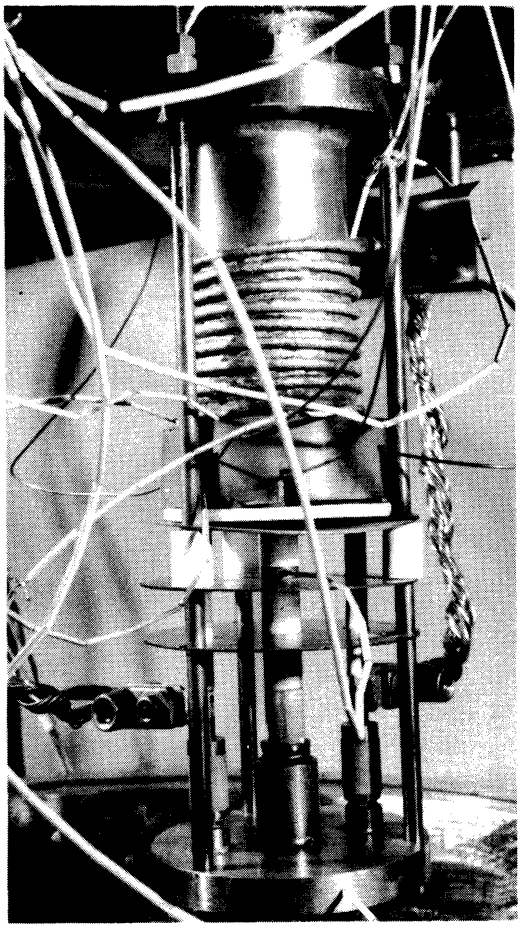

Figure 12. Instrumented Boiler Assembly

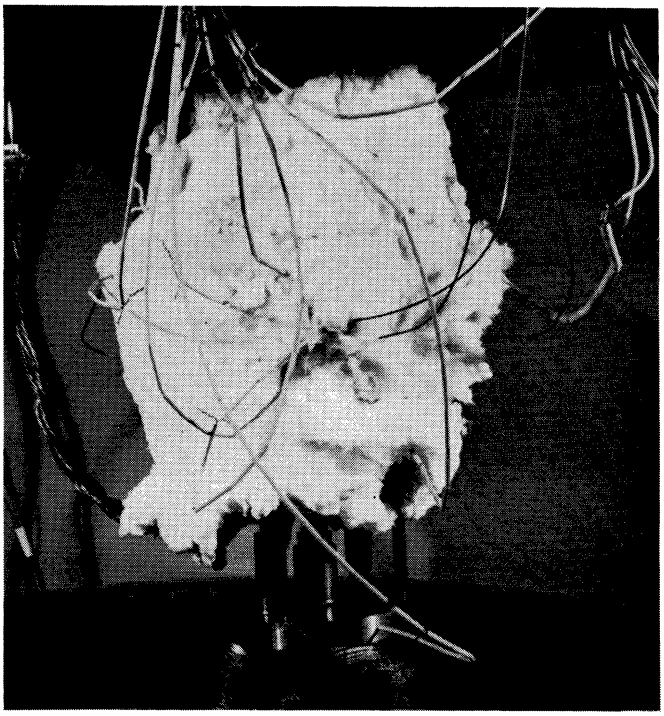

Figure 13. Instrumented and Insulated Boiler Assembly

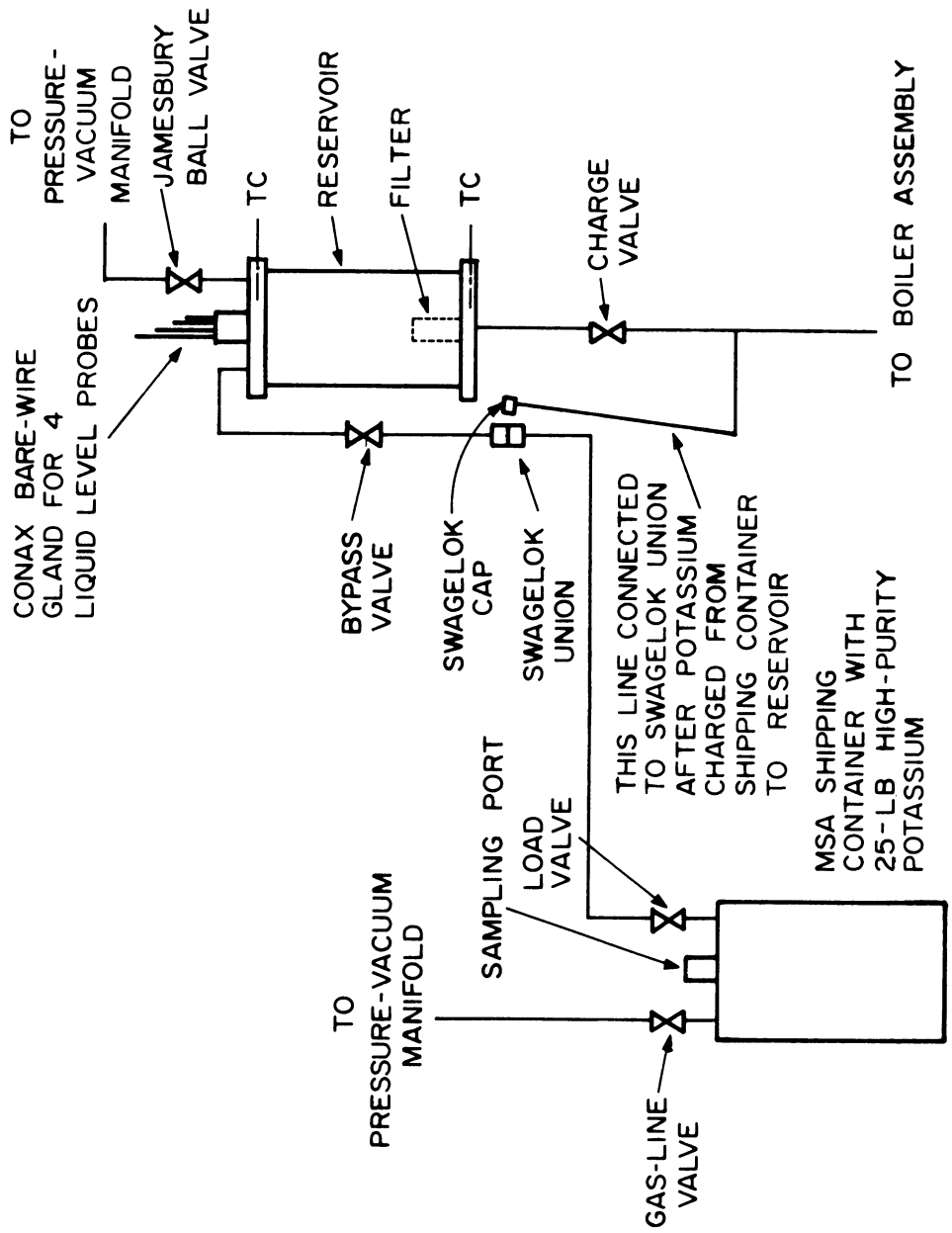

Figure 14. Diagram of Charging System

stainless steel vessel with a sintered stainless steel filter welded at the bottom for removing solid particles in the liquid. The filter is $\frac{1}{2}$-inch OD by $1\frac{1}{2}$-inch high with a 12-micron porosity and is the type used in Hoke in-line filters. The charge valve and bypass valve, as well as the two valves supplied with the 25-lb MSA shipping container, were Hoke TY 445 stainless steel bellows valves. A Conax gland at the top of the reservoir allowed for four 1/16-inch diameter stainless steel rods to be inserted into the reservoir to detect the liquid level. The rods were located just above the bottom (to detect the initial flow of potassium from the shipping container), and at 4, $4\frac{1}{4}$, and $4\frac{1}{2}$-inches above the bottom. Heating tapes were used on the reservoir, shipping container, and lines to maintain the temperature approximately 100°F above the melting point of potassium during charging operations.

5. Instrumentation

Figure 15 is a schematic diagram showing the location of the temperature measurements made in the system. The six thermocouples in the boiling plate (see Figure 10 for location) and the thermocouple in the 3/16-inch OD well located $\frac{1}{4}$-inch above the boiling surface, TC1 through TC7, were 1/16-inch OD, Inconel-sheathed, Pt-Pt 13% Rh swaged thermocouples with magnesium oxide insulation and grounded junctions made by the Claud S. Gordon Company. These seven thermocouples were hooked up to an 8-point thermocouple switch and utilized a common cold junction, another swaged thermocouple immersed in an ice bath. The

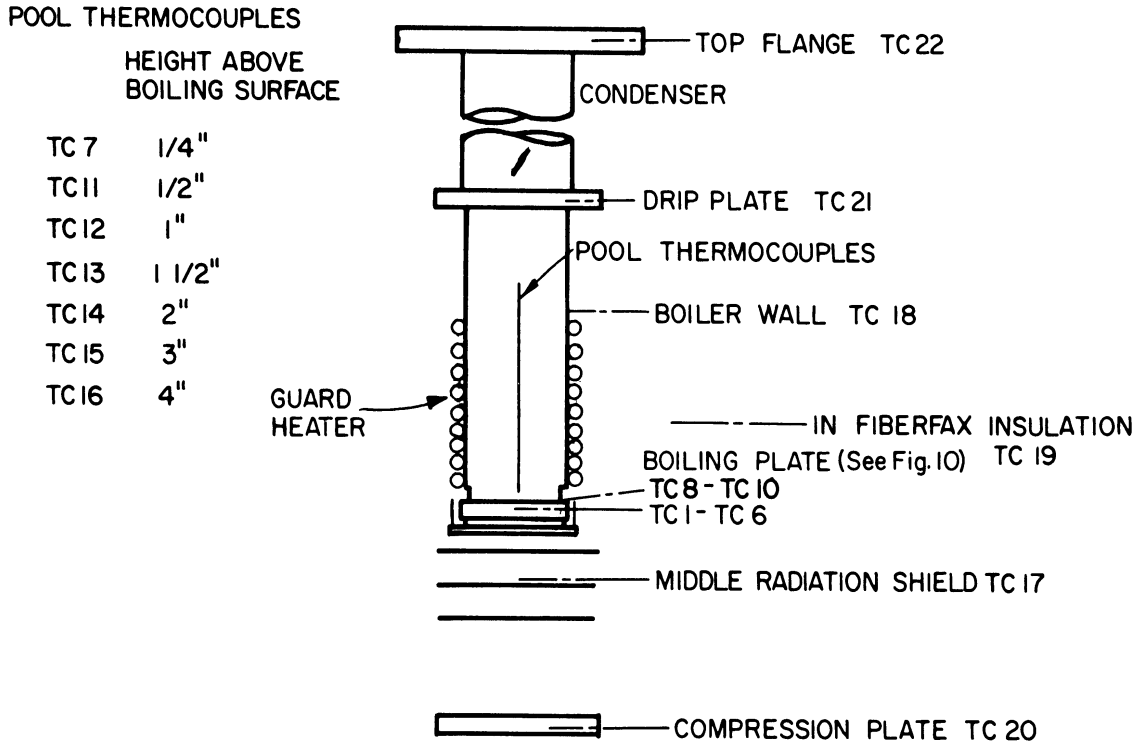

Figure 15. Location of Temperature Measurements

thermocouples located at the junction of the boiling plate and the 0.050-inch wall, TC8 through TC10, were made from 20-gauge Chromel-Alumel wires (Hoskins grade 3G-178) and were heli-arc-welded to insure good thermal contact. Pieces of stainless steel foil were placed around the junctions to avoid radiation error. These three thermocouples were hooked up to a second 8-point thermocouple switch and utilized a common cold junction, a thermocouple made from 24-gauge Chromel-Alumel wires (Hoskins grade 3G-178) immersed in an ice bath.

Each of the thermocouple switches was hooked up to a Leeds and Northrup Speedomax H Compact Azar recorder. A third thermocouple switch and recorder was available but was used only during the start up phase. The output of any of the thermocouple switches could be switched to a Leeds and Northrup No. 8662 portable precision potentiometer. Hence, two temperatures could be monitored constantly until steady state conditions were achieved but only one temperature at a time could be taken using the potentiometer. A picture of the two recorders and the potentiometer is shown in Figure 16. The six thermocouples in 3/16-inch OD wells located between $\frac{1}{2}$-inch and 4 inches above the boiling surface (TC11 through TC16) and the other check thermocouples located throughout the boiler assembly and potassium reservoir were made from 24-gauge Chromel-Alumel wires (Hoskins grade 3G-178) and were hooked up to a 12-point Brown Electronik recorder.

Pressure was measured with a U-tube manometer with a 100-cm scale graduated in millimeters. A Matheson gauge with a 30-inch vacuum to 15 psig range at the pressure-vacuum manifold was used primarily for outgassing and flushing with helium. Thermocouple

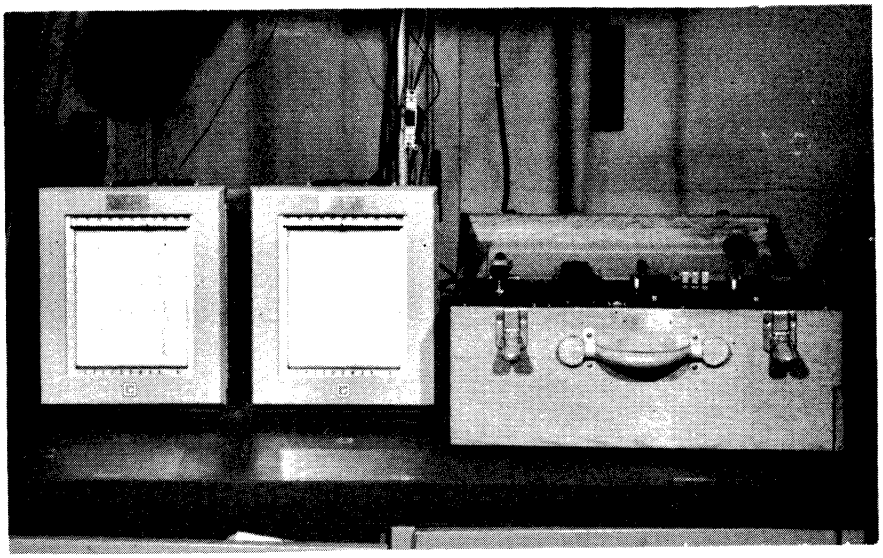

Figure 16. Temperature Recorders and Potentiometer

vacuum gauges with 1 micron-1 atm ranges are located in the environmental vessel and just before the diffusion pump. A Stokes McLeod gauge with a pressure range of .03 to 5000 microns could be used just before the diffusion pump or could be hooked up to the pressure-vacuum manifold.

6. Power Supply

Power to the main heater (graphite heater) was furnished by a 12 KW, 3-phase, full wave Udylite rectifier with a rated output of 250-2000 amps at 48-6 volts DC respectively. The rectifier is supplied with a 0-75 v voltmeter, a 0-250 a ammeter and a 0-2000 a ammeter. Copper welding cables carried the current from the rectifier to the Conax electrode glands passing through the top section of the environmental vessel. The glands used $\frac{1}{2}$-inch diameter copper busbars and Teflon sealants. Inside the vessel, copper braid carried the current from the electrode glandsto the mechanical clamps on the molybdenum busbars. The copper power lead system was designed to carry a current of 200 amps.

Power to the guard heater (3/16-inch OD, Inconel-sheathed 1 KW Nichrome heater), the condenser heater (400-watt beaded Nichrome heater), and the heating tapes on the charging system was supplied by 1 KW, 110 volt AC powerstats. Simpson 0-10 amp AC ammeters were used on all three guard heater circuits.

7. Miscellaneous

All equipment coming into contact with potassium was made from stainless steel or Haynes 25. Type 316 stainless steel tubing was used for the 3/16-inch OD pool thermocouple wells and

type 304 was used for gas lines. Hoke TY 445 bellows valves made from type 316 stainless steel were used on the potassium charging system but Jamesbury ball valves made from brass were used for the gas lines. Heli-arc welding between stainless steel or Haynes 25 components was utilized whenever possible. Where welding was impractical, connections were made using Swagelok compression fittings made from type 316 stainless steel. Glands operating over 200^{o}F used sealants made of Viton or Teflon; otherwise, neoprene sealants were used.

IV. EXPERIMENTAL PROCEDURE

The MSA Research Corporation stainless steel shipping container with 25 lbs. of high-purity potassium (less than 10 ppm oxygen) was hooked up to the reservoir just below the bypass valve (see Figure 14 for diagram of charging system). The entire system was then leak-checked under vacuum using a helium mass spectrometer. The reservoir and the lines between the reservoir and shipping container were then heated to approximately 250°F while under vacuum and then flushed three times with helium. The reservoir was back-filled with helium at 0 psig and slight helium pressure was then applied to the MSA shipping container to force the potassium liquid through the lines into the reservoir. The first liquid into the reservoir was detected by making electrical contact with the liquid level probe just above the bottom surface. The rising liquid level was detected by the probes at higher levels and the reservoir was filled to a level of $4\frac{1}{2}$ inches above the bottom surface. The load valve on the MSA shipping container was then closed and the lines allowed to cool to room temperature. The shipping container was disconnected from the reservoir under helium pressure to avoid introducing air into the system. This Swagelok connection below the bypass valve was then leak-checked using the helium mass spectrometer.

Before the commencement of boiling, a heat loss calibration was carried out. For various power settings of the main heater,

the power to the guard heater was adjusted to minimize heat conduction from the boiling plate to the boiler wall and radiation from the boiling surface. The heat generated in the main heater would then consist mainly of radiation losses at the outer edge of the boiling plate and losses below the plate, including conduction down the molybdenum busbars. It is assumed that these heat losses are approximately the same during boiling for the same boiling plate temperatures. The heat loss calibration data are presented in Appendix A and the heat loss curve is shown in Figure E-1. The calibration was carried out with the system under vacuum to facilitate outgassing.

To obtain film boiling, the boiling plate was first heated up to approximately 1600°F under vacuum. The reservoir and charging lines were heated to approximately 250°F and the charge valve cracked to allow potassium liquid to drip slowly from the end of the fill line located $\frac{1}{2}$-inch above the boiling surface. Since the low pressure in the boiler corresponded to a saturation temperature of approximately 700°F, film boiling was obtained directly. The boiling plate temperature was continuously monitored and the power was incremented to compensate for the drop in plate temperature due to the slowly increasing potassium level. Electrical contact with the liquid level probes in the potassium reservoir was monitored with an ohmeter to detect the falling liquid level. The charge valve was closed after approximately $\frac{1}{4}$-inch of potassium had been charged to the boiler.

After film boiling was established, the system was allowed to come to steady state. The Chromel-Alumel check thermocouples throughout the system were monitored on the 12-point Brown

Electronik recorder. Since this recorder was relatively slow (one point every 15 seconds), it was left on continuously during operation. The boiling plate temperatures were checked periodically with the Speedomax recorders to determine whether steady state conditions had been achieved. Upon reaching steady state, the following data was recorded: the pressure from the mercury manometer, the amperage and voltage of the power from the rectifer to the main heater, the amperage of the power to the guard heater, and all the temperatures throughout the system. The thermocouples hooked up to the two 8-point thermocouple switches were read consecutively on the portable precision potentiometer and the check temperatures on the 12-point recorder corresponding to this time were later tabulated. The power to the main heater and guard heater were then changed and the system allowed to achieve steady state again.

The time required for the system to reach steady state after a change in the power level was approximately 30 to 60 minutes. Even after several hours of operation at the same power level, the boiling plate temperatures sometimes drifted very slowly due to changes in the line voltage of the power supply to the rectifier. This was evidenced by the fact that relatively large temperature shifts were encountered at approximately 8 a.m. and 5 p.m. The Speedomax recorders were used to insure that the boiling plate temperatures were not changing more than $1^{o}F$ during the time that the temperatures could be read on the potentiometer.

The film boiling experimental data are tabulated in Appendix B. The first run was made at a constant pressure of 2 mm Hg and the measured saturation temperature varied slightly between $714^{o}F$

and 733°F probably due to slight changes in the liquid level. The first four data points were taken while increasing the temperature of the boiling plate and the remaining while decreasing the temperature. At a temperature difference (between the boiling plate and the liquid) of approximately 207°F, the boiling plate temperatures started to decrease rapidly and natural convection was quickly obtained. Thus, 207°F is probably the lower limit of the minimum heat flux at a pressure of 2 mm Hg.

The second run was at a constant pressure of 50 mm Hg and the measured liquid temperatures were between 983°F and 986°F. Almost half of the data points were taken while increasing the temperature. At a temperature difference of approximately 351°F, the boiling plate temperatures started to decrease rapidly but film boiling was maintained by quickly raising the power level of both the main heater and the guard heater. The third run consisted of increasing the pressure in small increments from 61 mm Hg to 300 mm Hg corresponding to liquid temperatures of 1011°F to 1243°F respectively, Data at higher pressure levels could not be obtained because it was decided to keep the boiling surface below 1700°F to avoid severe corrosion of the stainless steel by the potassium.

Nucleate boiling data were also obtained and are tabulated in Appendix C. Since it was unnecessary to charge the potassium on a hot surface, these runs started with an initial liquid level of $\frac{1}{2}$ inch above the boiling surface. The charging procedure was to adjust the tip of the fill line at the $\frac{1}{2}$ inch level and empty the contents of the reservoir into the boiler, which was maintained at approximately 400°F. The boiler was

then pressurized and the excess liquid above the $\frac{1}{2}$ inch level pushed back up into the reservoir. One of the purposes of these runs was to attempt to determine the critical heat flux at very low pressure. Another reason was to check the contention of Rallis and Jawurek (38) that a pressure exists below which the nucleate boiling regime cannot exist. They obtained data for ethanol where they were able to pass from natural convection directly into film boiling without experiencing the nucleate regime. However, nucleate boiling of potassium was obtained for pressures down to 1 mm Hg and heat fluxes up to 58,700 BTU/hr-sq ft were obtained at this pressure without any indication that the critical heat flux was imminent. It was undesirable to go to very much higher fluxes because of the thermal stresses induced in the boiling plate by the large thermal gradient in the boiling plate. Nucleate boiling data were obtained at 1-2 mm Hg and 602-751 mm Hg.

During the nucleate boiling runs and for the film boiling data at the higher power levels, it was necessary to blow air through the cooling coils welded on the outside of the condenser. As the power level during film boiling was decreased, it was necessary to reduce gradually and then shut off the air to the condenser cooling coils in order to maintain the top flange of the boiler assembly above 148°F, the melting point of potassium. At the lowest power levels, the beaded Nichrome heater around the condenser had to be turned on. Through past experience in preliminary runs, it was found that all of the potassium eventually froze in the condenser leaving the boiling surface dry if the condenser was not maintained above the melting point of potassium.

In the tabulated data of Appendices A, B, and C, the temperature of one of the thermocouples is sometimes missing. During operation, this thermocouple sometimes developed an open circuit. However, when the thermocouple was working, its resistance was the same as the other Pt-Pt 13% Rh thermocouples and the sensitivity of the potentiometer when making a reading was not affected. This indicated that the circuit became interrupted by a break in only one leg of the thermocouple and that an emf when received corresponded to the emf of the hot junction rather than an intermediate point.

The experimental data above were taken using an apparatus on which refinements had been made. Preliminary data were obtained on the initial apparatus which did not include a downcomer for the liquid return from the condenser and whose guard heater on the walls of the boiling chamber had burned out during the start-up. Also, the three thermocouples at the edge of the boiling plate had not been welded on yet. These preliminary data are tabulated in Appendix D and are characterized by large radial gradients due to heat conduction from the boiling plate up the boiler walls. Reasonable data could be obtained only at relatively high temperature differences. At lower temperature differences, the boiling on the boiler walls reverted to the transition or nucleate regime and caused temperature distortions in the boiling plate such that one side of the plate was hotter than the opposite side. These distortions rendered the temperature differences in the plate meaningless. One of the thermocouples in the plate also displayed an erratic behavior by sometimes indicating an open

circuit. When an emf signal was obtained, the resistance of the thermocouple was almost 20 times that of the other thermocouples in the boiling plate and a reading on the potentiometer was obtained with difficulty because of low sensitivity. Therefore, the temperature corresponding to this thermocouple was disregarded even for those cases where it was available.

V. EXPERIMENTAL RESULTS

Introduction

Data on the film boiling of potassium were obtained for pressures between 2 mm Hg and 300 mm Hg, corresponding to liquid temperatures between 714°F and 1243°F. The data are tabulated in Appendix B and the method of treating the data is discussed in Appendix E. The results are tabulated in Table 1 and plotted in Figures 17 and 18.

The boiling curves (q/A vs ΔT) for pressures of 2 mm Hg and 50 mm Hg are shown in Figure 17. The data for pressures between 61 mm Hg and 300 mm Hg do not determine a true boiling curve because the pressure was not held constant, but they were included to show the effect of pressure beyond 50 mm Hg. There appears to be a minimum in the heat flux at a temperature difference of 400°F for the 2 mm Hg film-boiling curve. For the 50 mm Hg curve, the trend at the lower temperature differences is not as well established but it appears that the minimum flux might occur at a higher temperature difference of 460°F although it may be as low as 351°F, the temperature at which the boiling plate temperatures started to fall rapidly. The heat transfer coefficient as a function of temperature difference is shown in Figure 18.

The effect of pressure on the heat flux at various constant temperature differences is shown in Figure 19. The points

TABLE I. Film Boiling Results

q/A (BTU/hr-sq ft)	ΔT (°F)	h (BTU/hr-sq ft-°F)	PRESSURE (mm Hg)
9,000	752	12.0	2
11,400	798	14.3	2
12,900	824	15.7	2
16,000	873	18.3	2
16,800	851	19.7	2
10,800	780	13.8	2
9,900	749	13.2	2
8,400	710	11.8	2
7,000	679	10.3	2
6,500	655	9.9	2
5,100	624	8.2	2
4,600	607	7.6	2
4,700	637	7.4	2
4,200	567	7.4	2
3,300	515	6.4	2
3,300	532	6.2	2
2,800	503	5.6	2
2,800	480	5.8	2
2,400	448	5.4	2
2,400	438	5.5	2
1,900	408	4.7	2
2,300	403	5.7	2
1,600	376	4.3	2
2,300	363	6.3	2
2,700	314	8.6	2
2,600	298	8.7	2
2,600	287	9.1	2
3,000	274	11.0	2
3,000	250	12.0	2
10,400	511	20.3	50
11,200	591	18.9	50
11,900	642	18.5	50
12,000	665	18.3	50
10,800	621	17.4	50
9,300	590	15.8	50
9,600	549	17.5	50
9,000	490	18.4	50
8,900	476	18.7	50
8,800	432	20.4	50
13,900	670	20.7	50

TABLE I (continued)

q/A (BTU/hr-sq ft)	ΔT (^{o}F)	h (BTU/hr-sq ft-^{o}F)	PRESSURE (mm Hg)
11,600	646	18.0	61
12,100	658	18.4	62
12,100	642	18.8	75
11,100	633	17.5	88
11,200	622	18.0	100
11,700	607	19.3	115
12,200	592	18.9	130
12,700	579	21.9	146
11,700	560	20.9	163
11,700	546	21.4	178
12,100	515	23.5	201
12,100	489	24.7	225
13,000	464	28.0	252
13,500	447	30.2	275
13,600	428	31.8	300

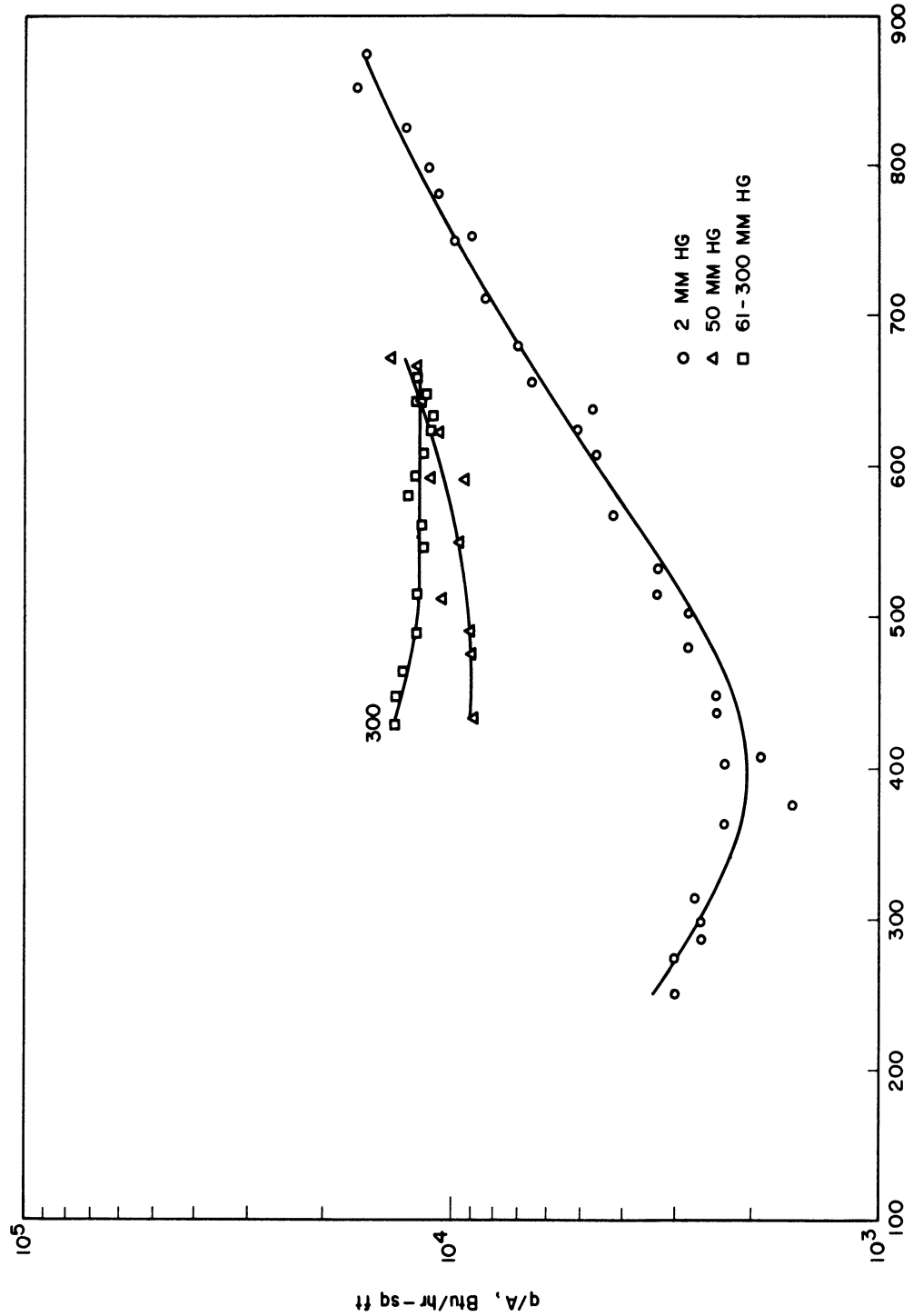

Figure 17. Heat Fluxes for Potassium in Film Boiling

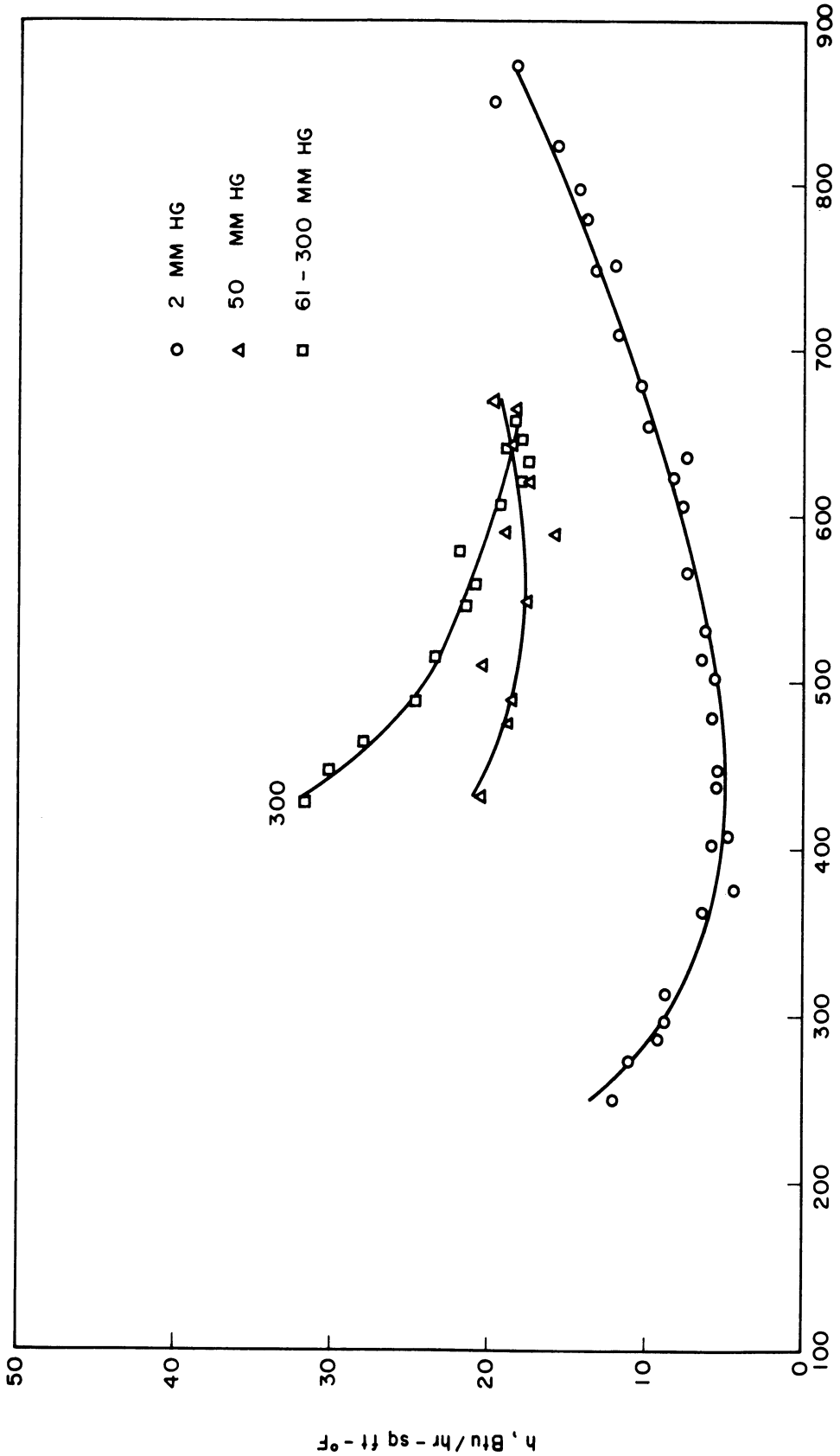

Figure 18. Heat Transfer Coefficients for Potassium in Film Boiling

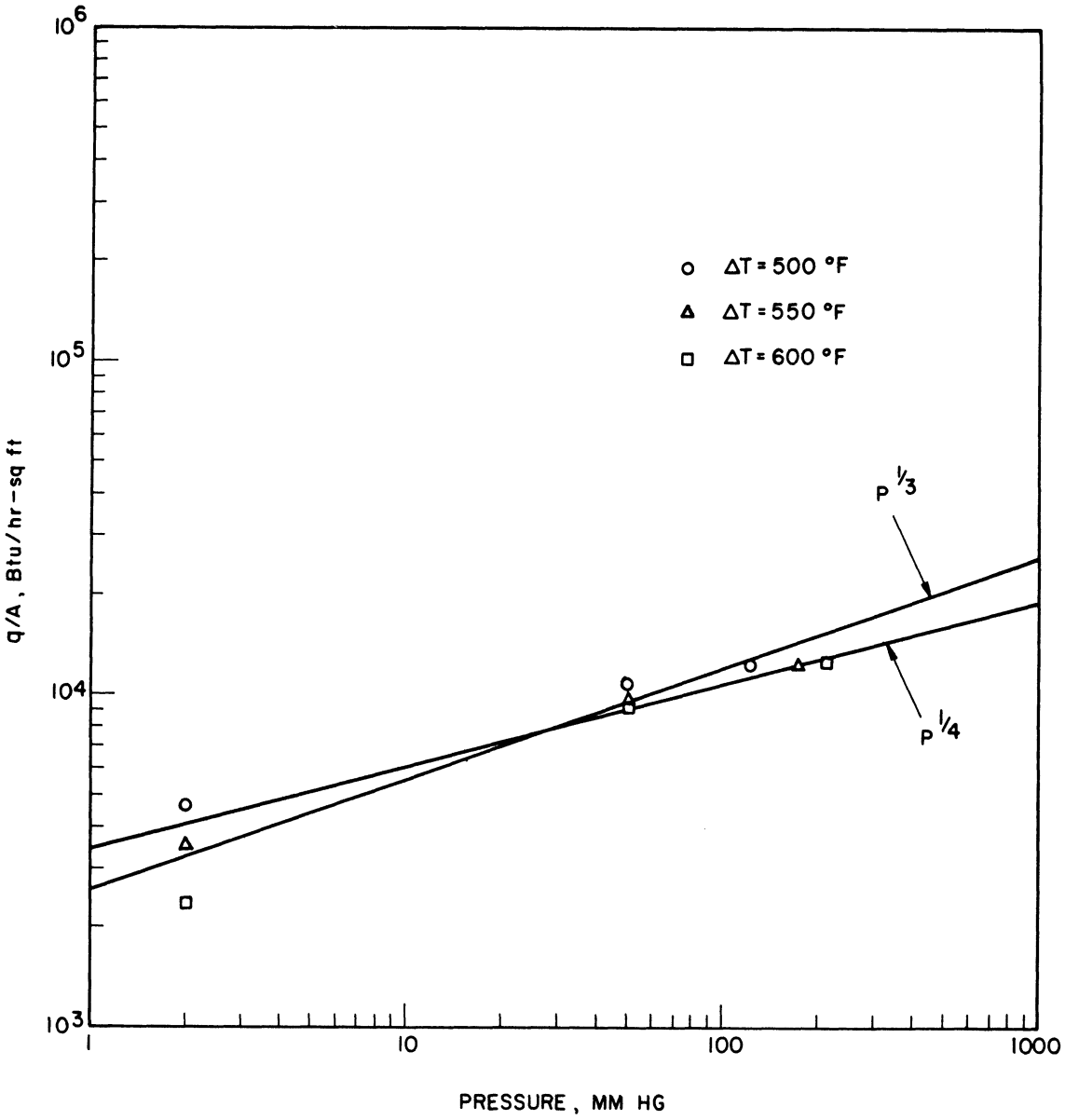

Figure 19. Effect of Pressure on the Heat Flux in Film Boiling

beyond 50 mm Hg were obtained by interpolating the results for 61-300 mm Hg. Although there are not enough points at different pressuresto accurately determine the dependency, it appears that the heat flux is proportional to the 1/4 to 1/3 power of the pressure.

In the absence of other film-boiling data for alkali metals, only a comparison with data for non-metallic fluids is possible. The results of Poppendiek et al (37) indicatethat the process for the stable film boiling of potassium droplets is the same as that for water and some organic fluids since the experimental lifetimes of the potassium droplets fell about the same amount above the predicted curve as the results for the non-metallic fluids. Hosler and Westwater (19) obtained film-boiling coefficients of 28 to 40 BTU/hr-sq ft-^{o}F for Freon-11 and water at one atm and the data of the present study at low pressure indicate that the film-boiling coefficient for potassium at one atm will be about the same order as that for water and Freon-11. Hence, additional factors which may be present in the film boiling of potassium, such as the vapor dimerization reaction and the effect of radiation, do not appear to be significant enough to increase the film boiling coefficients above the range of those for non-metallic fluids.

Nucleate boiling data were obtained for pressures of 1-2 mm Hg and 602-751 mm Hg. The results are tabulated in Table 11 and are plotted on Figure 20. Heat fluxes up to 63,000 BTU/hr-sq ft for temperature difference between 15^{o}F and 49^{o}F were obtained. There was essentially no difference between the low- and high-pressure data.

The experimental values of pressure and liquid temperature can be plotted and compared to the vapor pressure curves for potassium.

TABLE 11. Nucleate Boiling Results

Pressure (mm Hg)	q/A BTU/hr-sq ft	ΔT °F
2	7,000	14
2	4,000	2
1	47,400	32
1	47,700	29
1	26,200	20
1	58,700	33
2	5,700	10
2	13,900	17
2	20,600	17
2	25,600	19
2	32,500	25
2	40,000	28
2	47,200	28
709	18,000	20
659	23,200	24
684	29,200	26
704	36,000	30
728	46,600	37
707	36,900	35
721	46,600	38
736	53,700	49
751	63,600	44
730	46,600	44
717	41,200	39
724	32,900	31
723	26,000	24
708	21,000	20
640	13,400	15
602	9,600	31
680	17,400	19
707	21,900	24
700	28,300	32

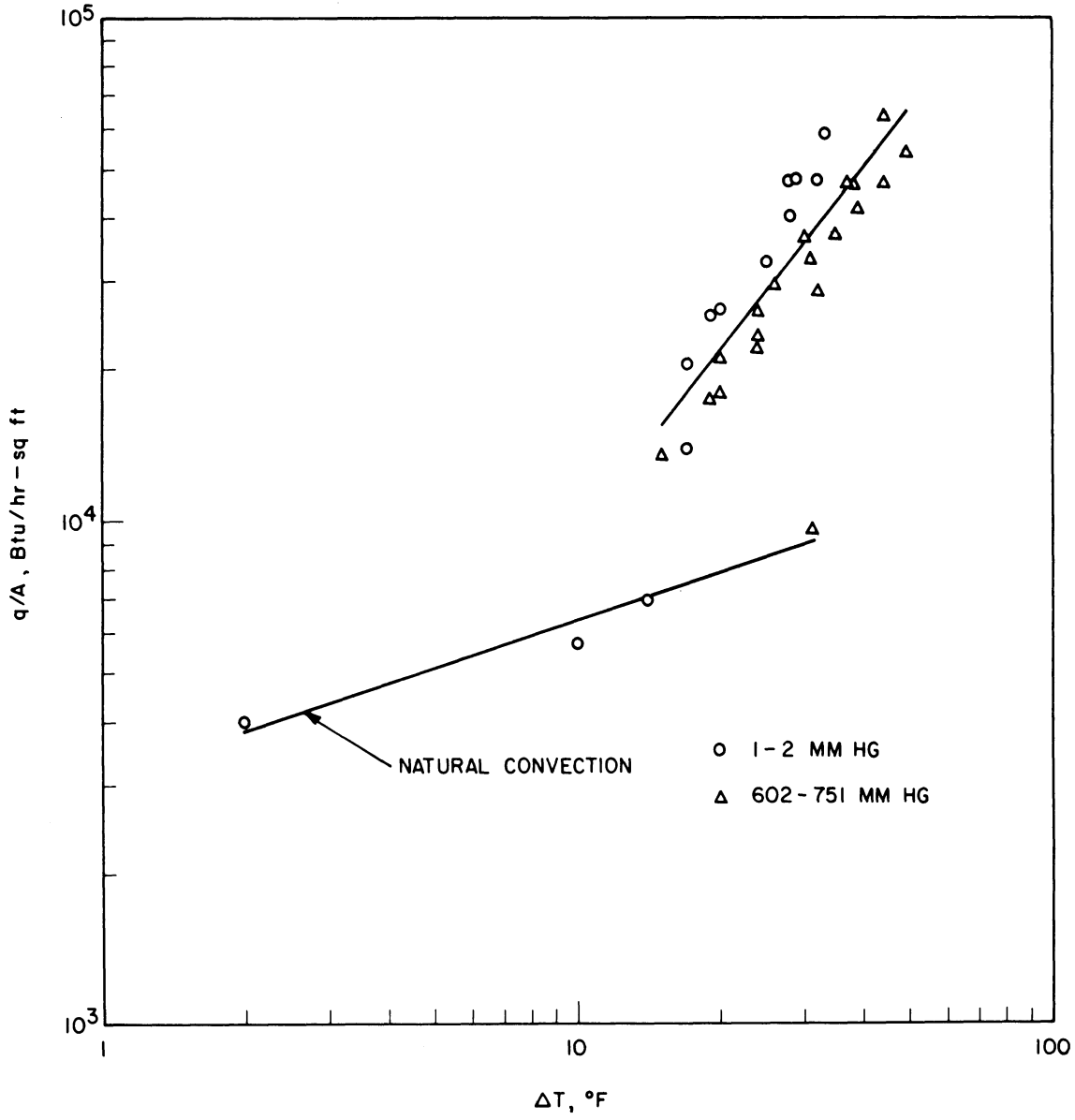

Figure 20. Heat Fluxes for Potassium in Nucleate Boiling

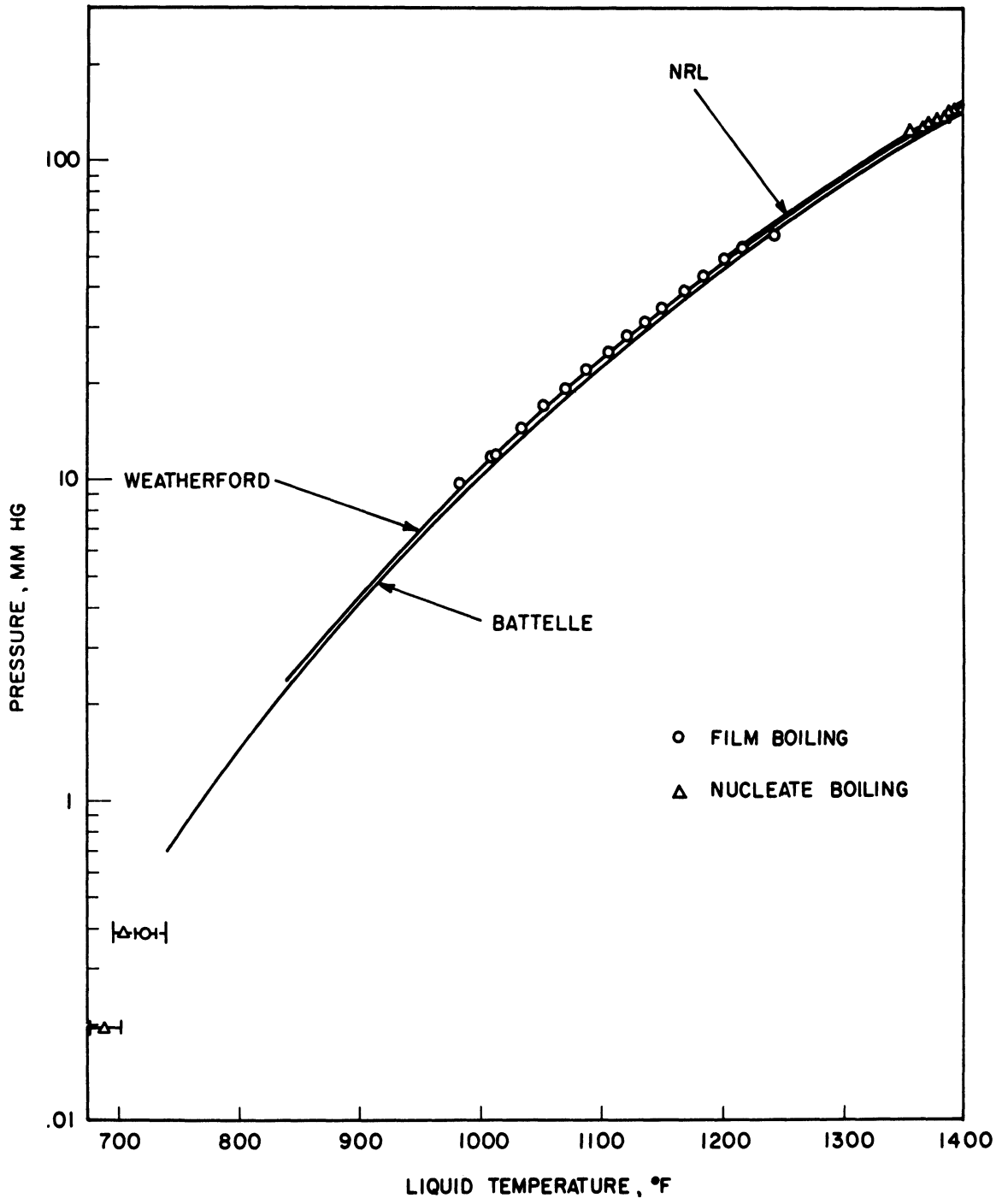

Figure 21. Vapor Pressure of Potassium

Figure 21 shows the data obtained in this study along with the curves from Weatherford (42), the Battelle Memorial Institute (24), and the Naval Research Laboratory (13). The data compares favorably with the curves indicating that saturated conditions prevailed during boiling.

VI. DISCUSSION OF RESULTS

1. Comparison of Experimental Results with Theoretical Predictions

The heat transfer coefficients for the film boiling of potassium at 2 mm Hg and 50 mm Hg are plotted in Figure 22 along with the theoretical predictions of Berenson (4) at 0.1 and 1 atm, and of Frederking (15) at 0.1 atm. The basis for the physical properties of potassium used in evaluating the correlations is discussed in Appendix F. The experimental results uncorrected for radiation and other effects which might increase the heat transfer above that due to conduction and convection are about twice the predicted values. It is interesting to note that at 0.1 atm Frederking's prediction for spheres which assumes a turbulent, free convection process is very close to that of Berenson for horizontal surfaces which assumes that heat is transferred across the vapor film by pure conduction alone. From the predicted curves at 0.1 and 1 atm, the predicted effect of pressure on the heat transfer coefficient, and thus the heat flux, can be determined. The ratio of the heat transfer coefficient at 0.1 atm to that at 1.0 atm is relatively constant at 0.57. Using this value, the heat transfer coefficient is found to be proportional to the .244, or approximately 1/4, power of pressure. Hence, the heat flux is proportional to the 1/4 power of pressure for constant temperature difference. This agrees qualitatively with what was found experimentally. In Figure 19, the heat flux was found to be approximately proportional to the 1/4 to 1/3 power of pressure.

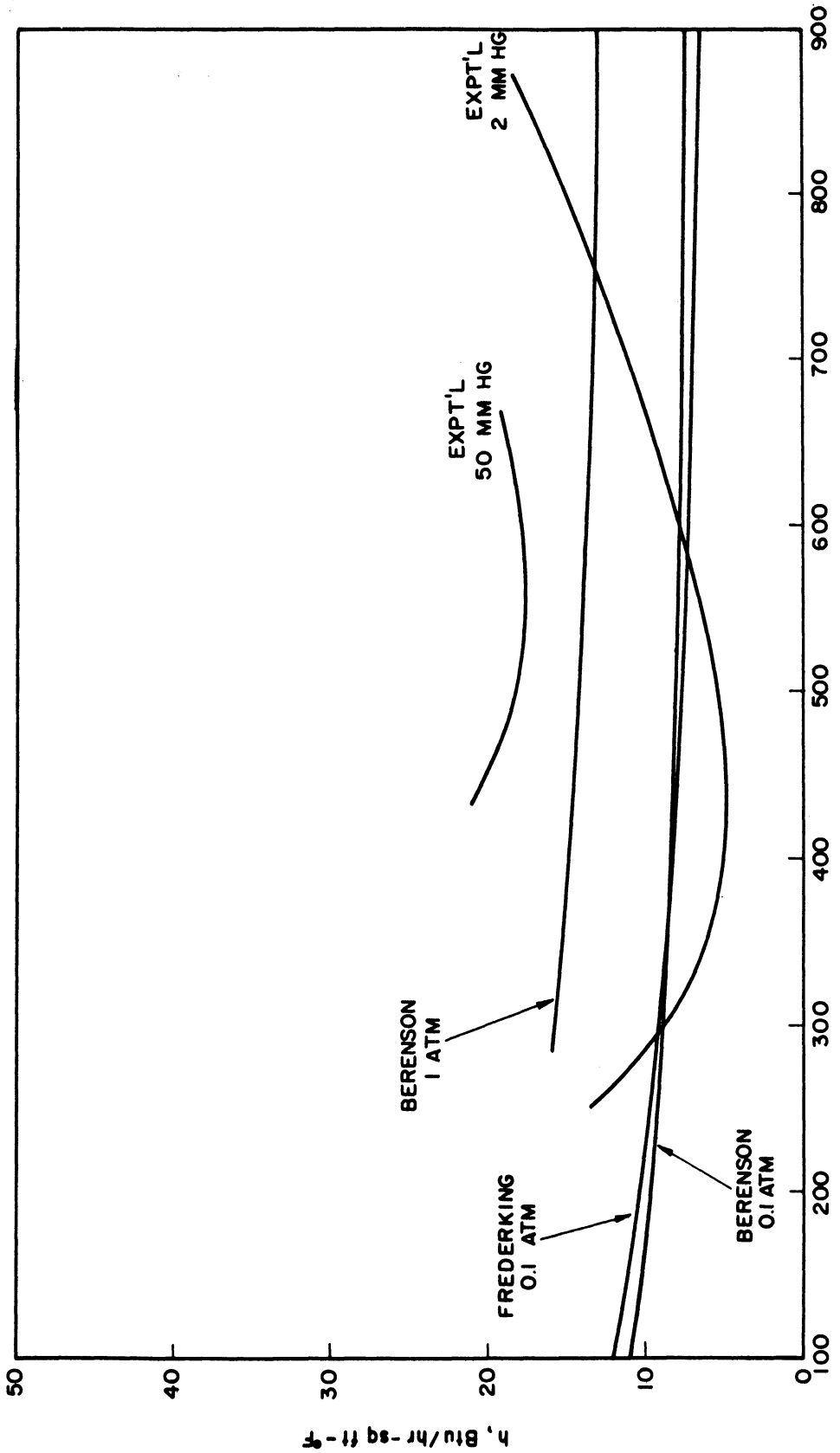

Figure 22. Comparison of Film Boiling Coefficients with Correlations

The heat fluxes obtained experimentally at the minimum are substantially above the predictions of Berenson and Zuber. The comparisons are summarized in Table III. It is seen that Berenson's equation for predicting the temperature difference at the minimum gives abnormally low values of $2^{o}F$ and $36^{o}F$ for film boiling at 2 mm Hg and 0.1 atm, respectively. An estimate of the minimum heat flux at one atm can be obtained by extrapolating to 760 mm Hg in Figure 19. This estimate is three times higher than Berenson's prediction but is not far from the upper limit of the range predicted by Zuber.

2. Effect of Radiation

At the high surface temperatures required for the film boiling of potassium, the radiative contribution to the heat flux can be significant. The heat transfer due to radiation can be estimated by assuming parallel plate geometry. The results are quite sensitive to values of the emissivities used in the calculations. Experimental data for the emissivity of the stainless steel boiling surface were taken from the Handbook of Thermophysical Properties of Solid Materials (17). The emissivity varied from .15 at $970^{o}F$ to .58 at $1780^{o}F$. However, the emissivity of the liquid potassium surface was calculated using an equation suggested by Jakob (21) based on the electrical resistivity.

$$\epsilon_o = 0.576 \sqrt{r_e T} + 0.124 r_e T \qquad (18)$$

The normal emissivity ϵ_o is easily converted to the total emissivity by means of a table presented by Jakob. Using Equation (18),

TABLE III

Comparison of Minimum Heat Fluxes
with Theoretical Predictions

	Minimum Heat Flux BTU/hr-sq ft	ΔT at Minimum Flux °F
Experimental (2 mm Hg)	2,000	400
Berenson (2 mm Hg)	200	2
Zuber (2 mm Hg)	222-518	
Experimental (50 mm Hg)	9,000	460
Berenson (0.1 atm)	513	36
Zuber (0.1 atm)	660-1,540	
Estimated from Figure 19 (1 atm)	15,000	
Berenson (1 atm)	4,810	287
Zuber (1 atm)	5,350-12,500	

the theoretical prediction for the emissivity of a molten copper surface agrees with the experimental value given by Jakob within 10%. Using experimental data for the electrical resistivity of potassium obtained by the Battelle Memorial Institute (24), emissivities of 0.11 and 0.14 were calculated for film boiling at 2 mm Hg and 50 mm Hg respectively. The heat transfer due to radiation using the calculated potassium emissivities and assuming parallel plate geometry is shown in Figure 23. Since the emissivity of the potassium liquid is so low, the calculations are very sensitive to increases in its value. It is seen that doubling the potassium emissivity essentially doubles the heat flux due to radiation. The calculations were also done for an emissivity of 0.30 since this number is within the realm of possibility. Jakob notes an experimental emissivity of 0.31 for a molten iron surface.

The experimental values for the heat transfer coefficients in film boiling can be corrected for the effect of radiation by subtracting the radiative contribution corresponding to the heat fluxes in Figure 23. The results are shown in Figure 24 and comparison of the corrected curve for 50 mm Hg with Berenson's prediction for 0.1 atm shows that the predicted values are still about 40% lower than the experimental values. However, a higher potassium emissivity of 0.30 brings the corrected experimental curve to within 11% of the predicted curve. Thus, the effect of radiation is seen to be very significant but an accurate quantitative measure of this effect is limited by uncertainties in the emissivity of potassium liquid. It is possible that radiation alone can account for the difference between the experimental and

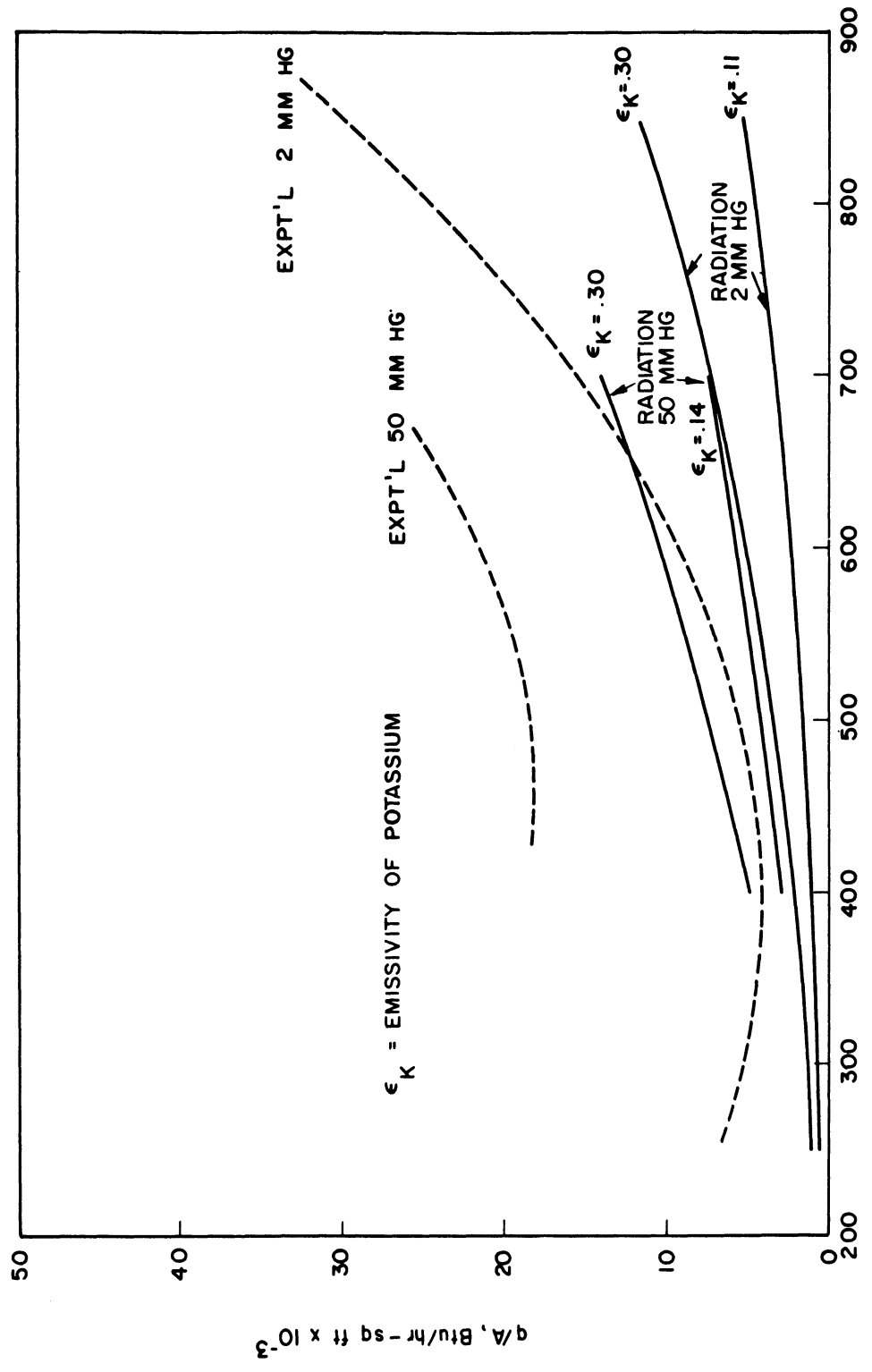

Figure 23. Heat Transfer Due to Radiation

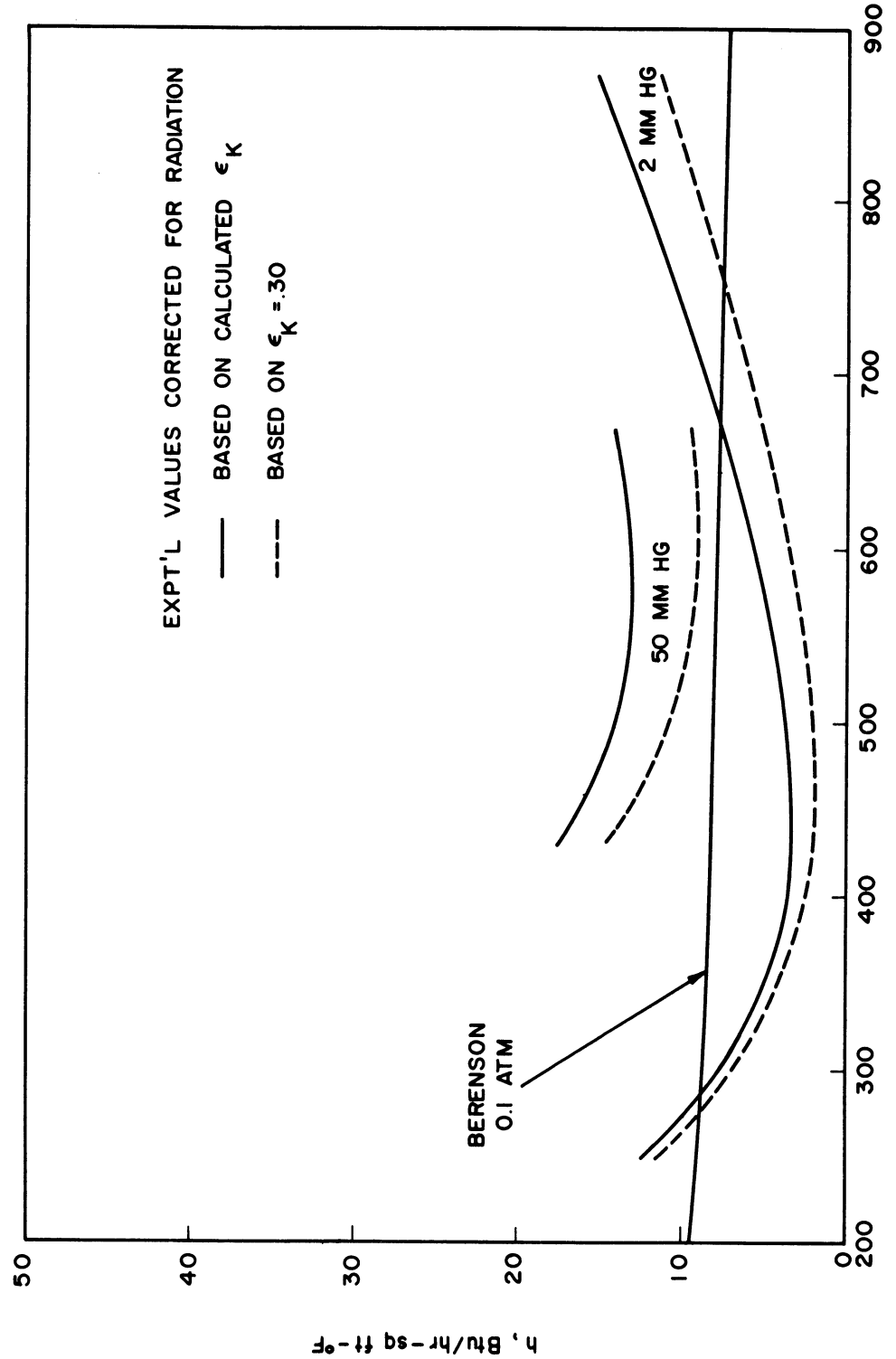

Figure 24. Correction of Film Boiling Heat Transfer Coefficients for Radiation

predicted values of the heat transfer coefficients in film boiling.

3. Effect of Vapor-phase Dimerization Reaction

A process which could add to the heat transfer is a chemical reaction in the vapor between the solid heating surface and the boiling liquid. To illustrate the process involved, consider a gas which undergoes an endothermic dissociation reaction being heated by a solid surface. The molecules near the wall are heated and they dissociate, absorbing the energy associated with the endothermic heat of reaction. A concentration gradient in the gas is established and the products of the dissociation reaction diffuse away from the wall. As they enter regions of lower temperature, the molecules begin to associate thereby releasing the heat of reaction to the new surroundings. Hence, heat is transferred by molecular diffusion in addition to the normal modes of conduction, convection, and radiation. This diffusional mechanism may be significant depending on the temperature level and the kinetics of the reaction.

The only type of reaction which has been treated extensively in the literature has been the "equilibrium" reaction in which the reaction rate is so high that the fluid may be assumed to have its equilibrium composition instantaneously after a change in temperature. A chemically reacting gas that has a temperature gradient across it, and whose local chemical composition can be described by the condition of local chemical equilibrium, can be considered as a non-perfect gas with temperature-dependent anomalies in its specific heat and transport properties. Use of the

equilibrium theory corresponds to predicting the maximum effect of the chemical reaction on heat transfer.

Potassium vapor undergoes the dimerization reaction $K_2 = 2K$ in the vapor phase and the method of calculating the effect of this reaction is presented in Appendix G. In Figure 25, the effect of the dimerization reaction has been subtracted from the radiation-corrected experimental curve for 50 mm Hg. It is seen that the contribution from the reaction is relatively small, being a maximum of 10% at the lower temperature differences and decreasing as the vapor is superheated. Since the effect decreases with pressure, the experimental results for 2 mm Hg would not be expected to be significantly influenced.

4. Evaluation of Film-boiling Correlations

The ultimate value of any correlation is determined by its ability to predict reliably film-boiling behavior regardless of whether it is applied in a range where some of the assumptions used in its derivation are known to be invalid. The results of the analyses of Zuber (44), Chang (8), and Berenson (4) for film boiling on a horizontal surface were presented in the Literature Review. Zuber predicts only the heat flux at the minimum. Chang obtained a relationship for the heat transfer coefficient as a function of temperature difference. Berenson derived an expression for the minimum heat flux identical in form to that of Zuber, and also predicted a relationship between the heat transfer coefficient and temperature difference. By dividing the two, he obtained an expression for predicting the temperature difference at which the minimum heat flux occurs. Berenson's

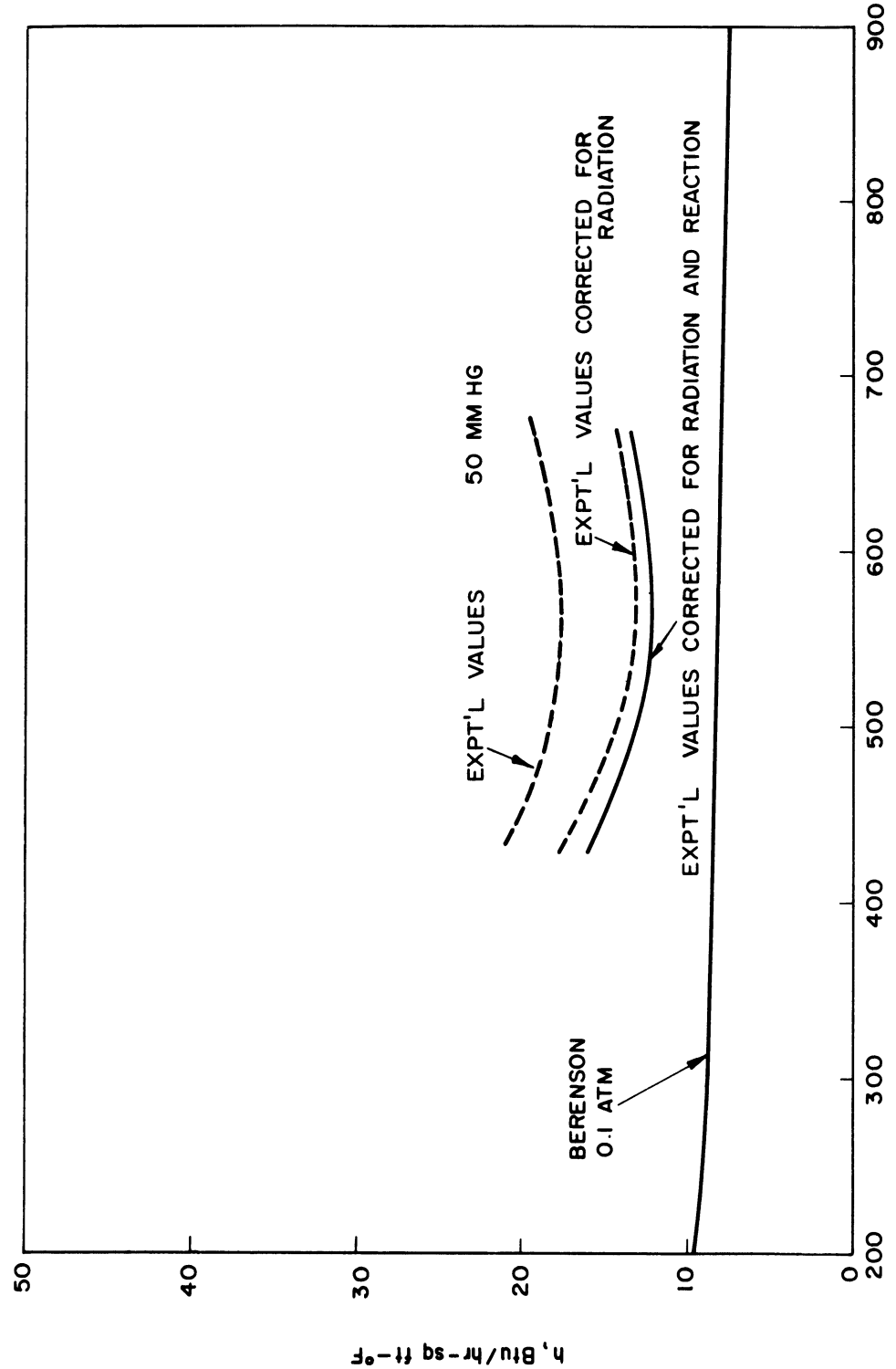

Figure 25. Correction of Film Boiling Heat Transfer Coefficients for Vapor Dimerization Reaction

correlation for the heat transfer coefficient is theoretically correct only near the minimum heat flux because he showed that the bubble spacing is unaffected by the vapor velocity and vapor film thickness only in the neighborhood of the minimum. Also, Berenson used his experimental results at the minimum to evaluate the constants in his expressions for the minimum heat flux and the heat transfer coefficient. Therefore, Berenson's equations agree well with his data for n-pentane and carbon tetrachloride at the minimum but not at higher temperature differences. However, the data of Hosler and Westwater (19) for film boiling of water and Freon-11 agrees with Berenson's correlation at the higher temperature differences but his predictions for the minimum heat flux were found to be seriously in error. The data for mercury do not seem to apply to any of the present correlations in that the heat transfer coefficients are about an order of magnitude higher than predicted at the lower temperature differences. Hosler and Westwater obtained heat transfer coefficients which were essentially constant with temperature difference whereas the results of Berenson and the present study yield coefficients which increase rapidly as a function of temperature difference.

In spite of the difference in flow characteristics, film boiling from horizontal tubes, vertical surfaces, spheres, and horizontal flat surfaces are described by equations of the same form providing the proper characteristic length is used:

$$Nu = a(Ra')^b = a(Gr' Pr)^b \tag{19}$$

where Ra' and Gr' are modified Rayleigh and Grashof numbers, respectively. Some of the correlations are presented in Table IV.

For film boiling on a horizontal flat surface, Equation (19) can be written in the form:

$$h = a\left[\frac{k_v^{\left(\frac{1}{b}-1\right)} \rho_v(\rho_l-\rho_v)g\, L'^{\left(\frac{1}{b}-3\right)}}{\mu_v\, \Delta T\, D_b}\right]^b \tag{20}$$

From the observed pressure effect in Figure 19 and noting the correlations in Table IV, it would seem appropriate to assume a value of 1/3 or 1/4 for b. If b is 1/3, then there is no effect of the characteristic length, which does not seem reasonable. Therefore, let b be equal to 1/4. Then the coefficient a is given by

$$a = h\left[\frac{\mu_v\, \Delta T\, D_b}{k_v^3 \rho_v(\rho_l-\rho_v)g\, L'}\right]^{1/4} \tag{21}$$

Values of the coefficient, a, can now be calculated from experimental data and plotted against some significant parameter to see whether it is actually a constant or whether any trends exist. Bromley (7) carried out a detailed analysis and concluded that if experimental values of the coefficient are plotted against

TABLE IV

FILM BOILING CORRELATIONS

Author	Geometry	Equation	Characteristic Length
Berenson	Horizontal flat surface	$Nu = 0.63(Ra')^{1/4}$	Bubble diameter
Bromley	Horizontal tube	$Nu = 0.62(Ra')^{1/4}$	Tube diameter
Bromley	Vertical tube or plate	$Nu = 0.62(Ra')^{1/4}$	Distance along tube or plate
Chang	Horizontal flat surface	$Nu = 0.43(Ra')^{1/3}$	Unspecified
Chang	Vertical surface	$Nu = 0.72(Ra')^{1/4}$	Distance along surface
Ellion	Vertical surface	$Nu = 0.72(Ra')^{1/4}$	Distance along surface
Frederking	Sphere	$Nu = 0.14(Ra')^{1/3}$	Sphere diameter
Hsu	Vertical surface	$Nu = 0.943(Ra')^{1/4}$	Height of critical thickness

the group $\frac{\Delta T\ C_p}{L'\ Pr}$, the effect of the various assumptions in the analysis should be shown. In Figure 26, the experimental data of Berenson for n-pentane and carbon tetrachloride, that of Hosler and Westwater for water and Freon-11, that of Merte for mercury and that of the present study for potassium were used to calculate values of the coefficient a, which were then plotted against the parameter $\frac{\Delta T C_p}{L' Pr}$. The characteristic length used in the calculations was the bubble diameter as determined experimentally by Hosler and Westwater (73% of the most dangerous wavelength) rather than Berenson's prediction of 75% of the critical wavelength. The mercury data of Bonilla was not included since his results were inconsistent and incompatible with other data, showing an increase in the heat flux for a decrease in pressure and exhibiting abnormally high temperature differences in nucleate boiling. Instead of including all of the experimental points, only the values corresponding to the minimum heat flux and the highest temperature difference obtained experimentally were calculated but flags were used to indicate the limits of the coefficient due to scatter in the experimental data. The values for potassium correspond to the experimental results which have been corrected for radiation and the effect of the dimerization reaction. The results of Figure 26 are summarized in Table V for discussion purposes.

From Figure 26 and Table V, the following conclusions can be drawn:

a. The data for mercury at the minimum heat flux do not conform to the rest of the experimental data.

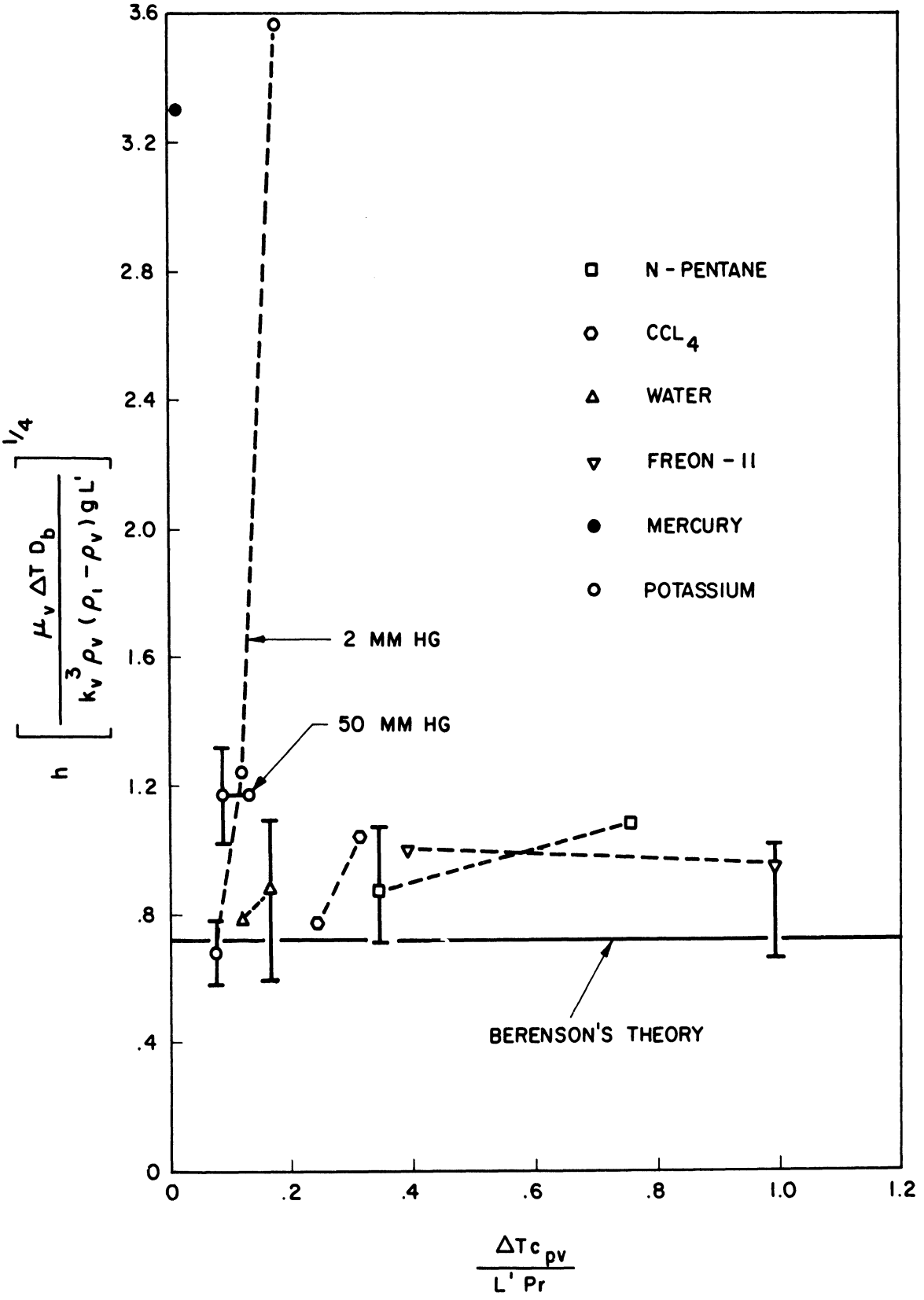

Figure 26. Correlation of Film Boiling Data for Horizontal Surfaces

TABLE V

Comparison of Experimental Film Boiling Data

		Coefficient a (Equation 21)		Deviation from Berenson's Coefficient .72	
Fluid	ΔT range	Minimum heat flux	Highest ΔT	Minimum heat flux	Highest ΔT
n-pentane	155°F	.87	1.08	21%	50%
CCl_4	52°F	.76	1.04	6%	44%
water	115°F	.79	.87	10%	21%
Freon-11	300°F	1.00	.95	39%	32%
Hg(1 atm)		6.11		749%	
Hg(80 psia)		3.33		362%	
K(50 mm Hg)	210°F	1.17	1.17	62%	62%
K(2 mm Hg)	473°F	.68	3.46	-6%	381%
K(2 mm Hg)	200°F	.68	1.22	-6%	69%

Clearly, the correlation does not correspond to the physical process taking place.

b. With the exception of Freon-11, the value of the coefficient increases with increasing temperature difference. This means that the experimental heat transfer coefficients are increasing with temperature difference more rapidly than can be accounted for by the assumed value of 1/4 for the power b in the equation $Nu = a(Ra')^b$.

c. The experimental results for potassium at high temperature differences give coefficients about four times higher than the rest of the data. However, the experimental results for n-pentane and carbon tetrachloride show that the heat transfer coefficients are increasing at such a rate that if data had been obtained at higher temperature differences, large values for the calculated coefficient in Figure 26 would also have been obtained. Figure 27 shows the heat transfer coefficients as a function of temperature difference for potassium, n-pentane, and carbon tetrachloride. The heat transfer coefficients for the two organic fluids are increasing more rapidly at moderate temperature differences than those of potassium at high temperature differences.

d. If the data for potassium is limited to a moderate range of temperature differences (last entry in Table V.) reasonable agreement is obtained with the other non-metallic data. Essentially all of the data are above the value of the coefficient assumed by Berenson although

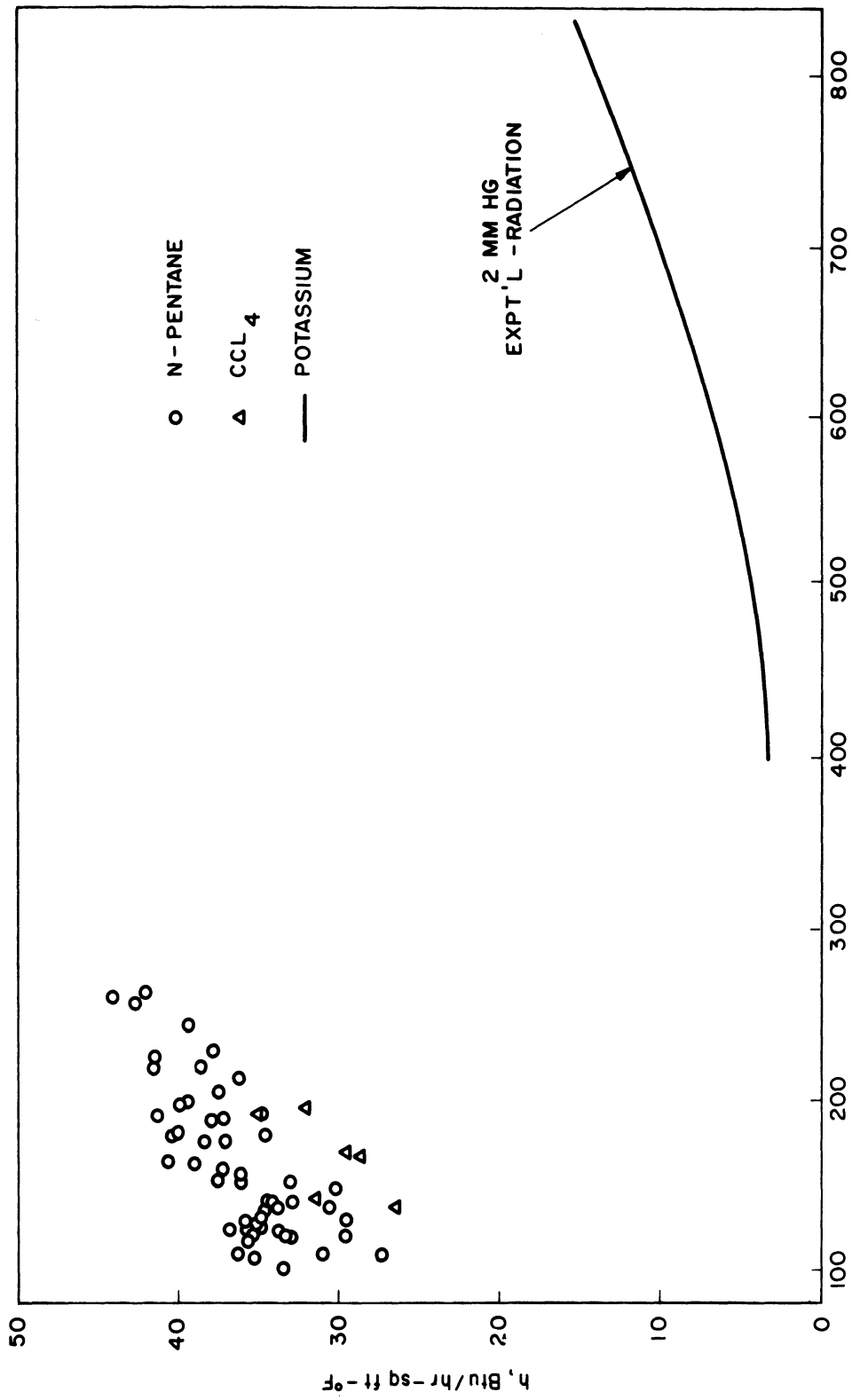

Figure 27. Rapidly Increasing Film Boiling Heat Transfer Coefficients

the flags showing the estimated scatter of the data indicate that some points will fall below Berenson's coefficient. The reason why Berenson's coefficient is below his points for n-pentane and carbon tetrachloride at the minimum is that the value assumed gave reasonable agreement with the data and also was within the theoretical limits set by his theory. Consideration of all of the non-metallic data gives an average value for the coefficient of 0.92 instead of Berenson's value of 0.72. Including the potassium data for a moderate range of temperature differences gives only a slightly higher coefficient of 0.97 since the potassium results bracket the non-metallic data. Therefore, the equation for the heat transfer coefficient which gives the best fit to all the experimental data is:

$$h = 0.97 \left[\frac{k_v^3 \rho_v (\rho_l - \rho_v) g \, L'}{\mu_v \, \Delta T \, D_b} \right]^{1/4} \tag{22}$$

$$D_b = 4.7 \sqrt{\frac{3 g_c \sigma}{g(\rho_l - \rho_v)}} \tag{23}$$

Equation (22) predicts the heat transfer coefficient up to moderate temperature differences ($\sim$200^{o}F) from the minimum flux but does not account for rapidly increasing coefficients at high temperature differences exhibited by some of the experimental data.

In Table III, it was shown that the minimum heat fluxes obtained for boiling of potassium at 2 mm Hg and 50 mm Hg were an order of magnitude higher than Berenson's and Zuber's predictions. The equation for the minimum heat flux is:

$$(q/A)_{min} = a' \rho_v L' \left[\frac{g(\rho_l-\rho_v)}{(\rho_l+\rho_v)}\right]^{1/2} \left[\frac{g_c\sigma}{g(\rho_l-\rho_v)}\right]^{1/4} \qquad (24)$$

The value of the coefficient a' assumed by Berenson was 0.09 and was evaluated from his experimental data at the minimum. Zuber predicts a range of values for a' of 0.10 to 0.233 because of uncertainties in the assumptions used in the analysis. The coefficient a' is given by:

$$a' = \frac{(q/A)_{min}}{\rho_v L'} \left[\frac{(\rho_l+\rho_v)}{g(\rho_l-\rho_v)}\right]^{1/2} \left[\frac{g(\rho_l-\rho_v)}{g_c\sigma}\right]^{1/4} \qquad (25)$$

Similar to the treatment of the relationship for the heat transfer coefficient, experimental data for various fluids on horizontal surfaces can be used to calculate the coefficient a' to see whether it is truly a constant. The results are summarized in Table VI. The potassium values used for 2 mm Hg and 50 mm Hg were corrected for radiation and vapor dimerization reaction. The minimum heat flux for potassium at one atm was estimated by Figure 19, giving $(q/A)_{min}$ = 15,000 BTU/hr-sq ft.

From Table VI it is apparent that the minimum heat flux data for potassium at low pressures does not agree with the rest of the data. It is also seen that Berenson's value of 0.09 for

TABLE VI

Comparison of Minimum Heat Flux Data

Fluid	Coefficient a' (Equation 24)
n-pentane	.134
CCl_4	.091
water	.189
Freon-11	.167
Mercury (Merte)	.119
Potassium (2 mm Hg)	6.74
Potassium (50 mm Hg)	1.16
Potassium (est., 1 atm)	.285

the coefficient is much too low for the average of all the experimental data presented. The average value for the coefficient for water, organics, and mercury is 0.140, which is more than 50% above Berenson's value but well within the theoretical range predicted by Zuber. Including the estimated value for potassium at one atm raises the average value to 0.164. However, the estimated minimum does not include corrections for the effects of radiation and vapor dimerization reaction, which would probably bring the calculated value for the coefficient down close to 0.2. Hence, it is concluded that the equation for the minimum heat flux is best represented by:

$$(q/A)_{min} = 0.14\ \rho_v L' \left[\frac{g(\rho_l-\rho_v)}{\rho_l+\rho_v}\right]^{1/2} \left[\frac{g_c\sigma}{g(\rho_l-\rho_v)}\right]^{1/4} \qquad (26)$$

It is felt that this equation is not valid at low pressures, although more data is needed to substantiate this contention.

Berenson obtained an expression for the temperature difference at the minimum merely by dividing his equation for the minimum heat flux by his expression for the heat transfer coefficient. In Table III, it was shown that this method predicts unreasonably low minimum temperature differences of $2^{o}F$ and $36^{o}F$ for potassium at 2 mm Hg and 0.1 atm, respectively. Although this approach can be followed using the modified equations, it is felt that very large errors might result. The scatter in the experimental data produces an already large uncertainty in the expressions for the minimum heat flux and the heat transfer coefficient and dividing one by the other may compound the uncertainty. However, it is the only available method for estimating the location of the

minimum heat flux and thus it may have to be used to see whether a reasonable value is obtained.

In the comparisons between experimental data and correlations, deviations might occur due merely to the uncertainties in determining the physical properties of the various fluids. The properties for n-pentane and carbon tetrachloride were taken from Berenson's report, those for Freon-11 were given by Hosler and Westwater in their paper, and those for water were taken from McAdams (30). The properties for mercury were taken from Weatherford (42). The properties of potassium were obtained from Weatherford, the Naval Research Laboratory Report 6233, the Battelle Memorial Institute Report 4673 and Coe (9). Values for the liquid and vapor densities, latent heat of vaporization, and specific heat were taken from Battelle. The density and latent heat values given by NRL were for a higher pressure than what was needed but agreed well with the Battelle values, thus providing an independent check. The surface tension was taken from Coe. The vapor thermal conductivity, and vapor viscosity were taken from Weatherford and it is these properties about which there is much uncertainty. The viscosity of potassium vapor was calculated theoretically and then used along with calculated values of the specific heat to determine the vapor thermal conductivity assuming a constant Prandtl number of 0.73. There is no experimental evidence to substantiate these calculated values although work is currently in progress at MSA Research Corporation (vapor thermal conductivity) Aerojet-General Nucleonics (vapor thermal conductivity and viscosity) and The University of Michigan (vapor thermal conductivity). Previous experimental work had been carried out by Battelle but the contract

was terminated before results could be obtained. The apparatus for determining thermal conductivity gave values for nitrogen which agreed well with published values, thereby providing a check on the soundness of the experimental technique. However, anomalous results were obtained for potassium vapor which could not be rectified within the time allowed for the experimental work. On the other hand, no extensive proof exists for the soundness of the technique and apparatus for determining the vapor viscosity but the difficulties were believed to be largely mechanical ones. Hence, the conformity of potassium and other alkali metals to the film boiling correlations cannot be more accurately determined without precise values for the transport properties of their vapors.

A by-product of the calculations to determine whether potassium film boiling agrees with correlations proven for non-metallic fluids is the estimation of the bubble diameter. Using equation (23), which predicts values for the bubble diameter approximately 80% higher than Berenson's equation, the bubble diameter for potassium in film boiling is found to be of the order of one inch. For the boiling surface used, this corresponds to only three bubble diameters and hence there may be an edge effect due to using too small a vessel. Consequently, the results for potassium may have to be verified by film-boiling experiments on a large vessel.

5. Effect of Radial Gradients in the Boiling Plate

In the present experimental system, the heat flux at the boiling surface must be calculated by measuring the temperature at several points in the boiling plate using thermocouples. The temperature measurements are then used with the known distance

between thermocouples and the thermal conductivity to establish the heat flux across the plate. This heat flux is equal to the flux at the boiling surface only if there are no radial gradients. The boiling plate is connected to a tube which serves as the containment vessel for the boiling liquid. The flux lines in the boiling plate depend on the relative resistances to heat flow of the boiling surface and conduction up the tube wall. If the boiling coefficient is very low, as in film boiling, then conduction up the tube wall can severely distort the flux lines in the plate. Because of this radial heat flow, the temperature gradient in the plate is no longer an accurate measure of the flux occurring at the boiling surface. The relationship between the boiling surface flux and the flux calculated by measuring the temperature gradient in the plate in the presence of radial gradients requires a knowledge of the entire temperature field in the boiling plate.

In order to assess the effect of radial gradients, a computer simulation of the boiling plate was carried out. Figure 28 is a diagram of the boiling plate and the model used for the analysis. Finite difference techniques were applied to Laplace's equation in cylindrical coordinates assuming polar symmetry and the resulting system of equations were then solved on the IBM 7090 digital computer.

In the preliminary film boiling runs where the guard heater on the boiler wall was inoperative and thus there was no effective way of limiting the heat flow from the boiling plate up the boiler wall, the computer simulation indicated that the isotherms in the boiling plate were severely distorted and that temperature measurements in the plate could not be used reliably to calculate the heat flux at

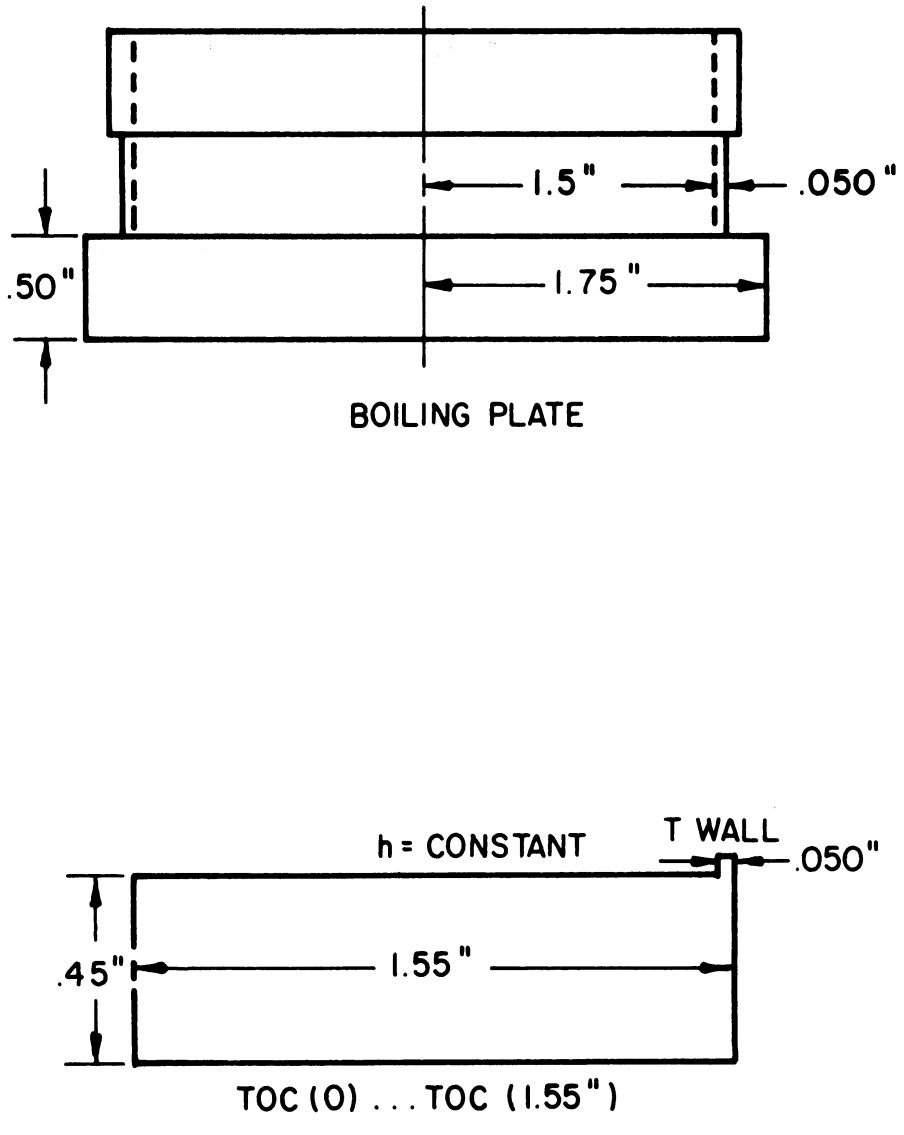

Figure 28. Model for Computer Simulation of Boiling Plate

the boiling surface. Thermocouple measurements indicated that the radial gradient from the center of the boiling surface to the boiler wall was in the order of 100°F. When the guard heater on the boiler wall was replaced, it was possible to adjust this heater during operation so that the temperature at the outer edge of the boiling plate was within a few degrees of the temperature in the interior of the plate.

The analysis is complicated by the fact that the heat loss calibration and the film boiling data indicate the existence of two isolated cold spots at the outer edge of the boiling plate above the location of the busbars to the graphite heater. However, the calibration data also show that the interior of the boiling plate, at least out to a radius of 1/2-inch from the center, is not affected by this heat drain. The effect during film boiling would be expected to be less severe, since the heat flow would smooth out the isotherms in the region above the busbars.

Although the heat drain down the busbars negates the assumption of polar symmetry, the computer simulation can be carried out in two parts. If the simulation is carried out considering the temperatures along the diameter perpendicular to the line connecting the two busbars as representative of the entire boiling plate, then the calculated isotherms in the boiling plate, shown in Figure 29, are essentially horizontal and the error involved in using the temperatures at the 1/2-inch radius corresponding to the thermocouple locations to calculate the heat flux would be negligible. However, if the simulation is carried out considering the temperatures along the diameter connecting the two busbars as representative of the entire boiling plate, then the calculated isotherms are more

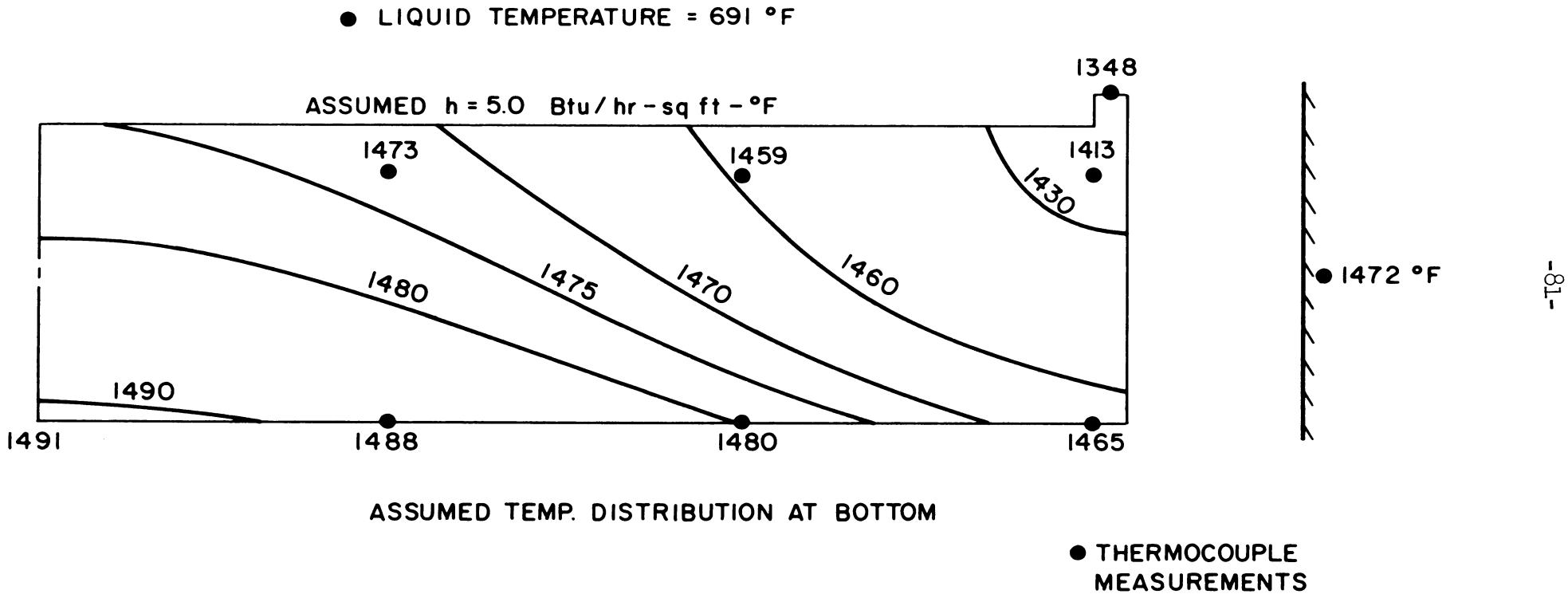

Figure 29. Temperature Distribution in Boiling Plate Obtained by Computer Simulation

severely distorted, as shown in Figure 30. Figure 30 predicts the maximum effect of the busbars since it assumes that the heat drain is occurring over the entire outer edge in an annular ring rather than at two isolated spots. The experimental temperature measurement at the 1/2-inch radius just below the boiling surface indicates that the distortion of the isotherms is much less severe than is shown in Figure 30. Comparison of Figures 29 and 30 indicates that the temperature distribution along the boiling surface more nearly corresponds to Figure 29 than Figure 30.

The experimental situation corresponding to Figures 29 and 30 is for film boiling near the lowest fluxes encountered and would tend to aggravate the distortion of isotherms in the boiling plate rather than to help smooth out the isotherms. The results of the computer simulation cannot be used to obtain corrections for the experimental measurements but they can indicate whether these corrections would be significant or negligible. The maximum distortion of the isotherms as shown in Figure 30 would predict an error of 12% if the 1/2-inch radius temperatures at the thermocouple locations are used to calculate the heat flux. However, the experimental temperature measurements indicate the temperature is more nearly uniform along the boiling surface. Since the maximum error is much less than the scatter in the data, it is reasonable to assume that the thermocouples at the 1/2-inch radius in the boiling plate can be used to calculate the heat flux with negligible error due to radial gradients.

6. Accuracy of Heat Flux Calculations

The uncertainty in the experimental results lies mainly in the heat flux. The temperature difference between the boiling

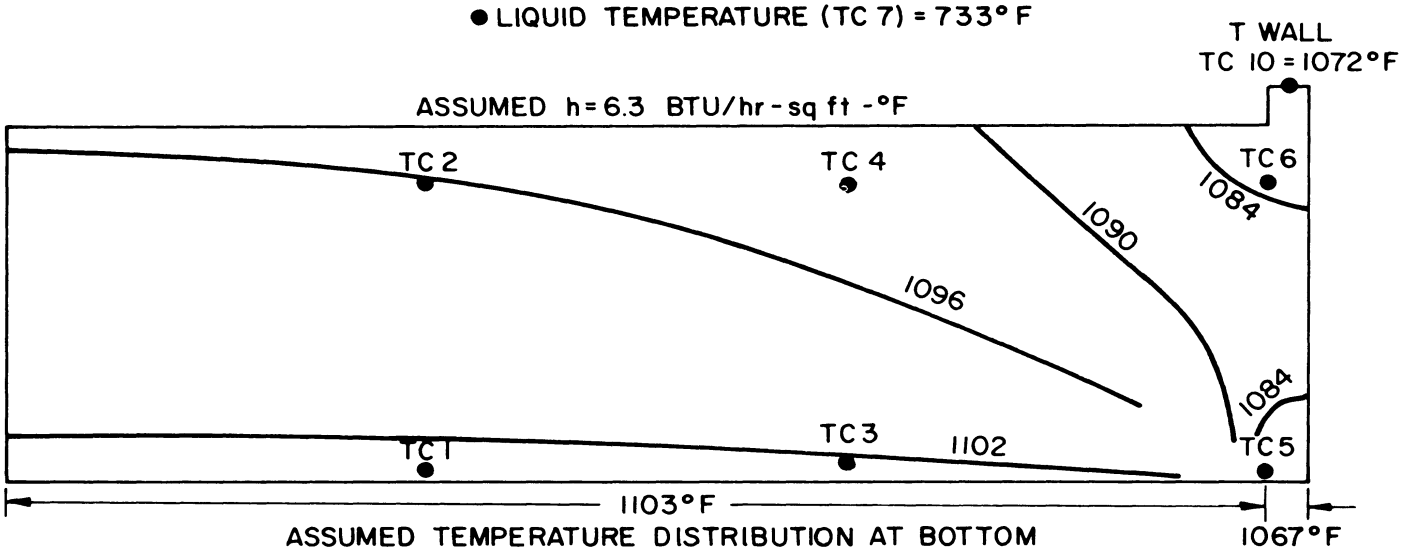

● THERMOCOUPLE MEASUREMENTS (See Figure 10 for Actual Location of Plate Thermocouples)

TC 1	1103° F
TC2	1097° F
TC3	1105° F
TC4	1097° F
TC5	1067° F
TC6	1064° F

Figure 30. Comparison Between Boiling Surface Flux and Flux Calculated from the Temperature Distribution Obtained by Computer Simulation

surface and the liquid is known to within a few percent because this quantity, although it is obtained by taking the difference between two large numbers, is also large. However, the heat fluxes during film boiling were calculated with temperature gradients in the boiling plate of $30^{o}F$ or less thereby introducing the possibility of a relatively large error. This uncertainty can be discussed in terms of random or accidental errors, systematic or constant errors, and errors of method.

An error of method can arise as a result of approximations and assumptions made in the theoretical development of an equation used to calculate the desired result. It can be assumed that the Fourier equation of heat conduction used to calculate the heat flux is theoretically accurate as long as the correct average thermal conductivity is used and the flow is unidirectional. For the temperature gradients in the boiling plate encountered during film boiling, the thermal conductivity varies a fraction of a percent. It was shown in the previous section on the discussion of radial gradients that the guard heater could be adjusted during operation such that the effect of radial gradients at the location of the thermocouples used to calculate the heat flux would be negligible. Hence an uncertainty in the heat flux due to an error of method can be neglected.

A systematic or constant error arises when some factor operates to continually bias the results. Such errors can be detected by performing the experiment with a number of different apparatus or by calculating the results by several independent methods. Two factors which might introduce systematic errors into the calculation of the heat flux are the thermal conductivity and the distance between the two temperatures used in the Fourier equation.

In Figure E-1 in Appendix E, the thermal conductivity of stainless steel as obtained by several researchers agree within 5 percent. Assuming that each of the thermocouple holes was drilled to within .010-inch and that the hot junction of each of the thermocouples is off by one-half the diameter of the thermocouple introduces a possible uncertainty of 23% in the distance used in the Fourier equation. These two factors could combine to give a maximum systematic error in the heat flux of 28%.

Random or accidental errors are inevitable in all measurements and result from errors of observation due to variation in the sensitivity of measuring instruments and the keenness of the senses of perception. They produce experimental scatter but a reliable average value can be calculated statisitically if enough measurements are obtained. The actual scatter of the experimental results shown in Figure 17 is relatively low. More than 80% of the points fall within one standard deviation of the curves fitted to the data and only one point falls outside of the 95% confidence limits.

The most significant factor which contributes to experimental scatter is the uncertainty in the temperature measurements used to compute the heat flux. It is important that the difference between the thermocouples used to calculate the heat flux is known accurately. All of the 1/16-inch OD Pt-Pt 13% Rh thermocouples were calibrated before use. The equipment and procedures used for the calibration are discussed in Appendix H. The thermocouples TC1 and TC2 were calibrated only to 1480^{o}F, the maximum anticipated saturation temperature of potassium, because they were originally used in the preliminary runs to measure temperatures in the liquid pool. They were used in the boiling plate

after modification of the apparatus because the thermocouples used initially could no longer be inserted into the holes. The thermocouple calibration data in Table H-1 in Appendix H shows that the agreement between TC1 and TC2 is very good and their average difference is 0.3°F over the calibration range 430-1480°F. After they had been in operation in the boiling plate for awhile, they were essentially re-calibrated during the heat loss calibration. The heat loss data in Appendix A show that TC1 and TC2 agree to within 1°F in the range 997-1632°F. These thermocouples were not re-calibrated in the constant-temperature furnace described in Appendix H since there was a high probability that they would develop open circuits if they were straightened. The two thermocouples that TC1 and TC2 replaced had developed open circuits after they were removed from the system and straightened.

Since the same potentiometer and the same observer were used in both the calibration and data runs, an estimate of the uncertainty in the temperature measurements during film boiling can be obtained from the statistical analysis of the thermocouples calibration data. From Table H-1, the standard deviations of the curves fitted to the calibration data for TC1 and TC2 are 0.9°F and 0.4°F respectively. The 95% confidence limits for TC1 and TC2 would be approximately 1.8°F and 0.8°F respectively, thus giving an uncertainty in their difference of 2.6°F. This corresponds to a maximum uncertainty of 43% which occurs at the lowest heat fluxes encountered during film boiling, whereas the data shown an actual scatter of 20% at the minimum for the 2 mm Hg results.

An independent method for calculating the heat flux to check that of using the temperature measurements in the boiling plate

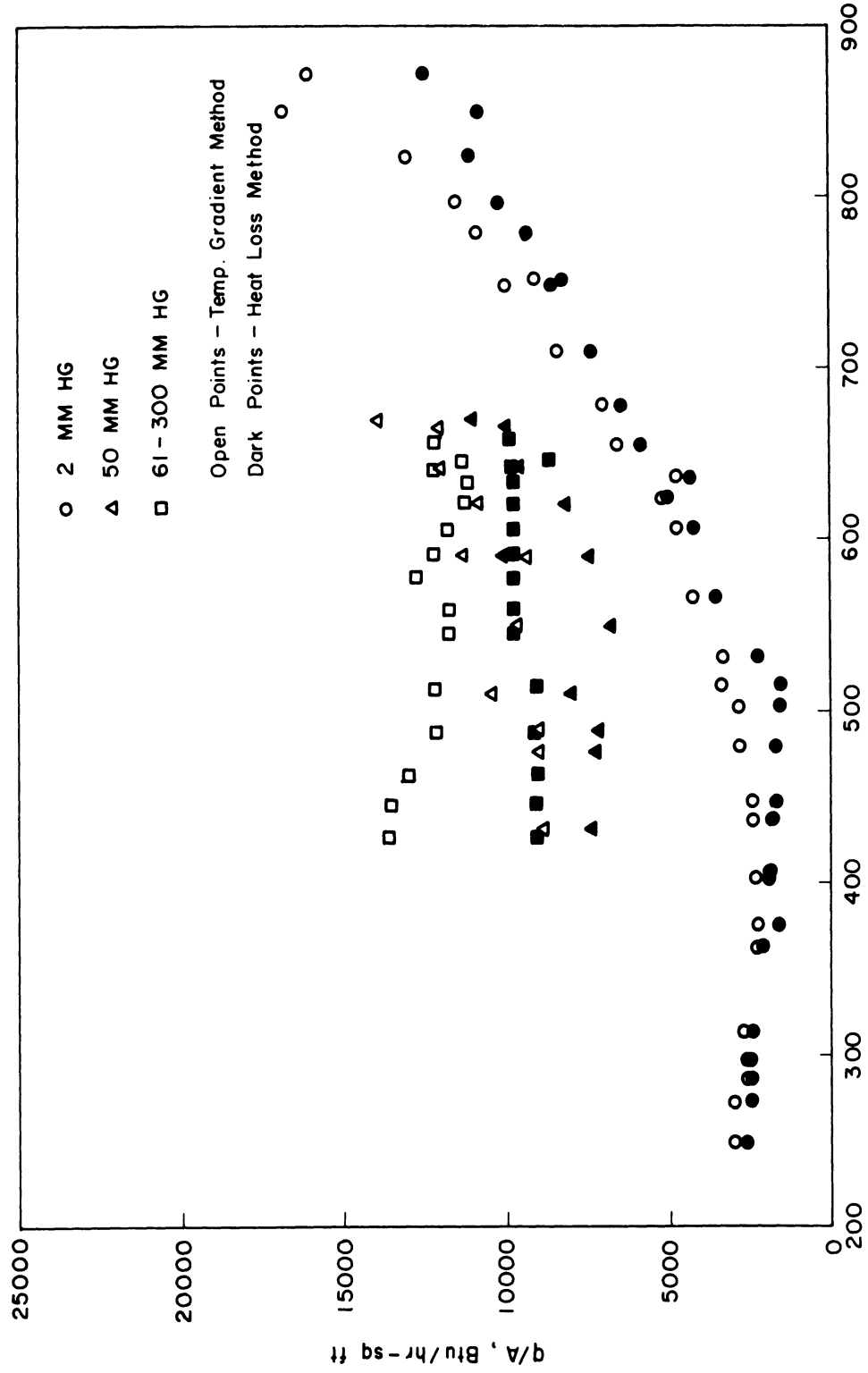

Figure 31. Comparison of Temperature Gradient Method and Heat Loss Method for Calculating the Heat Flux

consisted of subtracting an experimentally-determined heat loss from the power input to the main heater and dividing by the area of the boiling surface. The heat loss calibration curve is shown in Figure E-2 in Appendix E and it is seen that all of the points fall within 10% of the best line through the data. The comparison between the heat fluxes calculated by the two methods is shown in Figure 33. Except for two points, the heat flux calculated by the heat loss method is always lower than that obtained by Fourier's equation and the average deviation is 19%.

When one considers all of the possible factors which might introduce systematic or random errors, the maximum uncertainty in the calculated heat flux may be as high as 70%. However, the actual scatter of the data indicates that the uncertainty may be much less. Factors of unknown magnitude may bias the results upward or downward by almost 30% but an independent method of calculation agrees within 20%. It is felt that the present experimental results are accurate to within 30%.

VII. CONCLUSIONS

1. In stable film boiling, the heat flux increases with increasing pressure at a given temperature difference.
2. The heat fluxes encountered during film boiling of potassium are substantially above the theoretical predictions. However, the contributions to the heat flux of radiation and the vapor-phase dimerization reaction are significant. After correction for these two factors are made, the experimental results at moderate temperature differences can be correlated within 22% by the equation

$$h = 0.97 \left[\frac{k_v^3 \rho_v (\rho_l - \rho_v) g L'}{\mu_v \Delta T D_b} \right]^{1/4} \qquad (22)$$

where D_b is the bubble diameter given by

$$D_b = 4.7 \sqrt{\frac{3 g_c \sigma}{g(\rho_l - \rho_v)}} \qquad (23)$$

The constant 0.97 in Equation (22) gives the best fit to the present results and all the non-metallic data for film boiling from a horizontal surface at moderate temperature differences. Film boiling data for mercury do not apply to Equation (22) nor to any of the other correlations currently available.

3. The present results at low pressure do not agree with present correlations for predicting the minimum heat flux. However, the data indicates that the prediction of Zuber might be in agreement at higher pressures near 1 atm. The best fit to all of the metallic and non-metallic data is given by

$$(q/A)_{min} = 0.14\ \rho_v\ L' \left[\frac{g(\rho_l-\rho_v)}{\rho_l-\rho_v}\right]^{1/2} \left[\frac{g_c\ \sigma}{g(\rho_l-\rho_v)}\right]^{1/4} \qquad (26)$$

4. There is no reliable method for predicting the location of the minimum heat flux currently available.
5. The film boiling heat transfer to potassium, as well as to some non-metallic fluids, increases more rapidly at high temperature differences than can be accounted for by available correlations.

REFERENCES

1. Balzhiser, R. E., et al., "Literature Survey on Liquid Metal Boiling." ASD-TR-61-594, The University of Michigan, Ann Arbor, Michigan (December, 1961).

2. Baumeister, K. J., Hamill, T. D. and Schoessow, G. J., "A Generalized Correlation of Vaporization Times of Drops in Film Boiling on a Flat Plate." NASA TM X-52177 (1966).

3. Berenson, P. J., "Transition Boiling Heat Transfer from a Horizontal Surface." NP-8415, MIT Heat Transfer Laboratory (March, 1960).

4. Berenson, P. J., "Film Boiling Heat Transfer from a Horizontal Surface." J. of Heat Transfer, 83, No. 3 (1961).

5. Bonilla, C. F., "Alkali Metals Boiling and Condensing Investigations. Vol. I - Experimental Program." NASA CR-54050 (June, 1964).

6. Bonilla, C. F., "Pool Boiling Heat Transfer with Mercury." Reactor Heat Transfer Conference of 1956, TID-7529, Pt. 1, Book 2, 324-341.

7. Bromley, C. A., "Heat Transfer in Stable Film Boiling." Chem. Eng. Prog., 46, No. 5, 221 (1950).

8. Chang, Y. P., "Wave Theory of Heat Transfer in Film Boiling." J. of Heat Transfer, 81, (February, 1959).

9. Coe, H. H., "Summary of Thermophysical Properties of Potassium." NASA TN D-3120, (December, 1965).

10. Colver, C. P., "A Study of Saturated Pool Boiling Potassium up to Burnout Heat Fluxes." Ph.D. Thesis, The University of Michigan (September, 1963).

11. Drew, T., et al., "Boiling." Trans. AIChE, 23, (1937).

12. Ellion, M. E., "A Study of the Mechanism of Boiling Heat Transfer." JPL Memorandum No. 20-88 (March, 1954).

13. Ewing, C. T., et al., "High-Temperature Properties of Potassium." NRL Report 6233 (September, 1965).

14. Farmer, Liquid Metals Handbook, R. N. Lyon, editor, AEC and Bureau of Ships, Dept. of Navy, Washington, D. C. (1950).

15. Frederking, T. H. K., and Clark, J. A., "Natural Convection Film Boiling on a Sphere," Paper presented at 1962 Cryogenic Engineering Conference. Advances in Cryogenic Engineering, Vol. 8, K. D. Timmerhaus, Editor.

16. General Electric Company, "Alkali Metals Boiling and Condensing Investigations," Quarterly Report No. 8, Space Power Operations, Flight Propulsion Lab. Dept., NASA-CR-54138 (October, 1964).

17. Goldsmith, A., Waterman, T. E., and Hirschborn, H. J., Handbook of Thermophysical Properties of Solid Materials, Vol. II. Alloys, The Macmillan Company, New York (1961).

18. Hamill, T. D., and Baumeister, K. J., "Film Boiling Heat Transfer from a Horizontal Surface as an Optimal Boundary Value Process." NASA TM X-52183 (1966).

19. Hosler, E. R., and Westwater, J. W., "Film Boiling on a Horizontal Plate." ARS Journal, 32, 553-558 (1962).

20. Hsu, Y. Y., and Westwater, J. W., "Approximate Theory for Film Boiling on Vertical Surfaces." Chem. Eng. Prog. Sym. Ser., 56, No. 30, 15-24 (1960).

21. Jakob, M., Heat Transfer, Vol. I, Chapter 7, John Wiley and Sons, New York (1949).

22. Kepple, R. R., and Tung, T. V., "Two-Phase (Gas-Liquid) System: Heat Transfer and Hydraulics, An Annotated Bibliography." ANL-6734.

23. Kutateladze, S. S., "Heat Transfer on Condensation and Boiling." AEC TR 3770 (1952).

24. Lemmon, A. W., Jr., et al., "Engineering Properties of Potassium." NASA CR-54017 (Also BATT-4673-Final) (December, 1963).

25. Lewis, E. W., Merte, H., Jr., and Clark, J. A., "Heat Transfer at 'Zero Gravity'." Paper presented at 55th National Meeting of AIChE at Houston, Texas (February 7-11, 1965).

26. Lin, C., et al., "Boiling Heat Transfer of Liquid Metals." JPRS-3512 (1959).

27. Lyon, R. E., Foust, A. S., and Katz, D. L., "Boiling Heat Transfer with Liquid Metals." Ph.D. Thesis, The University of Michigan (1953).

28. Lyon, R. E., et al., "Boiling Heat Transfer with Liquid Metals." Chem. Eng. Prog. Sym. Ser., 51, No. 17, 41-47 (1955).

29. Madsen, H., and Bonilla, C. F., "Heat Transfer to Sodium Potassium Alloy in Pool Boiling." Chem. Eng. Prog. Sym. Ser., 56, (1960).

30. McAdams, W., Heat Transmission, 3rd ed., McGraw-Hill Book Co., New York (1954).

31. McFadden, P. W., et al. "High Flux Heat Transfer Studied. An Analytical Investigation of Laminar Film Boiling." ANL-6060 (October, 1959).

32. McFadden, P. W., et al. "An Analysis of Laminar Film Boiling with Variable Properties." Int. J. of Heat and Mass Transfer, 1, No. 4 (January, 1961).

33. Merte, H., Jr., "Investigation of Liquid Metal Boiling Heat Transfer." Contract No. AF 33(657)-11548, The University of Michigan (February, 1965).

34. Nukiyama, S., "Experiments on the Determination of the Maximum and Minimum Values of the Heat Transferred Between a Metal Surface and Boiling Water." AERE-TRANS-854 (1934).

35. Poppendiek, H. F., et al., "Quarterly Technical Report on High Acceleration Field Heat Transfer for Auxiliary Space Nuclear Power Systems." GLR-36, Geoscience Limited (May, 1965).

36. Poppendiek, H. F., et al., "Quarterly Technical Report on High Acceleration Field Heat Transfer for Auxiliary Space Nuclear Power Systems." GLR-32, Geoscience Limited (November, 1964).

37. Poppendiek, H. F., et al., "Summary Report on High Acceleration Field Heat Transfer for Auxiliary Space Nuclear Power Systems." GLR-42, AEC Contract No. AT(04-3)-409, Geoscience Limited (January, 1966).

38. Rallis, C. J., and Jawurek, H. H., "Latent Heat Transport in Saturated Nucleate Boiling." Int. J. of Heat and Mass Transfer, 7, 1051-1068 (1964).

39. Reid, R. C., and Sherwood, T. K., The Properties of Gases and Liquids, McGraw-Hill Book Co., New York (1958).

40. Richardson, J. L., Boynton, F. P., Eng, K. Y., and Mason, D. M., "Heat Transfer in Reacting Systems." Chem. Eng. Sci., 13, 130 (1961).

41. Rossini, F. D., et al., Selected Values of Chemical Thermodynamic Properties, Tables 84-96, Bureau of Standards Circular 500 (February, 1952).

42. Weatherford, W. D., Tyler, J. C., and Ku, P. M., "Properties of Inorganic Energy-Conversion and Heat Transfer Fluids for Space Applications." USAF, WADD-Tech. Report No. 61-96 (November, 1961).

43. Westwater, J. W., "Boiling of Liquids." Advances in Chemical Engineering, Vol. 1, T. B. Drew, editor, Academic Press Inc., New York (1956).

44. Zuber, N., "Hydrodynamic Aspects of Boiling Heat Transfer." AECU-4439 (June, 1959).

45. Zuber, N., and Tribus, M., "Further Remarks on the Stability of Boiling Heat Transfer." AECU-3631 (January, 1958).

APPENDIX A

Heat Loss Calibration Data

Main Heater Power (Watts)	Guard Heater Power (Watts)	Bottom Plate Temperatures (°F)			Top Plate Temperatures (°F)			Outer Tube Wall Temperatures (°F)		
		TC1	TC3	TC5	TC2	TC4	TC6	TC8	TC9	TC10
24	12	462	464	452	467	457	449	451	460	455
53	184	750	751	733	754	748	730	739	752	743
70	92	997	997	972	997	992	972	979	995	980
80	184	1224	1225	1195	1222	1225	1195	1210	1227	1211
92	254	1366	1368	1335	1367	1364	1336	1349	1369	1351
95	288	1418	1419	1385	1418	1415	1386	1400	1420	1400
104	288	1424	1425	1389	1423	1421	1391	1403	1424	1403
110	348	1526	1529	1490	1526	1524	1493	1506	1526	1506
113	374	1576	1579	1538	1576		1541	1554	1575	1553
120	428	1632	1634	1592	1632		1596	1607	1628	1605

APPENDIX B

FILM BOILING DATA

Main Heater Power (Watts)	Guard Heater Power (Watts)	Pressure (mm Hg)	Liquid Temperature (°F)	Bottom Plate Temperature (°F)			Top Plate Temperature (°F)			Outer Tube Wall Temperature (°F)		
			TC7	TC1	TC3	TC5	TC2	TC4	TC6	TC8	TC9	TC10
221.	428	2	718	1494	1495	1436	1474		1439	1445	1470	1435
256	428	2	717	1545	1544	1481	1520		1486	1492	1518	1481
270	407	2	718	1576	1575	1509	1548		1514	1517	1542	1505
296	400	2	720	1634	1631	1559	1600		1565	1568	1597	1555
270	407	2	728	1622	1619	1549	1586		1560	1564	1588	1546
242	400	2	721	1530	1532	1469	1506	1506	1474	1482	1508	1470
228	414	2	722	1497	1498	1436	1475	1474	1441	1448	1474	1438
208	414	2	722	1455	1456	1400	1436	1434	1402	1408	1432	1400
192	407	2	719	1417	1420	1367	1401	1398	1367	1375	1399	1369
180	407	2	718	1391	1393	1343	1376	1373	1343	1351	1375	1346
165	414	2	718	1356	1359	1313	1344	1340	1312	1322	1343	1317
154	421	2	714	1334	1337	1292	1323	1320	1293	1305	1325	1300
157	449	2	725	1375	1377	1331	1364	1361	1333	1344	1366	1338
143	421	2	720	1299	1301	1260	1289	1286	1260	1271	1291	1268
108	414	2	728	1253	1255	1218	1245	1243	1220	1234	1251	1230
120	414	2	718	1260	1262	1225	1252	1249	1226	1239	1254	1236
108	393	2	723	1234	1237	1200	1227	1225	1202	1215	1231	1212
108	367	2	720	1208	1211	1175	1201	1198	1175	1190	1207	1187
106	335	2	721	1176	1179	1144	1170	1167	1143	1157	1172	1155
106	317	2	719	1164	1166	1131	1158	1155	1130	1141	1160	1140
106	288	2	718	1132	1135	1100	1127	1122	1096	1107	1124	1107
106	293	2	723	1133	1136	1099	1127	1122	1098	1111	1129	1110

APPENDIX B (Continued)

Main Heater Power (Watts)	Guard Heater Power (Watts)	Pressure (mm Hg)	Liquid Temperature (°F) TC7	Bottom Plate Temperature (°F) TC1	TC3	TC5	Top Plate Temperature (°F) TC2	TC4	TC6	Outer Tube Wall Temperature (°F) TC8	TC9	TC10
106	265	2	732	1113	1117	1083	1109	1104	1082	1090	1110	1090
106	243	2	733	1103	1105	1067	1097	1097	1064	1071	1093	1072
106	233	2	731	1053	1055	1021	1046	1040	1017	1024	1043	1024
106	228	2	728	1034	1036	1004	1027	1022	1001	1010	1028	1009
103	223	2	725	1020	1021	988	1013	1008	985	992	1008	990
103	218	2	724	1008	1009	976	1000	995	973	983	997	980
103	213	2	724	984	985	952	976	968	950	961	969	952
221	414	50	983	1522	1519	1456	1499	1497	1464	1470	1498	1456
259	400	50	983	1603	1598	1532	1579		1540	1544	1570	1529
259	442	50	983	1655	1651	1585	1630		1594	1598	1624	1584
263	471	50	986	1681	1676	1610	1656		1620	1624	1650	1610
234	471	50	986	1635	1632	1569	1612		1578	1583	1608	1568
221	471	50	986	1600	1598	1537	1580		1546	1552	1577	1537
208	471	50	986	1560	1557	1498	1539		1508	1515	1539	1500
208	442	50	985	1499	1496	1438	1479	1478	1448	1456	1481	1441
208	414	50	984	1484	1481	1422	1464	1461	1430	1437	1463	1422
208	387	50	983	1439	1436	1377	1419	1416	1382	1387	1416	1375
278	414	50	983	1688	1681	1614	1659		1622	1624	1653	1610
245	428	61	1011	1686	1680	1617	1662		1624	1627	1654	1615
263	414	62	1013	1701	1695	1629	1676		1636	1639	1667	1626
263	414	75	1035	1707	1701	1636	1682		1643	1646	1674	1634
263	414	88	1052	1713	1707	1642	1690		1649	1653	1680	1642
263	414	100	1070	1720	1714	1650	1697		1657	1661	1688	1650

APPENDIX B (Continued)

Main Heater Power (Watts)	Guard Heater Power (Watts)	Pressure (mm Hg)	Liquid Temperature (°F)	Bottom Plate Temperature (°F)			Top Plate Temperature (°F)			Outer Tube Wall Temperature (°F)		
			TC7	TC1	TC3	TC5	TC2	TC4	TC6	TC8	TC9	TC10
263	414	115	1089	1725	1718	1654	1701		1660	1663	1690	1652
263	414	130	1106	1728	1721	1657	1703		1664	1669	1695	1658
263	414	146	1122	1732	1724	1660	1706		1667	1671	1697	1658
252	414	163	1137	1726	1719	1655	1702		1661	1662	1690	1652
252	414	178	1150	1725	1717	1654	1701		1661	1665	1694	1655
252	414	201	1169	1712	1706	1642	1689		1649	1650	1679	1639
252	414	225	1185	1704	1696	1632	1679		1639	1640	1670	1628
252	414	252	1202	1698	1689	1623	1671		1633	1634	1664	1620
252	414	275	1217	1698	1689	1622	1670		1634	1635	1663	1618
252	414	300	1243	1705	1696	1625	1677		1641	1642	1671	1625

APPENDIX C

NUCLEATE BOILING DATA

Main Heater Power (Watts)	Guard Heater Power (Watts)	Pressure (mm Hg)	Liquid Temperature (°F) TC7	Bottom Plate Temperature (°F) TC1	TC3	TC5	Top Plate Temperature (°F) TC2	TC4	TC6	Outer Tube Wall Temperature (°F) TC8	TC9	TC10
162	0	2	603	640	640	624	621	617	615	621	633	622
106	0	2	674	690	689	677	678	676	672	681	686	682
714	0	1	676	872	886	832	735		771	770	809	773
738	0	1	670	864	877	824	726		763	764	801	768
441	0	1	655	768	775	744	690		708	712	732	711
884	0	1	703	937	948	883	769		815	816	853	817
205	0	2	695	724	724	707	707	705	700	708	716	709
281	0	2	705	771	774	749	730		730	737	752	738
366	0	2	711	800	804	773	740		748	753	771	753
446	0	2	718	826	828	795	752		764	769	790	769
545	0	2	726	864	866	826	770		788	792	817	791
643	0	2	733	898	900	855	784		808	812	840	812
743	0	2	740	929	930	879	795		826	830	861	830
344	0	709	1381	1450	1451	1407	1409		1397	1406	1424	1404
432	0	659	1368	1455	1456	1408	1402		1393	1400	1422	1400
510	0	684	1376	1481	1483	1432	1415		1409	1416	1440	1416
604	0	704	1381	1508	1511	1452	1427		1425	1430	1458	1430
761	0	728	1387	1549	1552	1482	1445		1449	1452	1481	1451
626	0	707	1379	1513	1518	1453	1430		1427	1432	1460	1437
743	0	721	1384	1544	1550	1478	1442		1446	1446	1475	1444
856	0	736	1389	1573	1577	1498	1454		1463	1464	1492	1460

APPENDIX C (continued)

Main Heater Power (Watts)	Guard Heater Power (Watts)	Pressure (mm Hg)	Liquid Temperature (°F)	Bottom Plate Temperature (°F)			Top Plate Temperature (°F)			Outer Tube Wall Temperature (°F)		
			TC7	TC1	TC3	TC5	TC2	TC4	TC6	TC8	TC9	TC10
1008	0	751	1394	1606	1600	1525	1466		1482	1479	1506	1474
805	0	730	1384	1557	1561	1486	1449		1456	1460	1482	1454
696	0	717	1381	1530	1532	1466	1438		1440	1445	1467	1440
582	0	724	1384	1504	1508	1449	1430		1426	1434	1454	1429
485	0	723	1384	1479	1480	1430	1420		1413	1422	1440	1420
418	0	708	1378	1455	1453	1411	1407		1397	1453	1470	1452
285	0	640	1357	1409	1406	1370	1378		1365	1377	1392	1374
214	0	602	1269	1327	1323	1283	1304	1304	1284	1295	1313	1290
352	0	680	1373	1440	1440	1397	1400		1388	1397	1412	1394
127	0	707	1380	1464	1466	1417	1414		1404	1412	1428	1408
535	107	700	1377	1486	1490	1434	1422		1414	1422	1440	1418

APPENDIX D

PRELIMINARY FILM BOILING DATA

Main Heater Power (Watts)	Pressure (mm Hg)	Liquid Temperature (°F)	Bottom Plate Temperature (°F) 1/2" radius	1" radius	1 1/2" radius	Top Plate Temperature (°F) 1/2" radius	1" radius	1 1/2" radius	1/2" Radius Calculations q/A (Btu/hr-ft^2)	ΔT (°F)	h (Btu/hr-ft^2-°F)
419	N.A.	685	1565	1562	1556	1551	1535	N.A.	6,300	860	7.3
419	"	684	1568	1564	1553	1552	1536	"	6,600	863	7.6
388	"	693	1487	1471	1457	1470	1453	"	8,000	775	10.3
375	"	691	1488	1480	1465	1474	1460	"	6,500	781	8.3
403	"	684	1593	1587	1581	1577	1566	"	7,100	890	8.0
479	N.A.	815	1560	1554	1554	1549	1534	N.A.	4,800	730	6.6
493	"	814	1564	1557	1555	1552	1534	"	4,700	734	6.4
451	"	814	1482	1469	1461	1468	1447	"	5,900	650	9.1
457	"	814	1470	1458	1455	1460	1439	"	4,500	643	7.0
470	"	814	1506	1493	1492	1491	1471	"	6,700	673	10.0
476	"	814	1602	1590	1588	1573	1566	"	13,300	759	17.5
476	"	815	1636	1625	1618	1614	1598	"	10,700	795	13.5
476	"	815	1614	1603	1599	1594	1576	"	9,300	775	12.0
476	"	814	1592	1573	1572	1569	1553	"	10,300	753	13.7
476	"	814	1596	1578	1576	1573	1558	"	10,600	757	14.0
476	"	814	1609	1594	1592	1587	1571	"	10,500	769	13.7
467	N.A.	749	1669	1658	1654	1645	1631	N.A.	11,400	891	12.8
411	"	744	1552	1536	1534	1530	1518	"	10,000	785	12.7
419	"	742	1558	1543	1539	1536	1523	"	10,200	792	12.9
473	"	742	1677	1665	1663	1655	1639	"	10,300	907	11.4
452	"	741	1685	1673	1670	1666	1648	"	9,100	919	9.9
435	"	740	1658	1644	1640	1641	1620	"	7,900	895	8.8
342	2	773	1581	1572	1571	1564	1552	N.A.	7,800	788	9.9
319	2	773	1499	1489	1490	1484	1473	"	6,800	708	9.6
298	2	773	1462	1451	1453	1446	1434	"	6,800	670	10.2
277	2	773	1434	1425	1428	1422	1411	"	5,700	646	8.8

APPENDIX D (continued)

Main Heater Power (Watts)	Pressure (mm Hg)	Liquid Temperature (°F)	Bottom Plate Temperature (°F) 1/2" radius	1" radius	1 1/2" radius	Top Plate Temperature (°F) 1/2" radius	1" radius	1 1/2" radius	1/2" Radius Calculations q/A (Btu/hr-ft^2)	ΔT (°F)	h (Btu/hr-ft^2-°F)
348	1	727	1519	1506	1506	1502	1490	N.A.	7,500	773	9.7
396	"	"	1685	1675	1675	1667	1653	"	8,600	935	9.2
354	"	"	1597	1588	1587	1581	1568	"	7,300	850	8.6
314	"	"	1516	1508	1506	1501	1489	"	6,500	770	8.4
314	"	"	1502	1495	1493	1489	1477	"	5,600	759	7.4
298	"	"	1483	1475	1476	1471	1460	"	5,500	741	7.4
302	"	"	1466	1459	1458	1454	1443	"	5,200	725	7.2
282	"	"	1472	1465	1463	1459	1448	"	5,600	728	7.7
267	"	"	1360	1353	1355	1352	1342	"	3,700	623	5.9
256	"	"	1348	1340	1342	1339	1329	"	3,800	610	6.2
256	"	"	1443	1434	1442	1431	1425	"	5,100	702	7.3
208	"	"	1430	1428	1431	1420	1416	"	4,500	691	6.5
145	"	"	1371	1373	1383	1365	1365	"	2,400	636	3.8
174	"	"	1152	1145	1145	1142	1138	"	4,400	417	10.5
236	"	"	1480	1477	1480	1468	1463	"	5,200	739	7.0
204	"	"	1403	1400	1402	1392	1387	"	4,800	661	7.3
204	"	"	1393	1390	1392	1381	1376	"	4,800	651	7.4
186	"	"	1264	1261	1264	1256	1252	"	3,400	528	6.4
251	"	"	1226	1216	1214	1217	1206	"	3,600	489	7.4
409	2	750	1543	1537	1539	1530	1514	"	6,200	775	8.0
267	N.A.	724	1534	1530	1540	1515	1514	"	11,400	789	14.5
364	1	717	1434	1420	1421	1414	1408	"	8,800	700	12.6
382	"	714	1570	1562	1565	1550	1544	"	9,300	834	9.0
371	"	714	1577	1569	1570	1557	1550	"	9,100	841	10.8
347	"	713	1536	1529	1528	1518	1510	"	8,300	804	10.3
314	"	710	1428	1419	1417	1410	1402	"	7,800	700	11.1
318	"	711	1390	1378	1376	1372	1365	"	7,700	663	11.6
318	"	710	1372	1357	1358	1354	1348	"	7,700	646	11.9
342	"	714	1404	1387	1390	1384	1380	"	8,300	671	12.4
342	"	711	1451	1440	1442	1433	1426	"	8,000	722	11.1
382	"	713	1588	1580	1582	1570	1562	"	8,400	855	9.8
382	"	714	1607	1599	1603	1588	1579	"	8,900	871	10.2
369	N.A.	655	1569	1562	1565	1550	1542	"	8,700	892	9.7

APPENDIX E

TREATMENT OF DATA

Given: Power to main heater P, watts
Temperature of bottom 1/2-inch radius thermocouple in boiling plate TC1
Temperature of top 1/2-inch radius thermocouple in boiling plate TC2
Temperature of liquid TC7

1. Heat flux, q/A BTU/hr-sq ft

$$q/A = k \frac{TC1 - TC2}{x_1 - x_2} \qquad \text{(E-1)}$$

where k = thermal conductivity of type 316 stainless steel evaluated at

$$\frac{TC1 + TC2}{2}$$

and obtained from Figure E-1

x_1 = vertical distance between TC1 and boiling surface = .434 inch

x_2 = vertical distance between TC2 and boiling surface = .072 inch

2. Temperature difference, ΔT ^{o}F

$$\Delta T = TC2 - \frac{.072}{.362} (TC1 - TC2) - TC7 \qquad \text{(E-2)}$$

.072 = vertical distance between TC2 and boiling surface in inches

.0362 = vertical distance between TC1 and TC2 in inches

3. Heat transfer coefficient, h BTU/hr-sq ft-^{o}F

$$h = \frac{q/A}{\Delta T} \qquad \text{(E-3)}$$

APPENDIX E (Continued)

4. Average heat flux, $(q/A)_{avg}$ BTU/hr-sq ft-^{o}F

$$(q/A)_{avg} = \frac{(P-P_L)\ 3.412}{A} \qquad (E-4)$$

P_L = heat loss evaluated at TC1 and obtained from Figure E-2, watts

3.412 = conversion factor, watts to BTU/hr

A = area of boiling surface = .0491 sq ft

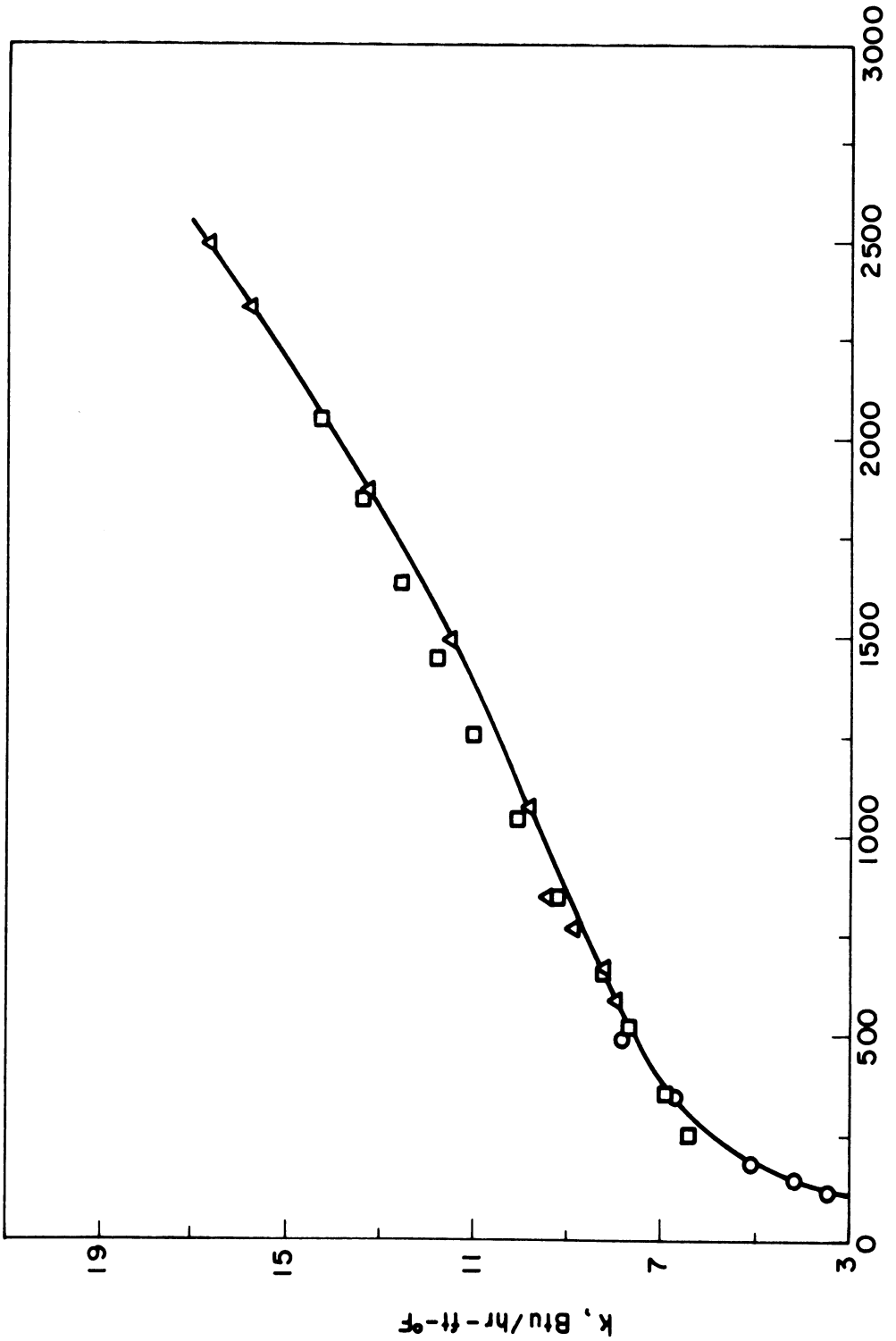

Figure E-1. Thermal Conductivity of Type 316 Stainless Steel (17)

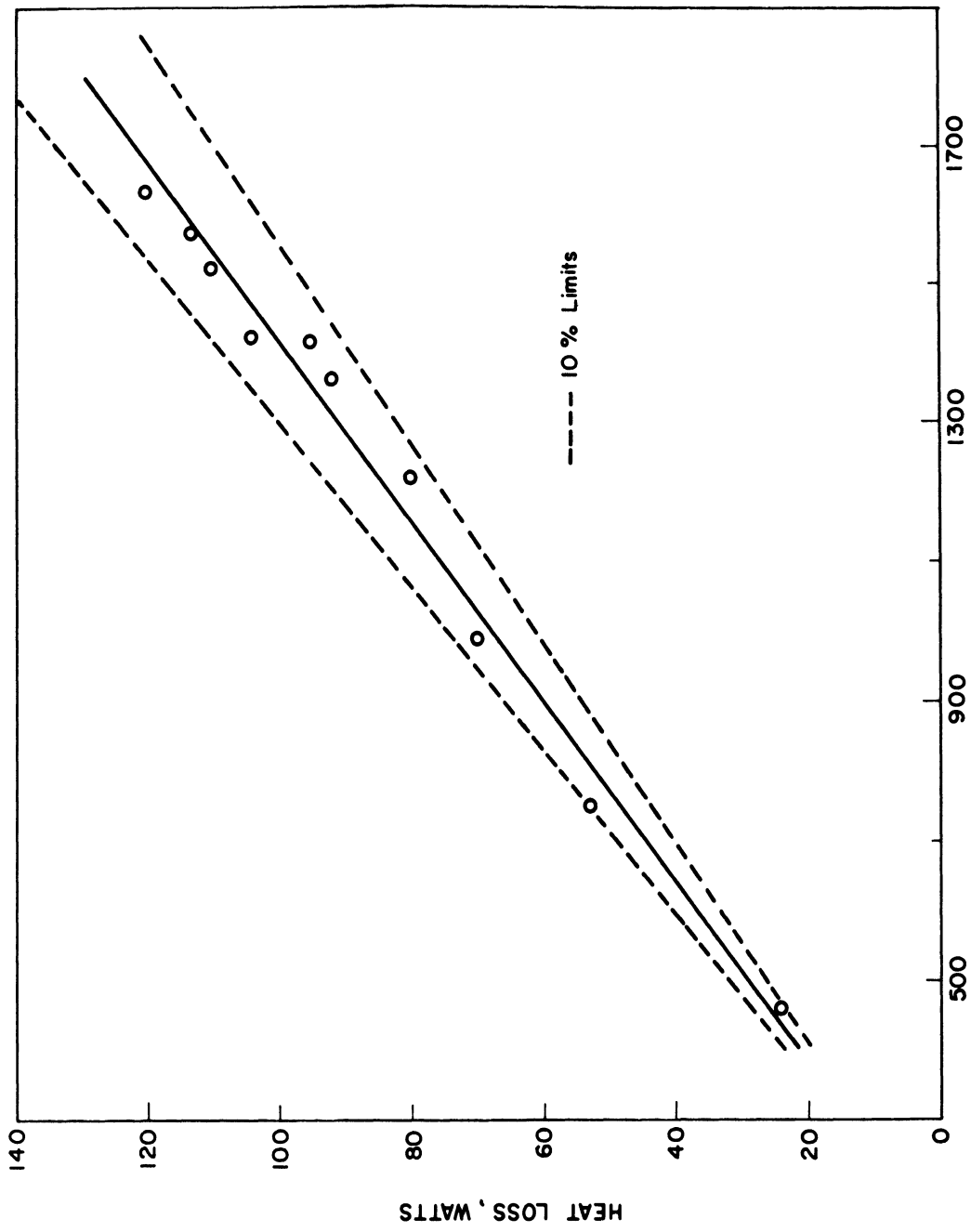

Figure E-2. Heat Loss Calibration

APPENDIX F

PHYSICAL PROPERTIES OF POTASSIUM

The vapor volumes of potassium as a function of temperature and pressure are tabulated in BATT-4673 (24) and the vapor density was obtained by taking the reciprocal of the vapor volume.* The surface tension was taken from Coe (9) and the vapor thermal conductivity and viscosity were obtained from Weatherford (42).

The thermal conductivity of superheated potassium vapor was calculated by taking the value for saturated conditions and employing Figure 7-3 in Reid and Sherwood (39). The viscosity of the vapor was assumed to be independent of pressure at low pressures and thus the temperature dependence was obtained by using the data for saturated conditions. The physical properties for potassium at 0.1 atm are summarized in Table F-1.

* Values for the liquid density, latent heat of vaporization, and vapor specific heat were also obtained from this report.

TABLE F-1

PHYSICAL PROPERTIES OF POTASSIUM AT 0.1 ATM

T ^{o}R	ρ_v lb/ft^3	k_v BTU/ft-hr-^{o}F	C_{pv} BTU/lb-^{o}F
1500	.00376	.00723	.1987
1600	.00348	.00772	.2060
1700	.00325	.00820	.2148
1800	.00306	.00869	.2172
1900	.00289	.00917	.2150
2000	.00275	.00965	.2103

Saturation temperature = $1500^{o}R$

ρ_l = $44.07\ lb/ft^3$ ($1500^{o}R$)

L = 887.4 BTU/lb ($1500^{o}R$)

σ = .0030 lb/ft

μ_v = .0418 lb/ft-hr

APPENDIX G

CALCULATION OF EFFECTIVE THERMAL CONDUCTIVITY OF POTASSIUM VAPOR

It has been found experimentally that the heat transfer rate to a gas undergoing a chemical reaction may be many times the rate predicted using accepted correlations and a weight average of the physical properties of the gas. This increase has been attributed to a diffusional mechanism associated with the chemical reaction. Thus, heat is transferred away from a wall by ordinary molecular collisions and by molecular diffusion associated with chemical reaction. The usual method of treating the effect on the heat transfer coefficient is to define an effective thermal conductivity:

$$k_{eff} = k_f + k_r \qquad \text{(G-1)}$$

where k_f is the thermal conductivity in the "frozen" system which has the equilibrium composition at a given temperature but is not undergoing a reaction and k_r is the contribution due to the reaction.

The only type of reaction which has been treated extensively in the literature has been the "equilibrium" reaction (40) in which the reaction rate is so high that the gas mixture may be assumed to have its equilibrium composition instantaneously after a change in temperature. The thermal conductivity due to reaction for this case is given by:

$$k_r = D_{12}\,\rho\,\frac{\alpha(1-\alpha^2)}{2\,RM}\left(\frac{\Delta H_r}{T}\right)^2 \qquad \text{(G-2)}$$

APPENDIX G (Continued)

For the reaction

$$2K = K_2 \tag{G-3}$$

the degree of dissociation, α, can be expressed in terms of the mole fraction of K_2

$$y_{K_2} = \frac{1 - \alpha}{1 + \alpha} \tag{G-4}$$

Equation (G-2) can then be written as

$$k_r = D_{12} \rho \frac{y_{K_2}(1 - y_{K_2})}{RM(1 + y_{K_2})^2} \left(\frac{\Delta H_r}{T}\right)^2 \tag{G-5}$$

Assuming the ideal gas law, the gas density is given by

$$\rho = \frac{PM}{RT} \tag{G-6}$$

substituting Equation (G-6) into Equation (G-5) gives

$$k_r = 0.692\, D_{12} \rho \frac{y_{K_2}(1 - y_{K_2})}{(1 + y_{K_2})^2} \frac{\Delta H_r^2}{T^3} \tag{G-7}$$

Equation (G-7) can be used to calculate the thermal conductivity due to reaction provided that the composition of the gas, the binary diffusion coefficient, and the heat of reaction can be determined.

Since Weatherford has tabulated the equilibrium molecular weight of potassium vapor as a function of temperature for

APPENDIX G (Continued)

saturated conditions, it is possible to calculate the vapor composition from this data. Using fugacity charts, the equilibrium constant for the reaction described by Equation (G-3) can be determined. Since the equilibrium constant is a function of temperature only, it can then be used to calculate y_K and y_{K_2} at various constant pressures.

Several methods are available for calculating binary diffusion coefficients: the Arnold equation, the Gilliland equation, the Slattery equation, and the Hirshfelder equation. These equations are presented and discussed by Reid and Sherwood (39) and the Hirschfelder equation was arbitrarily chosen.

Values for the heat of formation of K and K_2 at 25°C are tabulated in Rossini (41). Using these values and the enthalpy differences for the ideal monatomic and diatomic species tabulated in Weatherford, the heat of reaction as a function of temperature can be calculated.

The method for calculating the frozen thermal conductivity was presented in Appendix F. The results are summarized in Figure G-1 for a pressure of 0.1 atm.

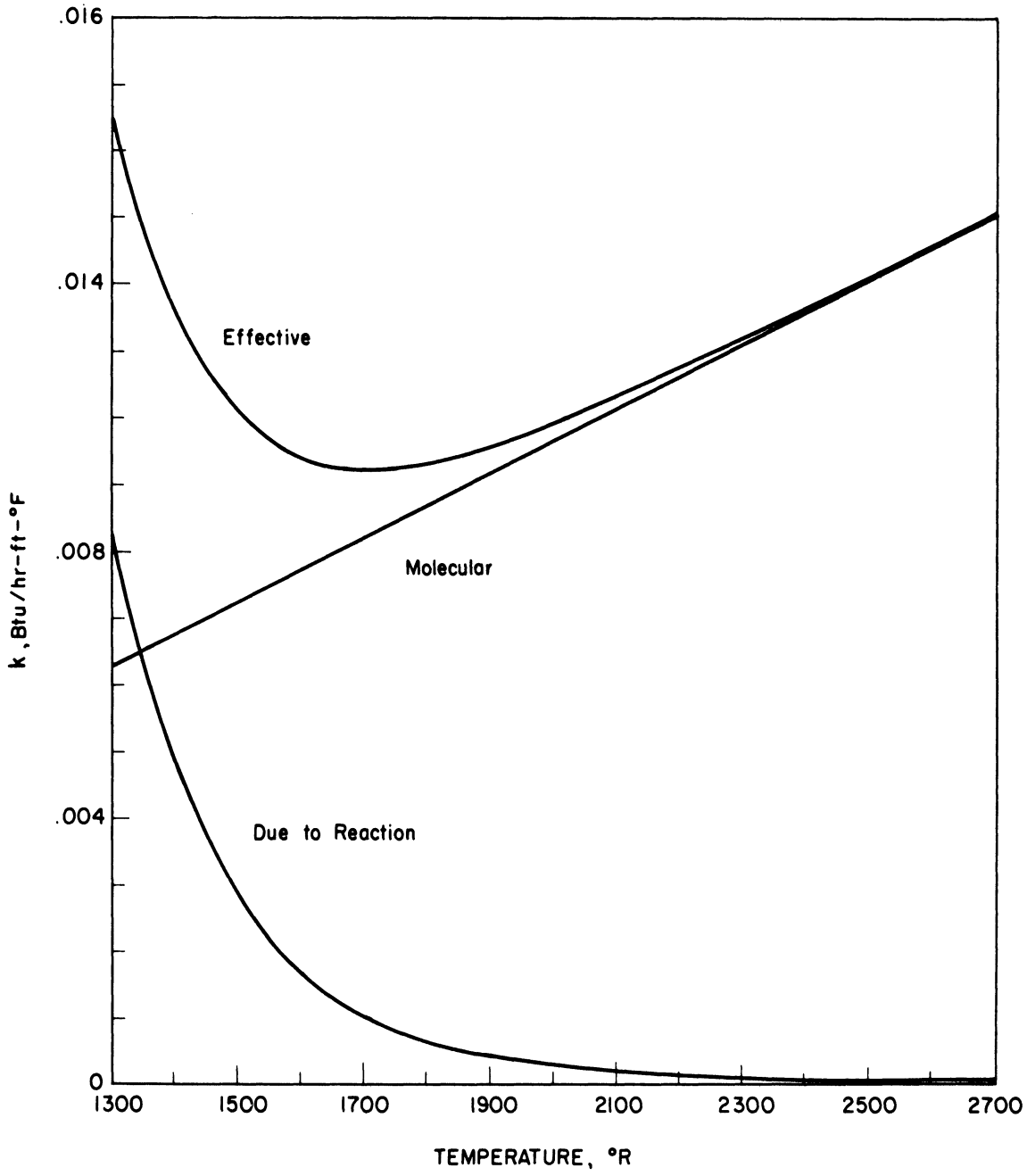

Figure G-1. Effective Thermal Conductivity of Potassium Vapor at 0.1 Atm.

APPENDIX H

CALIBRATION OF THERMOCOUPLES

The calibration of the 1/16-inch OD by 2-ft long thermocouples used in the boiling plate was carried out in a flanged stainless steel pipe 2-inches OD by 1 3/4-inches ID by 2-ft long. The brass head contained a Conax multi-hole gland for the swaged thermocouples, a Conax MPG gland for the standard thermocouple, and a 1/4-inch tube for evacuation. The standard was a Pt-Pt 10% Rh thermocouple made from 20-gauge wires which had been calibrated by the Bureau of Standards. A copper equilizing block 1 11/16-inches diameter by 2-inches long was used to insure isothermal conditions. The 1/16-inch OD thermocouples were inserted into .065-inch holes to a depth of 3/4-inch. When the thermocouples were calibrated inside of 1/8-inch OD wells, the wells were inserted into the copper block to a depth of 1-inch. The standard was contained in a 3/16-inch OD well which was inserted 1 1/4-inches into the copper equilizing block.

The stainless steel vessel was inserted into a Leeds and Northrup thermocouple checking furnace which has a maximum operating temperature of 1800^{o}F. The vacuum pump was turned on and the power to the furnace adjusted with a rheostat. After steady state conditions were reached, the emf output of the standard and the swaged thermocouples were recorded using a Leeds and Northrup No. 8662 portable precision potentiometer, and the rheostat was reset. Data were obtained while both increasing and decreasing the temperature of the furnace.

APPENDIX H (Continued)

A cubic equation was used to express the temperature-emf relationship for each thermocouple. The results of the calibration and a comparison with the theoretical values in the Leeds and Northrup Bulletin 07789, Issue 3, are presented in Table H-1. The thermocouples T1 and T2 in Table H-1 were calibrated in 1/8-inch OD stainless steel wells whereas the rest of the thermocouples were calibrated without wells.

TABLE H-1

CALIBRATION OF BOILING PLATE THERMOCOUPLES

EMF (mv)	TC1 (°F)	TC2 (°F)	RANGE (°F)	TC3 (°F)	TC4 (°F)	TC5 (°F)	TC6 (°F)	TC7 (°F)	RANGE (°F)	L & N* (°F)
2.012	497.4	496.5	0.9							500
2.547	597.0	597.0	0							600
3.103	697.5	697.8	0.3							700
3.677	798.0	798.5	0.5							800
4.264	897.8	898.1	0.3	896.8	896.9	897.1	897.2	898.3	1.5	900
4.868	997.6	997.6	0	999.1	998.4	998.9	999.0	998.7	0.7	1000
5.488	1097.3	1097.0	0.3	1100.4	1099.3	1099.9	1100.0	1098.8	1.6	1100
6.125	1197.2	1196.7	0.5	1201.0	1199.7	1200.4	1200.4	1198.9	2.1	1200
6.773	1296.5	1296.0	0.5	1300.1	1299.0	1299.6	1299.6	1298.1	0.5	1300
7.436	1396.2	1396.1	0.1	1398.7	1398.0	1398.4	1398.5	1397.2	1.5	1400
8.116				1497.5	1497.2	1497.5	1497.5	1496.5	1.0	1500
8.809				1596.3	1596.4	1596.5	1596.6	1595.8	0.8	1600
9.516				1695.7	1696.2	1696.2	1696.2	1695.3	0.9	1700
Average			$\overline{0.3}$						$\overline{1.2}$	
Std. dev. (°F)	0.9	0.4		0.8	1.0	1.1	1.2	0.9		

*L & N Bulletin 07789 Issue 3